Princeton University

Department of
Mechanical and
Aerospace Engineering

DISCLAIMER

DOE/ET/15352--T1

DE82 012938

DOE/ET/15352--T1

THE PLASMADYNAMICS AND IONIZATION KINETICS OF THERMIONIC ENERGY CONVERSION

by

John L. Lawless, Jr.

and

S. H. Lam

Department of
Mechanical and Aerospace Engineering
Princeton University, Princeton
New Jersey 08544

February 1982

LEGAL NOTICE

Table of Contents

Abstract

To reduce the plasma arc-drop, thermionic energy conversion is studied with both analytical and numerical tools. Simplifications are made in both the plasmadynamic and ionization-recombination theories. These are applied to a scheme proposed presently using laser irradiation to enhance the ionization kinetics of the thermionic plasma and thereby reduce the arc-drop. It is also predicted that it is possible to generate the required laser light from a thermionic-type Cesium plasma. The analysis takes advantage of theoretical simplifications derived for the ionization-recombination kinetics. It is shown that large laser ionization enhancements can occur and that collisional Cesium recombination lasing is expected. To complement the kinetic theory, a numerical method is developed to solve the thermionic plasma dynamics.

The effects of the complete system of electron-atom inelastic collisions on the ionization-recombination problem are shown to reduce to a system nearly as simple as the well-known "one-quantum" approximation. As a consequence the effects of other processes such as recombination lasing, resonant atom-atom collisions, and resonant radiation enhanced ionization can be analyzed simply, analytically, and quantitatively. A number of well-known

ionization-recombination approximations are limiting cases of this theory. The resonant radiation ionization enhancement process is analyzed and it is shown why large enhancements are possible. A Cesium recombination laser is predicted and the magnitudes for the population inversion and the laser efficiency are derived.

To combine the above analysis of ionization-recombination kinetics with the plasma dynamics of thermionic conversion, a finite difference computer program is constructed. It is capable of solving for both unsteady and steady thermionic converter behavior including possible laser ionization enhancement or atomic recombination lasing.

Using the above developments, a proposal to improve thermionic converter performance using laser radiation is considered. In this proposed scheme, laser radiation impinging on a thermionic plasma enhances the ionization process thereby raising the plasma density and reducing the plasma arc-drop. A source for such radiation may possibly a Cesium recombination laser operating in a different thermionic converter. The possibility of this being an energy efficient process is discussed.

I Introduction

The principles of operation and possible methods for improvement of thermionic energy conversion (T.E.C.) are explored in this study. A number of unusual or unexpected results are found. Two tools were developed for the consideration of the plasma dynamics. One is an isothermal model which features closure with simplicity. The other is a numerical computer program which is capable of examining unsteady as well as steady modes of operation. A motivating factor for this work is interest in possible improved performance using laser irradiation of the plasma. This involved two parts. The first is studying the effect of such radiation on T.E.C. operation. The second part involved finding a not too inefficient source for such radiation. For ionization-recombination, standard methods are supplemented with a new theory that simplifies the problem without loss of quantitative accuracy.

Using both analytical and computational methods, some unintuitive conclusions have resulted. For one, energy injection into a thermionic plasma actually causes a lower electron temperature. This is true for laser energy injected for absorption by the atomic levels. To some lesser extent, it is also true for direct heating of the electron translational modes. Another unintuitive result is that even though energy injection lowers the electron temperature it also simultaneously causes an increase in the electron density. A further counter-conventional result is that the double sheath which obstructs electron emission from the emitter does not reduce but rather improves T.E.C. performance. Suppression of this obstruction increases the arc-drop. These conclusions appear as immediate consequences of the analytical isothermal model that is developed presently. The trends predicted by this theory are verified by computational solution of the governing differential equations.

Towards a maximum of insight with a minimum of mathematical complexity, an isothermal model, built upon[5,6], is developed and closed. The roles of various physical processes and how they interrelate are clarified. A picture of the plasmadynamics is developed wherein the arc-drop is determined by an energy balance and the electron temperature is governed by an ignition condition. Physical causes of the results, even the unintuitive ones, are apparent. The consequences of this analysis and its application to the laser enhancement scheme are thoroughly discussed in chapter II.

To verify the conclusions drawn from analytical theory, a numerical algorithm has been created to solve the system of unsteady or steady thermionic converter differential equations. The present method of solution which uses a predictor-corrector relaxation scheme differs greatly from previously employed marching or shooting methods. In addition to allowing the study of unsteady situations, the exponentially growing error terms of shooting schemes are avoided.

Because of the importance of ionization and recombination on thermionic conversion and because these processes can be sensitive to inelastic collision cross-sections, the subject of these cross-sections is reviewed. In light of recent studies, cross-sections used in earlier studies with Cesium are found to be of poor accuracy. A set of cross-section formulas which appear to have the present backing of theory and experiment are selected for use in the present study.

A development which significantly simplifies the collisional transition network while retaining quantitative accuracy is presented herein. This is done by taking advantage of a property that the cross-section formulas selected as above have. The resulting model is nearly as simple as the well-known one quantum model. As a consequence, many otherwise subtle effects can be analyzed and explained with unlabored algebraic formulas. A number of examples are given. Many previous ionization-recombination theories are shown to be limiting cases of the present one. In particular, the process of laser ionization enhancement is made clear. It is shown to be a very energy efficient way to ionize. Recombination lasing is also discussed with this model.

A motivation for this work is interest in the possibility of improving T.E.C. behavior by altering the ionization kinetics. This is to be done by subjecting the plasma to light resonant with some atomic levels. For a given electron temperature, this causes a very large increase in the ionization rate constant. In contrast with other proposals, laser enhancement has the advantages of being a volume process and the energy used goes directly into ionization. As a consequence, the arc-drop is reduced. In principle, this process can be energy efficient overall. In practice, it is limited by the energy cost of producing such light. Steps towards removing this obstacle are taken by the present theoretical development of a thermionic Cesium recombination laser. A rapidly cooled Cesium plasma may have a population inversion on the infrared 7p-7s transition. The plasma dynamic studies indicate that this rapid cooling may be obtained in a thermionic type plasma by varying the current flow.

The laser ionization enhancement process developed herein appears to be similar to the opto-galvanic effect which has received much attention in the literature, e.g. [103-111]. While optogalvanic theories[103,106,110,111] have tended to be qualitative in nature, the present investigation proceeds from first principles in hopes of attaining quantitative accuracy.

These subjects and others are discussed in detail in the chapters to follow. Chapter II reviews the development of the governing equations, discusses the present isothermal model, and applies it to various problems of interest. Since the Cesium laser prediction is sensitive to inelastic collision cross-sections, available theories and experiments on this subject are discussed in chapter III. The elements of ionization-recombination theory are reviewed in chapter IV and some of the subtler implications are discussed with little mathematical complication. The new equivalent circuit ionization-recombination theory is presented in chapter V. The results of the computer solution of the T.E.C. plasma equations are given in chapter VI to verify earlier conclusions. Chapter VII summarizes and concludes this work. From this work a number of avenues for improving converter performance appear suggesting that much fruitful future work is possible.

II Introduction to Thermionic Energy Conversion Theory

Thermionic energy conversion involves a large number of physical phenomenon which interact in very complex ways. If the performance of thermionic converters is to be improved, it must be determined which effects dominate and how they can be controlled. It is the purpose of this chapter to outline the fundamental equations governing thermionic converter performance and discuss the concepts developed in simplified approximate models.

The isothermal theory of thermionic converter operation developed in Lam[6] culminated in relationships determining the arc-drop and electron temperature in terms of the plasma resistance and the ratio of output current to emitted current. This has shed much light on the determination of T.E.C. performance. In this chapter, the theory is further extended. First, it is shown how the plasma resistance can be determined a priori. Secondly, an a priori determination of the emitted current even in the double sheath regime is found. This closes the model and allows quantitative prediction of T.E.C. behavior.

Sections A through E and section G are largely reviews. They develop the general conservation equations, their boundary conditions, and their scaling laws. The fifth section, E, then develops simple approximate analytic models. This includes a discussion of the ignition condition and determination of arc-drop. This is based on Lam[5,6] but differs in emphasis which is placed here on approximating converter behavior subject to ionization-recombination kinetics rather than the concept of the ideal screwed-down-ion converter. Section G develops the physical basis of the Lam transformed energy equation theory[9]. This theory has important implications for the development of numerical methods for thermionic plasmas.

The remaining sections extend the simplified theories to conditions of present interest. Section F explains how the well known faster-than-Boltzmann voltage rise can occur in a one dimensional T.E.C. This is done by extending the concept of an ignition temperature to nonlinear conditions. Section H discusses how laser enhanced ionization can reduce the plasma arc-drop. Section I discusses unsteady thermionic converter behavior with application to the possibility of creating a thermionic Cesium plasma recombination laser. These theories will be used to explain the numerical results presented in a later chapter.

II.A Conservation Equations

The conservation equations to be used in this work are cast in a form somewhat different from those commonly used. This form, developed in Lam[5] and Lam[9], simplifies the equations by uncoupling the electrostatic potential from the momentum and energy equations. These equations will, with the continuum approximations to be made in section II.B, lead to the ambipolar diffusion and Lam[9] energy equations. The usual energy equation, the one which explicitly includes the electrostatic field, will also be discussed here. Further formal simplification of the usual energy equation is shown when the total as opposed to the sensible enthalpy is considered.

These equations are presently developed from a fundamental point of view. The derivation proceeds starting with the mass, momentum, and energy moments of the Boltzmann equation. This is done mainly for two reasons. First, it is desired to emphasize what assumptions and approximations are and are not necessary to develop the ambipolar diffusion equation. This will lead to results which differ from some conventional conclusions, particularly with regard to the role of electron-ion momentum transfer effects on ambipolar diffusion. Secondly, this procedure provides an alternative but fully equivalent derivation of the Lam[9] energy equation. Again, to emphasize where approximations are and are not made, the collisional source terms are left in a general unspecified form in the present section. The usual approximations for them will be given in II.B. Because thermionic converters are typically one-dimensional and planar, the present derivation will be in one dimension. This avoids the complications of tensor notations.

To begin, the continuity equations for electrons and for ions may be stated:

$$A.1 \qquad \frac{\partial n_e}{\partial t} = S^{(n)} - \frac{\partial \Gamma_e}{\partial x} \quad ; \quad \frac{\partial n_i}{\partial t} = S^{(n)} - \frac{\partial \Gamma_i}{\partial x}$$

where: $\Gamma_e = n_e u_e$ = ELECTRON FLUX

$\Gamma_i = n_i u_i$ = ION FLUX

u_e = ELECTRON SPEED

u_i = ION SPEED

And $S^{(n)}$ is the chemical source term. n_e and n_i are the electron and ion number densities, respectively. Since ions

are assumed to exist only in the singly ionized form, the electron and ion source must be identical.

An immediate consequence of the mass conservation equations is the conservation of total current J:

$$A.2 \qquad \frac{\partial J}{\partial x} = 0 \qquad \text{WHERE} \qquad J = e(\Gamma_e - \Gamma_i)$$

Because of this conservation property, it is convenient to formulate T.E.C. theory as if the converter were placed in a constant current circuit. Thus, J may be considered given.

It is a definition of the term plasma that quasi-neutrality hold as a good approximation. In the present situation this means that, outside of the sheaths, the electron and ion densities must be very nearly equal. Thus from here on, the explicit distinction between these densities will be dropped, their densities simply denoted by n. Note however that electrons and ions may have quite different temperatures.

Next, the momentum equation may be considered. Thus:

$$A.3 \qquad mn \frac{D_e u_e}{Dt} = -\frac{\partial p_e}{\partial x} - n\frac{\partial e\psi}{\partial x} + S_{ea}^{(p)} + S_{ei}^{(p)}$$

$$A.4 \qquad Mn \frac{D_i u_i}{Dt} = -\frac{\partial p_i}{\partial x} + n\frac{\partial e\psi}{\partial x} + S_{ia}^{(p)} - S_{ei}^{(p)}$$

Where $S_{ea}^{(p)}$, $S_{ei}^{(p)}$, $S_{ia}^{(p)}$ are source terms for momentum caused by electron-atom, electron-ion, and ion-atom collisions respectively. Here p_e and p_i are the x-x components of the electron and ion pressure tensors, respectively. m and M are electron and ion masses, respectively. ψ is the electron motive. e is the elementary charge. D_e /Dt and D_i /Dt are, respectively, the electron and ion substantial derivatives.

Asymmetries may be immediately noted between the electron and ion momentum equations: both the electric field and electron-ion momentum transfers appear in each equation with equal magnitude but opposite signs. By adding these two equations both of these effects exactly cancel and disappear from the result:

$$A.5 \qquad mn\frac{D_e u_e}{Dt} + Mn\frac{D_i u_i}{Dt} = -\frac{\partial p}{\partial x} + S_{ea}^{(p)} + S_{ia}^{(p)}$$

Where: $p = p_e + p_i$

The above when combined with the continuity equation and

assumed behaviors for the source terms becomes the well known ambipolar diffusion equation, as will be shown later. Again, it is to be noted that in addition to eliminating the electric field, the electron-ion momentum transfer also cancelled. Furthermore these cancellations occurred using no approximations other than quasi-neutrality and the Boltzmann equation.

Energy conservation is considered next. For ions under T.E.C. conditions, it is generally adequate to replace their energy equation with the approximation that their translational temperature is the same as that of the neutrals. The situation for the electrons however is quite different. Determination of the electron temperature turns out to be quite complex and has a dominating effect on T.E.C. performance. Taking the appropriate moment of the Boltzmann equation for electrons results in the energy equation:

$$\text{A.6} \qquad \frac{\partial n\epsilon}{\partial t} + \frac{\partial \Gamma_e h_1}{\partial x} + \frac{\partial q_e}{\partial x} + \Gamma_e \frac{\partial e\psi}{\partial x} = S^{(\epsilon)} + \epsilon S^{(n)}$$

Where ϵ and h are the stagnation energy and enthalpy defined by:

$$\text{A.7} \qquad \epsilon = \tfrac{1}{2} n u_e^2 + \tfrac{3}{2} k T_e$$

$$\text{A.8} \qquad h = \epsilon + p_e/n$$

and where $S^{(\epsilon)}$ is a collisional energy source term. In principle, this should include both elastic and inelastic collisional effects but, under T.E.C. conditions, the inelastic effects dominate. The quantity q_e is the heat conduction flux. The inelastic energy source, or sink, occurs only under disequilibrium conditions such as may be caused by ionization-recombination or radiative energy loss or absorption.

In the usual development of the T.E.C. energy equation, integration by parts of the electric field term followed by application of the continuity equation is used resulting in:

$$\text{A.9} \qquad \frac{\partial n(\epsilon + e\psi)}{\partial t} + \frac{\partial}{\partial x}\left[\Gamma_e(h + e\psi) + q_e\right] = n\frac{\partial e\psi}{\partial t} + S^{(\epsilon)} + (\epsilon + e\psi)S^{(n)}$$

In steady state with the collisional source terms neglected,

a first integral is obtained:

$$A.10 \qquad Q_e \equiv \Gamma_e (h + e\Psi) + q_e = \text{CONSTANT}$$

which is probably the most common form for the T.E.C. energy equation. In a next better approximation, a part of the energy source is written as being the energy into ionization-recombination. thus, let:

$$A.11 \qquad S^{(E)} = -E_o S^{(n)} + R$$

Where Eo is the ionization energy and R is the remaining contributions that are often neglected. The energy equation can then be rewritten as:

$$A.12 \qquad \frac{\partial}{\partial t}[n(\epsilon + e\Psi + E_o)] + \frac{\partial}{\partial x}[\Gamma_e(h + E_o + e\Psi) + q_e] = n\frac{\partial e\Psi}{\partial t} + R + (\epsilon + e\Psi)S^{(n)}$$

where, when steady-state is assumed and R neglected, the equation still has a first integral:

$$A.13 \qquad Q_e' \equiv \Gamma_e (h + E_o + e\Psi) + q_e = \text{CONSTANT}$$

The quantity (h+Eo) is often called the total as opposed to sensible enthalpy.

The above equations explicitly include the electric field or electron motive. This creates some difficulties. To remedy this, there is an alternative formulation that has been developed in Lam[9]. That theory eliminates the explicit appearance of the electric field from the energy equation. Thus this energy equation when combined with the ambipolar diffusion equation will allow for the T.E.C. behavior to be solved without reference to the electric field. The problem is reduced from a system of simultaneous equations with three unknown variables to a system with just two. The development in Lam[9] proceeded from the usual T.E.C. transport equations. Here, an equivalent development is given which starts with the moments of the Boltzmann equation as above and before the additional approximations for the collisional source terms are made.

The elimination of the electric field term from the energy equation is done simply. Taking the momentum equation and multiplying through by the electron speed, there results:

$$A.14 \quad m\Gamma_e \frac{D_e u_e}{Dt} + u_e \frac{\partial P_e}{\partial x} + \Gamma_e \frac{\partial e\psi}{\partial x} = u S_{ea}^{(p)} + u S_{ei}^{(p)}$$

Note that the term involving the electric field here has the same form as in the energy equation. Eliminating this term between the two equations there results:

$$A.15 \quad \frac{\partial n\epsilon}{\partial t} + \frac{\partial \Gamma_e \epsilon}{\partial x} + \frac{\partial q_e}{\partial x} + p_e \frac{\partial u_e}{\partial x} = S^{(E)} + \epsilon S^{(n)} + m\Gamma_e \frac{D_e u_e}{Dt} - u\left(S_{ea}^{(p)} + S_{ei}^{(p)}\right)$$

Now, the only unknowns in this energy equation are the density and temperature. As will be apparent later, the plasma dynamics of the T.E.C. can be solved now without reference to the electric field at all. With this the number of equations involved is of course less and thus the whole problem is much simpler.

These equations cannot be solved without a model to quantify the collisional source terms. This will be remedied in the next section. With section D to discuss non-dimensionalization and section C to describe the boundary conditions, the equations will be complete.

II.B Approximations for a Weakly Ionized Plasma

The conservation equations stated in the last section are quite general. Before such equations can be used rules for determining the various unknowns such as the collisional source terms must be specified. For this to be done in a practical way, more approximations are necessary. The end result of this section will be the plasma convection-diffusion equations. The approximations to be made, the usual ones for a T.E.C. plasma, are mostly based on a small mean free path assumption. This is reasonable since there are typically at least ten mean free paths between the electrodes. The specific approximations are listed below:

1). Viscous components of the pressure tensor are neglected. Thus, the x-x component of the pressure tensor, which is the one which appears in the conservation equations, can be given by the ideal gas law:

B.1 $$p_e = n \cdot kTe$$

B.2 $$p_\lambda = n \cdot kTn$$

where Te is the electron temperature and Tn is the heavy particle temperature. k is Boltzmann's constant.

2). The momentum source terms are approximated to first order by a small mean free path or continuum assumption as linear in the relative speed of the two interacting species. Thermal diffusion is neglected. The constant of proportionality is written as a product of the mass of the target particle and a momentum transfer collision frequency:

B.3 $$s_{ea}^{(e)} = -m \nu_{ea} \Gamma_e$$

B.4 $$s_{ei}^{(e)} = -m \nu_{ei} (\Gamma_e - \Gamma_i)$$

B.5 $$S_{ia}^{(p)} = -M \nu_{ia} \Gamma_i$$

3). The unsteady terms in the momentum equations will be neglected. This is based on the assumption that the time scales under consideration are much longer than particle mean free times. Since mean free times are typically the order of ten nanoseconds or less, this will generally be a good assumption.

4). Terms in the momentum equations involving the convection of momentum are neglected. This is based on the assumption that the momentum transfer collisions occur sufficiently often to keep the Mach numbers small.

5). The term q_e is given by Fourier's law of heat conduction:

B.6 $$q_e = -k_e \frac{\partial T_e}{\partial x}$$

With these approximations, the plasma conservation equations may be written. First, the electron-ion momentum equation, A.5, using approximations 2 and 4, is rewritten as:

B.7 $$0 = -\frac{\partial p}{\partial x} - \frac{\Gamma}{\mu_i}$$

where Γ is called the ambipolar flux and is defined by:

B.8 $$\Gamma = \Gamma_i + \frac{\mu_i}{\mu_{ea}} \Gamma_e$$

and where the quantities μ_i and μ_{ea} are called mobilities and are defined by:

B.9 $$\mu_i = 1/M\nu_{ia}$$
$$\mu_{ea} = 1/m\nu_{ea}$$

Combining the above relations for the ambipolar flux with the mass conservation equation A.1 yields the ambipolar diffusion equation:

B.10 $$\left(1 + \frac{\mu_i}{\mu_{ea}}\right)\frac{\partial n}{\partial t} = \frac{\partial}{\partial x}\mu_i \frac{\partial p}{\partial x} + \left(1 + \frac{\mu_i}{\mu_{ea}}\right) S^{(n)} + \Gamma_e \frac{\partial}{\partial x}\left(\frac{\mu_i}{\mu_{ea}}\right)$$

Turning to the energy equation A.15, by using approximations 1 through 5 there results:

$$\frac{3}{2} n \frac{\partial k T_e}{\partial x} + \frac{3}{2} \frac{\partial \Gamma_e k T_e}{\partial x} - \frac{\partial}{\partial x} k_e \frac{\partial T_e}{\partial x} + p \frac{\partial u_e}{\partial x}$$

B.11

$$= S^{(E)} + \frac{3}{2} k T_e S^{(n)} + \frac{\Gamma_e^2}{n \mu_{ea}} + \frac{\Gamma_e}{n} \frac{\Gamma_e - \Gamma_i}{\mu_{ei}}$$

Employing conservation of mass A.1 and rearranging yields the energy equation:

$$\frac{3}{2} n \frac{\partial k T_e}{\partial x} = \frac{\partial}{\partial x} k_e \frac{\partial T_e}{\partial x} - \frac{3}{2} \Gamma_e \frac{\partial k T_e}{\partial x} - n k T_e \frac{\partial \Gamma_e / n}{\partial x}$$

B.12

$$+ \frac{\Gamma_e^2}{n \mu_{ea}} + \Gamma_e \frac{\Gamma_e - \Gamma_i}{n \mu_{ei}}$$

To complete the energy equation, expressions are needed to determine the electron and ion fluxes, Γ_e and Γ_i. The ion flux can be determined from conservation of mass, A.1:

B.13 $$\frac{\partial \Gamma_i}{\partial x} = S^{(n)} - \frac{\partial n}{\partial t}$$

From the above and the definition of total current J, the electron flux can be found:

B.14 $$\Gamma_e = \frac{J}{e} + \Gamma_i$$

where, again, J is a conserved quantity determined by factors outside of the thermionic converter. Since electron mobility is much larger than ion mobility, it is often the case that:

B.15 $$\Gamma_e \cong \frac{J}{e} \quad ; \quad \Gamma_i << \Gamma_e$$

The limits of this approximation will be discussed later. When it is valid, it can be used to replace B.14 and simplify equations B.10 and B.12. This is often very useful.

The remaining unspecified functions are the mass and energy source terms. The mass source term is to be given by detailed consideration of the ionization-recombination kinetics of the plasma. This term is generally written in the phenonemological form:

B.16 $$S^{(n)} = (\alpha N_0 - \beta n_e^2) n_e$$

where No is the neutral Cesium ground state density and where α is called an ionization coefficient and β is called the recombination coefficient. Both these coefficients are generally strong functions of temperature and possibly density as well. They may also depend on radiative disequilibria. If the time scales were sufficiently short, they would also depend on the time history of the plasma. These considerations will be discussed in chapters IV and V.

The electron collisional energy source term can be accurately modeled as being due to inelastic electron-atom collisions. This includes effects of the energy of formation of ions as well as of the excited states of the atom and radiative gains or losses. A quantitative model for these effects will be developed in chapters IV and V also.

As appropriate for this type of plasma, the ion temperature will be assumed to be the same as the neutral temperature for all regions not near the sheaths. Further, it is a good approximation that the neutral temperature near the electrodes is the same as the electrode temperature and that it varies linearly in the gap between the electrodes.

To summarize, the governing equations of the thermionic converter are the ambipolar diffusion equation B.10 and the energy equation B.12, as supplemented by relation B.14 and either B.13 or B.15. For sections II.D and onward, B.15 will be assumed. The next section will present the boundary conditions for these equations. Following that, they will be scaled and nondimensionalized. the remaining sections discuss analytical methods to simplify and clarify the roles of the various physical processes involved.

II.C Sheaths and the Plasma Boundary Conditions

To solve the plasma equations developed in the previous sections, it is of course necessary to have boundary conditions. The electrode walls are characterized by their behavior as sources or sinks of ions, electrons, and energy. Their behavior determines the boundary conditions for the problem. These conditions cannot be applied directly to the plasma convection-diffusion equations, however, as the quasineutral assumption generally fails in a small region near the boundaries. While the non-neutral regions, sheaths, are typically quite small being the order of ten microns or smaller in width typically, they have a major effect on the overall T.E.C. performance. Analyzing a sheath is a difficult problem in itself. In the present work, the sheath theory of Lam[5] is employed. The assumptions used in this theory will be outlined presently. In particular, the relationship between the mono-energetic approximation and the presumably more precise half-Maxwellian distribution is discussed. Also, the Bohm criterion matching between the sheath and the outer plasma will be compared with the more common ad hoc approximations. Using this sheath analysis, the plasma boundary conditions will then be stated.

The assumptions of plasma sheath theory are discussed presently. The results are not derived; they are merely stated. For the derivations and more detailed discussions, the reader is referred to Lam[5].

Since a goal of the present work is to further understanding of thermionic conversion, simple models are used to describe the wall behavior. To this end:

1). The walls are perfectly absorbing, no reflection.

2). The collector is assumed to emit nothing.

3). The emitter is assumed to emit only electrons.

These assumptions reduce the number of phenomena involved.

To solve Poisson's equation for the potential drop in a sheath, it is necessary to know the charge densities. To start, consider the electrons emitted from the emitter. They have a current density:

$$J_E = e\, n_E\, \bar{v}_E / 2 = e\,\Gamma_E$$

Where n_E is the emitted density, and $\bar{v}_E$ is the mean thermal speed of electrons at the emitter temperature. The emitter sheath may or may not have a potential peak as shown in figure two. If it has no peak, then the emitted density is given by the Richardson density, possibly as modified for the Schottky effect. Otherwise, it must be solved for as an unknown in the sheath theory. The density of these emitted electrons varies as they travel through the sheath as a function of the potential, V. If one assumes the usual half-Maxwellian form of the distribution function for emitted electrons at the potential peak, the density of these electrons as they fall down the peak towards the plasma is given by an error function:

$$\text{C.2} \quad n_E(V) = n_E \exp\left(e(V_E - V)/kT_E \right) \operatorname{erfc}\left(\sqrt{e(V_E - V)/kT_E} \right)$$

where V_E is the total voltage drop of the sheath and V is the potential in the sheath with respect to the potential at the sheath-quasineutral region interface. T_E is the emitter wall temperature. At large potential drops, the above behaves like:

$$n_E(V) \simeq \frac{n_E}{\sqrt{\pi \frac{e(V_E - V)}{kT_E}}} \qquad \text{FOR } e(V_E - V) \gg kT_E$$

It is found moreover that the the whole function, C.2, is well approximated by the simple form:

$$\text{C.3} \quad n_E(V) \cong \frac{n_E}{\sqrt{1 + \pi \frac{e(V_E - V)}{kT_E}}}$$

which is exactly the density one would find if the mono-energetic assumption for the emitted electrons had been made to begin with. Considering now the density of the ions which are accelerated into the sheath and making the mono-energetic approximation, their density is given by:

$$\text{C.4} \quad n_i(V) = n_o / \sqrt{1 + 2\alpha_E V / kT_E}$$

where n_o is the density at the emitter sheath-quasineutral region interface. The subscripts 0 and 1 will be used to indicate that a plasma variable should be evaluated near the

emitter and collector sheaths, respectively. The parameter alpha in the ion density function is determined from the speed with which the ions enter the sheath. If it is assumed that the ions enter with a speed associated with the neutral particle temperature, it follows that:

C.5 $$\alpha_E = \pi / 2$$

A common correction to account for non-Maxwellian effects is to assume that the ions arrive at the sheath with twice the mean Maxwellian speed. This would make alpha one quarter of the value above.

$$\alpha_E = \pi/8$$

There is a more precise method for determining alpha. Detailed analysis indicates that ions must arrive with at least a certain speed or else Poisson's equation is ill-behaved. This speed is determined by Bohm's criterion. See Lam[5].

In contrast to ions and emitted electrons, the plasma electrons entering the sheath generally face a potential barrier. It is assumed that the barrier, V_E, is sufficiently high that a near equilibrium density distribution is obtained:

C.6 $$n_e(V) = n_o N_e e^{-eV/kT_e}$$

Where Ne is the ratio of the density of near equilibrium electrons at the sheath-quasineutral region interface to the density of ions there. Ne must be less than one if there is emission of electrons from the wall.

At this point there are four unknowns: Ne, the ion speed parameter α_E, the emitted density n_E, and the sheath height itself V_E. These can be solved for, as in Lam[5], with the following four conditions:

1). Charge neutrality must exist at the sheath-quasineutral region interface.

2). The emitted density must be given by the double-sheath or Richardson conditions.

3). The Bohm criterion must be satisfied.

4). The net current flow must match that of the plasma.

Information about the sheath heights can be obtained by examining the conservation of current conditions. For emitter and collector, the total current is J. Evaluated at the emitter sheath-quasi-neutral region interface, it is found that:

$$C.7 \qquad J = J_E - e n_0 N_e \frac{\bar{v}_0}{4} e^{-eV_E/kT_e} + n_0 \sqrt{\frac{kT_E}{\alpha_E M}}$$

Here, J_E is the emitted current. Similarly, at the collector plasma-sheath interface it is found that:

$$C.8 \qquad J = n_1 \frac{\bar{v}_1}{4} e^{-\frac{eV_C}{kT_e}} - n_1 \sqrt{\frac{kT_C}{\alpha_C M}}$$

where Ne has been set to one since collector emission is assumed negligible, n_1 is the plasma density at the collector sheath-quasineutral region interface, and $\bar{v}_1$ is the electron mean thermal speed.

In the plasma equations it is often accurate to assume that the ion current is negligible compared to the electron current. This will be true when:

$$e n_1 \sqrt{\frac{kT_e}{\alpha_C M}} \ll J$$

With the ion current neglected, the above equations when solved for the sheath height result in:

$$C.9 \qquad V_E = \frac{kT_0}{e} \ln \frac{n_0 N_e \bar{v}_0 / 4}{\Gamma_E - \Gamma_e}$$

$$V_C = \frac{kT_1}{e} \ln \frac{n_1 \bar{v}_1 / 4}{\Gamma_e}$$

n_1 is the ion density in the quasi-neutral region near the collector sheath. T_0 and T_1 are the electron temperatures evaluated near the emitter and collector sheaths, respectively. The above equations for the sheath heights will be useful in later sections.

Turning attention now to the implications of the plasma sheath on the boundary conditions for the plasma equations, the mass and energy boundary conditions will be stated. Using the above mass flux equations, the ambipolar diffusion boundary condition at the emitter can be written:

$$C.10 \qquad \Gamma_0 = -\mu_i \frac{\partial P}{\partial x}\Big|_0 = -n_0 \sqrt{\frac{kT_E}{\alpha_E M}} \left(1 + \frac{\mu_i}{\mu_{ea}}\right) + \frac{\mu_i}{\mu_{ea}} \frac{J}{e}$$

The corresponding condition at the collector is:

$$C.11 \qquad \Gamma_1 = -\mu_i \frac{\partial P}{\partial x}\Big|_1 = n_1 \sqrt{\frac{kT_C}{\alpha_C M}} \left(1 + \frac{\mu_i}{\mu_{ea}}\right) + \frac{\mu_i}{\mu_{ea}} \frac{J}{e}$$

Under some circumstances, an approximation to these boundary conditions can be used to advantage. By analyzing the orders of magnitude for the variables in these equations, it is found that the densities at the walls are typically of the order of a Knudsen number. This is typically a small number, as was assumed to derive the plasma diffusion equations. Thus, it is often a reasonable first approximation that:

$$n_0 \cong 0 \quad ; \quad n_1 \cong 0$$

While the above can be quite reasonably accurate for many purposes, it is inadequate for use in the T.E.C. electric field or electron energy equations since all of these are singular as density goes to zero.

The energy equation boundary conditions are found by considering the fluxes of energy through the sheath. At the emitter, it follows that[5,6]:

C.13 $$Q_e = (e\psi + eV_E + 2kT_E)\Gamma_E - (e\psi + eV_E + 2kT_0)(\Gamma_E - \Gamma_e)$$

Using the approximations of section B for the electron heat flux Qe, it follows that:

C.14 $$-k_e \frac{\partial T}{\partial x}\Big|_0 = -2\Gamma_E(kT_0 - kT_E) + \Gamma_e\left(eV_E - \frac{kT_0}{2}\right)$$

And, at the collector:

C.15 $$Q_e = (e\psi + eV_c + 2kT_1)\Gamma_e$$

and similarly:

C.16 $$-k_e \frac{\partial T_e}{\partial x}\Big|_1 = \Gamma_e\left(eV_c - \frac{kT_1}{2}\right)$$

In summary, the boundary conditions on the T.E.C. plasma equations have been stated. For the ambipolar diffusion equation these are C.10 and C.11. For the energy equation, C.14 and C.16 are used. The sheath heights and ion acceleration parameters are determined from the sheath theory of Lam[5].

II.D Scaling and Nondimensionalization

The equations presented in sections II.B and II.C contain many quantities which are of uncertain magnitude. This makes it difficult to judge the importance of each and the sensitivity of the solutions of the equations to each of them. To alleviate this problem, the equations can be non-dimensionalized. When this is done the number of uncertain problems will be reduced to a smaller number of dimensionless parameters which are just groups of the old parameters. A further benefit of non-dimensionalization is that scaling laws obeyed by these equations will be apparent.

Reference quantities should be chosen so that the resulting non-dimensionalized variables have easily estimated magnitudes. Electron temperature, Te, and heavy particle temperature, Tn, are non-dimensionalized by the emitter temperature, T_E. Thus:

$$\tau = T_e / T_E \quad ; \quad \tau_n = T_n / T_E$$

The voltages and sheath heights are scaled similarly by the emitter temperature:

$$\chi = \frac{e\Psi}{kT_E} \quad ; \quad \chi_E = \frac{eV_E}{kT_E} \quad ; \quad \chi_c = \frac{eV_c}{kT_E}$$

The mobilities are scaled by reference, or characteristic, values:

$$\bar{\mu}_{ei} = \mu_{ei} / \mu_{ec}$$

$$\bar{\mu}_e \equiv \left(\frac{1}{\bar{\mu}_{ea}} + \frac{1}{\bar{\mu}_{ei}} \right)^{-1} ; \quad \bar{\mu}_{ea} = \mu_{ea} / \mu_{ec} ; \quad \bar{\mu}_i = \mu_i / \mu_{ic}$$

The ratio of the ion to electron mobilities is expected to be the order of the square root of the mass ratio. Thus define:

$$\Lambda_c = \sqrt{\frac{M}{m}} \frac{\mu_{ic}}{\mu_{ec}}$$

where, according to kinetic theory, Λ_c is the ratio of the ion to electron mean free paths.

The x-location of a point is scaled by the distance between the plates:

$$\xi = x / d$$

The density is scaled by some fixed value n_c:

$$\bar{n} = n/n_c$$

Sometimes for steady-state analysises, n_c may be chosen to be the maximum density in the field. More commonly it will be chosen to be a fixed value like 1(14) cm-3*. The currents are scaled by an expected diffusion current:

$$I = J / J_D \quad ; \quad I_e = e \Gamma_e / J_D$$

$$I_i = e \Gamma_i / J_D \qquad I_E = J_E / J_D$$

Where: $$J_D = e\, n_c \mu_{ec} kT_E / d$$

The ambipolar flux is also nondimensionalized:

$$\bar{\Gamma} = e\Gamma / J_D$$

The time is scaled by a reference characteristic time for electrons to diffuse across the gap:

$$\bar{t} = t/t_c \quad \text{WHERE} \quad t_c \equiv \frac{d^2}{\mu_{ec} kT_E}$$

In the boundary conditions, a group of parameters occurs repeatedly: let it be called Kn since it is related to a knudsen number:

$$K_n = \frac{\mu_{ec} kT_E/d}{v_E}$$

The remaining nondimensionalizations are listed here:

$$\bar{S}^{(n)} = \frac{S^{(n)}}{n_c \mu_{ec} kT_E/d^2}$$

$$K = \frac{k_e}{n_c \mu_{ec} k^2 T_E}$$

$$\bar{S}^{(E)} = S^{(E)} / (n_c \mu_{ec} (kT_E)^2/d^2)$$

$$\bar{p} = (p_e + p_i)/(n_c kT_E)$$

---

* The notation 1(14) signifies one times ten to the fourteenth.

With these definitions above, the conservation equations can be written. The ambipolar diffusion equation is:

$$\text{D.1} \qquad \frac{\partial \bar{n}}{\partial \bar{t}} = -\lambda_c \sqrt{\frac{\pi}{M}} \frac{\partial}{\partial \bar{x}} \left(\bar{\mu}_i \frac{\partial \bar{p}}{\partial \bar{x}} + \frac{\bar{\mu}_i}{\bar{\mu}_{ea}} I_e \right) + \bar{S}^{(n)}$$

The Lam[9] energy equation is:

$$\text{D.2} \qquad \frac{3}{2} \bar{n} \frac{\partial \tau}{\partial \bar{t}} = \frac{\partial}{\partial \bar{x}} K \frac{\partial \tau}{\partial \bar{x}} - \frac{3}{2} I_e \frac{\partial \tau}{\partial \bar{x}} - \bar{n} \tau \frac{\partial I_e / \bar{n}}{\partial \bar{x}} + \bar{S}^{(E)} + \frac{I_e^2}{\bar{n} \bar{\mu}_e} + \frac{I_e I_i}{\bar{n} \bar{\mu}_{ei}}$$

Equations can be closed by setting the electron current equal to the total current. Otherwise, the continuity equations are needed:

$$\text{D.3} \qquad \frac{\partial \bar{n}}{\partial \bar{t}} = \frac{\partial I_i}{\partial \bar{x}} + \bar{S}^{(n)} \quad ; \quad I_e = I - I_i$$

For completeness, the usual energy equation will also be given here:

$$\text{D.4} \qquad \frac{3}{2} \bar{n} \frac{\partial \tau}{\partial \bar{t}} = - \frac{\partial \bar{Q}_e}{\partial \bar{x}} + \bar{S}^{(E)}$$

where: $$\bar{Q}_e = I_e \left(\frac{5}{2} \tau + \chi \right) - K \frac{\partial \tau}{\partial \xi}$$

Since this equation introduces the additional variable of the electric potential, it must be used in combination with another equation such as the electron momentum equation:

$$\text{D.5} \qquad -\bar{n} \frac{\partial \chi}{\partial \bar{x}} = \frac{\partial \bar{n} \tau}{\partial \bar{x}} + \frac{I_e}{\bar{\mu}_e} - \frac{I_i}{\bar{\mu}_{ei}}$$

The mass and energy boundary conditions are written:

$$\text{D.6} \qquad \begin{aligned} \bar{\Gamma}_0 &= -\bar{\mu}_i \frac{\partial \bar{p}}{\partial \bar{x}}\Big|_0 = -\frac{\bar{n}_0}{\lambda_c K_n} \sqrt{\frac{\pi}{8 \alpha_E}} + \frac{\bar{\mu}_i}{\bar{\mu}_{ea}} I \\ \bar{\Gamma}_1 &= -\mu_i \partial \bar{p} / \partial \bar{x}\Big|_1 = \frac{\bar{n}_1}{\lambda_c K_n} \sqrt{\pi / 8 \alpha_E} + \frac{\bar{\mu}_i}{\bar{\mu}_{ea}} I \\ -K \frac{\partial \tau}{\partial \bar{x}}\Big|_0 &= -2 I_E (\tau_0 - 1) + I_e (\chi_E - \tau_0 / 2) \\ -K \frac{\partial \tau}{\partial \bar{x}}\Big|_1 &= I_e (\chi_c - \tau_1 / 2) \end{aligned}$$

where the subscripts 0 and 1 refer to conditions in the quasineutral region near the emitter and collector, respectively. The approximate sheath heights are written:

$$\text{D.7} \qquad \chi_E = \tau_0 \lambda_{D1} \frac{\bar{n}_0 N_e \sqrt{\tau_0}}{4 K_n (I_E - I_e)}$$

$$\chi_c = \tau_1 \lambda_{D1} \frac{\bar{n}_1 \sqrt{\tau_1}}{4 K_n I_e}$$

This summarizes the T.E.C. equations as written in nondimensional form.

II.E Some Fundamental Concepts in Thermionic Conversion

The system of equations that has just been developed is quite complex. The variables interact with each other in peculiar ways and even the qualitative behaviors of some variables in response to others is controversial. Yet, it has been found that there are some guiding principles capable of at least qualitatively describing overall thermionic converter behavior. Principally these are the concept of an ignition temperature and the isothermal theory [5,6]. As these will be of great use in later sections, they will be reviewed here.

Each of these concepts is developed by dividing the T.E.C. problem into two parts. One of these is to find what the response of the density is to some given temperature. This leads to the ignition temperature concept. The second is to find the temperature given a density distribution. This will lead to a simple relationship between temperature and arc-drop. These will be combined only at the end to determine the overall characteristics of the T.E.C.

The essential assumption of isothermal theory is that the electron temperature varies little across the thermionic plasma. this assumption is justified only empirically. while it is known to be somewhat inaccurate, it is extremely useful since it eliminates unnecessary mathematical complexities. In light of Lam[9], however, an additional assumption generally associated with isothermal theory has to be abandoned. This assumption is that the gradients of temperature are small, and is invalid even when the first assumption is accurate. Thus, in this thesis, the theory is formulated so that only the first assumption is used.

Let us first consider the ignition temperature concept. For this purpose the electron temperature is regarded as being imposed upon the problem and the response of the density to this temperature is studied. To avoid the obscurational effects of unnecessary mathematical detail, a simple case will be analyzed. Suppose that the densities under consideration are sufficiently low that recombination can be neglected. assume constant mobilities and neglect ion current. From D.1, the steady state density equation is:

$$\text{E.1} \qquad \frac{d^2\bar{p}}{d\xi^2} + A\bar{p} = 0$$

Where A, the non-dimensional ionization coefficient is

defined by the dimensional quantities:

E.2 $$A = No\ d^2 \alpha / Da$$

Where α is the ionization coefficient (cm3/sec), No is the cesium density, d is the inter-electrode distance, and Da is the ambipolar diffusion coefficient:

E.3 $$Da = \mu_i (kT_e + kT_n)$$

For the present purposes, the simple density boundary conditions C.12 are quite adequate (use of more precise density boundary conditions would change the results a small amount but would add much complication and not alter the general conceptual result.).

The above equation is an eigenvalue problem for A. From WKB analysis, the only solution with positive density occurs when:

E.4 $$\int_0^1 A\, d\xi = \pi^2$$

If A were too small to meet this condition, the density would decrease to zero. If it were too large, the density would increase until recombination became important (thus invalidating an assumption of the equation).

Thus, the coefficient A must at least meet a minimum value of π^2 somewhere in the interval or else the density will go to zero. A, through α, is exponentially sensitive to the electron temperature, τ. The electron temperature at which A is pi squared is called the ignition temperature, τ_I:

E.5 $$A(\tau_I) = \pi^2$$

The qualitative behavior of the maximum density n_m as a function of temperature for the isothermal case can be summarized by:

E.6 $$\bar{n}_m = \begin{cases} 0 & \text{FOR } \tau < \tau_I \\ 0 < \bar{n}_m < \bar{n}_{SAHA} & \text{FOR } \tau = \tau_I \\ \sim \bar{n}_{SAHA} & \text{FOR } \tau > \tau_I \end{cases}$$

Density is thus strongly dependent on temperature. Further, this theory imposes strict limitations on how low the plasma

electron temperature may be in a thermionic converter. Implications of this on the reduction of the arc-drop will soon be apparent.

Let us turn attention now to the question of what determines the electron temperature. By integrating the electron energy conservation equation across the gap, and applying the boundary conditions a very important but simple overall energy conservation equation results:

$$E.7 \qquad -IV_d = 2(I_E - I)\tau_0 - 2I_E + 2I\tau_1 - \Delta Q$$

Where: $$\Delta Q = \int_0^1 \left[\bar{S}^{(E)} - \frac{3}{2}\bar{n}\frac{\partial \tau}{\partial \bar{t}}\right] d\bar{x}$$

and vd is the voltage at the top of the collector sheath less the voltage at the peak of the emitter sheath. The subscripts 0 and 1 refer to conditions in the quasi-neutral regions near the emitter and collector, respectively. Other useful voltage differences will be defined later. This equation is exact. This relates the electrical power loss in the gap, -Ivd, to the various inflows, outflows, sources, and sinks of energy. In fact, this equation could have been derived by thermodynamic analysis of the T.E.C. as a system. This simple relationship has many uses. Because of its simplicity, it enhances understanding of the loss mechanisms in thermionic conversion. More will be said on this below. It is also useful numerically to compute the arc-drop from a simple well-behaved equation.

For present purposes, let us consider a steady state situation. It is useful to rewrite the arc drop equation, E.7, as:

$$E.8 \qquad -IV_d = 2I_E(\tau_0 - 1) + 2I(\tau_1 - \tau_0) - \Delta Q$$

Considering the currents and ΔQ as known, this equation has three unknowns: the emitter electron temperature, the collector electron temperature, and the arc-drop itself.

A second equation for the arc-drop can be found by integrating the electron momentum equation across the gap:

$$E.9 \qquad V_d = \chi_c - \chi_E + \tau_0 - \tau_1 - IR - \int_0^1 \tau \frac{d \ln \bar{n}}{d\bar{x}} d\bar{x}$$

Where R is the electrical resistance of the thermionic converter defined by*: $R = \int_0^1 \frac{d\bar{x}}{\bar{\sigma}}$ WHERE $\bar{\sigma} = \bar{\mu}_e \bar{n}$

* this definition differs from that of [5] wherein the density was normalized additionally be the emitted density, n_E.

Even with the final integral ignored, R considered given, and the sheath heights considered as known functions of temperature, this equation still has three unknowns, the same ones as the previous equation. Thus we now have two equations in three unknowns.

It is possible to obtain valuable qualitative results with a simple ad hoc model: the isothermal model, Lam [6]. The electron temperature is thus assumed independent of position. By virtue of its simplicity, this model accents the main features of the fundamental physical processes occurring in the T.E.C.

The first of the equations above, E.8, which expresses gross energy conservation changes in the isothermal form to:

$$E.11 \qquad -IV_d = 2I_E(\tau - 1) - \Delta Q$$

Again, this equation is expressing a balance between the net electrical power out and heat input. The second of the above equations, E.9, which details the mechanisms by which the electrical energy is lost to heat simplifies greatly under the isothermal assumption. Using the expressions for the sheath heights, D.7, many cancellations occur and there results:

$$E.12 \qquad -V_d = IR + \tau \lambda_1 \frac{N_e I}{I_E - I}$$

The dependence of the sheath heights on the plasma density has cancelled with the "ambipolar motive drop" (Lam[6] p.10). As shown above, two terms remain on the right-hand-side of the equation. The first of these is the plasma ohmic arc-drop. The second is due to the difference in sheath heights. The quantity Ne which appears above comes from the sheath theory and may be set to one as a first approximation. The two equations above may be equated and solved for the electron temperature:

$$E.13 \qquad \tau = \frac{2I_E + I^2R + \Delta Q}{2I_E + I\lambda_1\left(\frac{I_E}{I} - 1\right)} \equiv \tau_E$$

This indicates how temperature behaves as a function of the currents and the resistance. From the above it can be seen that, for fixed current, temperature rises as density decreases. This is because resistance, R, is inversely proportional to density. This contrasts with the well-known behavior along a steady-state I-V characteristic where temperature and density rise and fall together as current varies.

With the above information the approach to steady-state operation of a thermionic converter can be described. Suppose the output current is held constant by some

constant-current load. The initial density distribution, whatever it is, determines a resistance and through sheath theory an I_E. This then determines a temperature by equation E.13. Two conditions are then possible. (1) if the temperature is high, more ionization occurs, the density rises, and hence the resistance declines and the thus the temperature declines. Or, (2) the temperature is low and recombination occurs. Thus the density falls, the resistance rises, and hence the temperature will rise. It is apparent that in either case an equilibrium density and temperature will be approached. This temperature then determines the arc-drop through equation E.11.

vd was defined as the voltage drop from the peak of the collector sheath to the peak of the emitter sheath. Some other voltage drops are also in common use. One such, to be called v_T here, measures the voltage at the collector-sheath interface less the voltage at the emitter-sheath interface. This differs from vd only if a double sheath exists, as depicted in figure 2. Generally a double sheath can exist in a T.E.C. only at the emitter sheath. Denoting its magnitude as $\Delta\hat{\chi}$, it follows that:

E.14 $$V_T = V_d + \Delta\hat{\chi}$$

The magnitude of the double-sheath height can be expressed in terms of the emitted and Richardson currents so that:

E.15 $$V_T = V_d + \ln \frac{I_R}{I_E}$$ WHERE I_R IS THE RICHARDSON CURRENT (NON-DIMENSIONAL)

The output voltage, v, seen at the terminals is obtained from v_T by adding the collector work function and subtracting the emitter work function. A third common measure of the converter performance is the difference between the actual voltage drop and that which would occur in a converter with an interelectrode spacing so small that the free electron space charge would be negligible. Such a converter is called a vacuum ideal converter and has a voltage drop:

E.16 $$V_I = \ln \frac{I_R}{I}$$

this is a consequence of the Maxwell-Boltzmann distribution of the emitted electrons. The difference between the actual drop, v_T, and the ideal drop is denoted as:

E.17 $$V_B \equiv V_+ - V_I = V_d + J_1 j$$

where j is the ratio of the net current to the emitted current, I/I_E. All these drops will be referred to later during discussions of T.E.C. performance. Note that all drops have been defined so that the more positive, or less negative, the voltages are the better the performance is.

There is also some terminology associated with the behavior of the voltage drops. Consider discharge current plotted as a function of voltage for a given thermionic converter. The plot of the vacuum ideal voltage drop, v_I, is called a Boltzmann line. Sometimes over some over range of current, v_B, the difference between the actual drop and the ideal drop, is roughly constant. Such a range is said to have a Boltzmann-like rise. If v_B decreases as current increases, this is said to be a faster than Boltzmann rise. As the current level is increased to near the level of the Richardson current, v_B may start to increase rapidly. This range where v_B increases rapidly is called the 'knee' of the current-voltage curve. These behaviors are illustrated qualitatively in figure 58.

In sum, the fundamental concepts of thermionic converter operation have been discussed. It was shown that the density is exponentially sensitive to temperature and that there is a minimum temperature below which the discharge collapses and the density goes to zero. It was also shown that the arc-drop is determined by thermal energy losses at the sheaths which in turn are dependent on the temperature of the electrons near the walls. Finally, it was shown that the conversion of electrical energy to thermal energy occurs through ohmic losses in the plasma as well as differences in the sheath heights. While these results were developed under the convenient and ad hoc isothermal approximation, it is apparent that the concepts that result have validity even in the general non-isothermal case.

II.F The Faster-than-Boltzmann Rise

It is an experimentally well-known fact that the T.E.C. current voltage characteristic in the region below the knee rises much faster than the vacuum ideal Boltzmann curve rises. Past one dimensional theories have not been able to explain this. For an explanation, it was considered necessary to invoke two-dimensional phenomenon, and there has been some experimental evidence to indicate that two-dimensionality may be important. It is shown herein that this faster-than-Boltzmann rise can be explained even in one dimension. In fact, there are a variety of phenomena which can cause it. The analysis here will be confirmed by numerical results to be presented later.

To complete this analysis it will be necessary to extend the theory discussed in the previous sections. The isothermal theory as developed so far has left two important parameters undetermined: the plasma resistance R, and the nondimensional current j. Examination of double sheath theory, energy conservation, and the ignition condition will lead to an a priori determination of R and j. This then makes possible quantitative predictions using isothermal theory of not only the arc-drop but also the the densities and sheath parameters. While a full computer calculation of the differential equations gives presumably more accurate results, this theory explains the interconnections among the many variables and parameters in a fairly simple and straightforward manner.

It is suggested herein that for one dimensional T.E.C.s, the cause of the faster-than-Boltzmann rise is in the ionization kinetics. The ionization kinetics contribute to this rise in three ways. First, the existence of spontaneous radiation alters the ionization rate constant so that it varies with density as well as temperature. Secondly, non-Maxwellian free electron distributions also cause the rate constant to vary with density. In both cases the rate constant declines as density declines leading to a faster than Boltzmann rise. The third effect is that spontaneous radiation becomes increasingly important as an energy loss mechanism as density decreases. Attention in this thesis is restricted to the first of these effects.

This effect will be studied quantitatively in later chapters, but the effects they have on T.E.C. performance can be analyzed in isothermal theory as below. The analysis herein is thus based on some simplifying assumptions. The value is that it illustrates the essential features of the real equations with minimum mathematical complication.

Presently the density equation will be considered for ionization rate constants that vary with density. Although the equation is now nonlinear, an ignition temperature concept can be recovered. This new ignition temperature will depend on the density level, as parameterized by, say, the maximum density. This will then be combined with the previously presented isothermal result relating temperature and ohmic drop. This will determine the T.E.C. density and temperature. From the other isothermal relation, this temperature implies a level of the plasma arc-drop.

As a note on mathematical technique, determination of the ignition temperature requires solution of a nonlinear eigenvalue problem. Standard methods yield approximate solutions to an equivalent calculus of variations problem. Under the isothermal assumption, it is shown that the solution can be found directly by quadratures. Thus the shape of the solution need not be assumed as in standard methods but can be determined explicitly.

To begin, let us write the steady-state density conservation equation:

$$\text{F.1} \qquad \kappa\sqrt{\frac{m}{M}}\,\bar{\mu}_i\,\frac{d^2\bar{p}}{d\zeta^2} + \bar{S}^{(n)} = 0$$

The source term is left in its general functional form, but the problem is assumed isothermal to eliminate unnecessary mathematical detail. In particular, by virtue of the isothermal assumption the solution of the above equation can be found by quadratures. The first integral, found by standard means, is:

$$\text{F.2} \qquad \pm\left(\frac{d\bar{p}}{d\zeta}\right)^2 = \int_{\bar{p}}^{\bar{p}_m} \frac{\bar{S}^{(n)}(\bar{p}')}{\kappa\sqrt{\frac{m}{M}}\,\bar{\mu}_i}\,d\bar{p}'$$

Where $\bar{p}_m$, the constant of integration, is the maximum pressure, i.e. the pressure when the first derivative $d\bar{p}/d\zeta$ is zero. The above can be integrated again to find:

$$\text{F.3} \qquad \zeta = \int_{\bar{p}_0}^{\bar{p}_m} \frac{d\bar{p}'}{\left(2\int_{\bar{p}'}^{\bar{p}_m} \frac{\bar{S}^{(n)}(\bar{p}'')}{\kappa\sqrt{\frac{m}{M}}\,\bar{\mu}_i}\,d\bar{p}''\right)^{1/2}}$$

Where $\bar{p}_0$ is the pressure at the emitter wall, i.e. $\zeta \cong 0$. Since this value is typically much less than the maximum, it can be taken to be about zero [see section II.D]. The above integral gives a relation between pressure and position.

There is an additional boundary condition that the above integral must satisfy: the pressure at the collector wall ($\zeta \cong 1$) must be a number, $\bar{p}_1$, determined by the collector boundary conditions as in section II.D. Again, $\bar{p}_1$ is also about zero. It follows that:

$$\text{F.4} \qquad 1 = \int_{\bar{p}_0}^{\bar{p}_m} \frac{d\bar{p}'}{\sqrt{2\int_{\bar{p}'}^{\bar{p}_m} \frac{\bar{S}^{(n)}(\bar{p}'')}{\kappa\sqrt{\frac{m}{M}}\,\bar{\mu}_i}\,d\bar{p}''}} + \int_{\bar{p}_1}^{\bar{p}_m} \frac{d\bar{p}'}{\sqrt{2\int_{\bar{p}_1}^{\bar{p}_m} \frac{\bar{S}^{(n)}(\bar{p}'')}{\kappa\sqrt{\frac{m}{M}}\,\bar{\mu}_i}\,d\bar{p}''}}$$

For this to be satisified, $\bar{p}_m$ and the source function obviously cannot both be specified independently.

At this point let us consider a form for the source function. For example:

F.5 $$\frac{\bar{S}^{(n)}(\bar{\rho})}{A_c \frac{\bar{n}^{n}}{\bar{M}} \bar{\Pi}_j} = \left(\bar{A}\bar{\pi}^{\rho-1}\right)\bar{\rho} = \left(\frac{\bar{A}}{(\tau+\tau_n)^{\rho-1}}\right)\bar{\rho}^{\rho}$$

For ρ=1, this function is linear in density as the one discussed in section II.E was. For ρ>1 however, this form illustrates the behavior of an ionization rate constant which declines as density declines, like a real rate constant does due to the spontaneous radiation effects mentioned previously. While the above form will not represent the actual form accurately over a wide range of data, it does have the appropriate general shape and suffices to illustrates the points to be considered here without great mathematical complications.

When this form of the source function is substituted into the integral, it becomes apparent that the values of the density at the walls may be set to zero with little resulting error and a relationship between $\bar{A}$ and $\bar{n}_m$ appears:

F.6 $$\bar{A}\bar{\pi}_m^{\rho-1} = C_\rho \bar{\pi}^2$$

where:

$$\bar{\pi}_m = \bar{\rho}_m/(\tau+\tau_n)$$

and where the function c_ρ is given in terms of the gamma (factorial) function by:

F.7 $$C_\rho = \frac{2}{\pi(1+\rho)}\left[\frac{\Gamma\left(\frac{1}{1+\rho}\right)}{\Gamma\left(\frac{1}{2}+\frac{1}{1+\rho}\right)}\right]^2$$

If the standard methods of calculus of variations had been employed, C_ρ could not have been determined explicitly as above.

If ρ=1, as in section II.E, then, also as before, $\bar{n}_m$ disappears from the above equation and the condition is solely a condition on $\bar{A}$. Even for the present more general form, $\bar{A}$ is still well approximated by an exponential in temperature:

F.8 $$\bar{A} = a e^{-\bar{E}_o/\tau} \quad \text{WITH } a, \bar{E}_o \text{ CONSTANTS}$$

With this form, the ignition temperature, now a function of the maximum density, can be found:

F.9 $$\tau_I = \frac{\bar{E}_o}{\ln\frac{a}{C_\rho \pi^2} + (\rho-1)\ln\bar{\pi}_m}$$

Let us now discuss the significance of this temperature. First, if the density distribution is given by the above solution with the same $\bar{n}_m$, then the density will be in steady state. Let us suppose this temperature remains fixed but the density is for some reason perturbed. The steady-state assumption made in this section will cease to hold but the physical unsteady behavior that would occur is apparent. First, if the density were perturbed to a lower value, the rate constant decreases, the ignition condition is no longer satisfied, and the density declines even further till it reaches zero. If on the other hand the density were perturbed to a greater value, the ignition condition would be more than satisfied, and the density would increase still further. In the physical problem, this increase in density would be stopped only when recombination, neglected here, became important. In summary, the steady-state solution found above is an unstable one for fixed temperature.

The temperature is not in reality fixed. As was shown in the discussion on isothermal theory, it itself is determined by density through, for example, the plasma resistance. To repeat the isothermal result of section II.E, the temperature is determined by:

F.10 $$\tau_E = \frac{2 + jIR + \Delta Q}{2 + j\beta_i\left(\frac{1}{j} - 1\right)}$$

Where $j=I/I_E$.

Consider how temperature changes with density for a fixed current I. To do this it is necessary to know how R, j, and Q behave as functions of density and current. The value of R declines as density rises. The exact form of the integral for R is written:

F.11 $$R = \frac{1}{\bar{\mu}_e}\int_0^1 \frac{ds}{\bar{n}}$$

This can be integrated analytically without further approximation. It is however simpler to use the quite good approximation that the density at the walls, though finite, is small compared with the maximum density. Employing the density boundary conditions of D.6 and using the preceding analysis of this section to determine the pressure gradients at the walls, the wall densities are given as:

F.12 $$\frac{\bar{n}_o}{\bar{n}_m} = \frac{\lambda_c K_n}{\sqrt{\pi/8\alpha_E}}\left(\frac{\bar{\mu}_i}{\bar{\mu}_{ea}}\frac{I}{\bar{n}_m} + \bar{D}_a \pi S_\rho\right)$$

F.13 $$\frac{\bar{n}_i}{\bar{n}_m} = \frac{\lambda_c K_n}{\sqrt{\pi/8\alpha_E}}\left(-\frac{\bar{\mu}_i}{\bar{\mu}_{ea}}\frac{I}{\bar{n}_m} + \bar{D}_a \pi S_\rho\right)$$

where:

$$S_\rho = \sqrt{2\varphi/(1+\rho)}$$

$$\bar{D}_a = \bar{\mu}_i(\tau + \tau_i)$$

It follows that, to a good approximation, the resistance is given by:

F.14 $$R = \frac{1}{\pi S_\rho \bar{n}_m \bar{\mu}_e}\left\{ \ln \frac{2^{\frac{1+3\rho}{1+\rho}}}{\pi\sqrt{\alpha_E \alpha_c}(\lambda_c K_n \bar{D}_a S_\rho)^2} - \ln\left[1 - \frac{I}{\pi S_\rho \bar{n}_m (1+\tau)\bar{\mu}_{ea}}\right]\right\}$$

This relation for R with the information on the character of j then shows how the isothermal temperature varies as a function of density. Note that, typically, the first natural log term dominates over the second.

By combining sheath theory with isothermal theory it is possible to determine j even when a double-sheath exists. For a single sheath with Schottky neglected, I and j can be considered known. For the double sheath case, I_E is a variable. I_E shall now be determined as a function of current and maximum density for the double-sheath case. In terms of the nondimensional emitted density, N_E, I_E is given by:

F.15 $$I_E = N_E \frac{\bar{n}_o}{2K_n}$$

where: $$N_E = n_E / n_o$$

From the sheath theory of Lam[5], N_E is a function of only two parameters:

F.16 $$N_E = N_E\left(\frac{I}{\bar{n}_o/K_n}, \tau\right)$$

Iterative solution of the sheath system of equations has been performed over a wide range of the parameters. Figure 7 displays a graph of N_E against τ with $IKn/\bar{n}_o$ as a parameter. It is seen that N_E is only weakly dependent on τ. For present purposes, the following functional fit is adequate:

F.17 $$N_E \cong 0.32 + 1.2\,\frac{I K_n}{\bar{n}_o}$$

Now, using the results of isothermal theory, it is possible to relate $\bar{n}_o$ to $\bar{n}_m$ and thus describe the behavior of I_E in terms of I and $\bar{n}_m$:

F.18 $$I_E = \left(0.6 + 0.26\sqrt{\alpha_E}\,\frac{\bar{\mu}_i}{\bar{\mu}_{ea}}\right) I + \left[0.8\lambda_c\sqrt{\alpha_E}\,\bar{D}_a S_\rho\right]\bar{n}_m$$

Thus I_E and j may be considered known functions of I and $\bar{n}_m$. Furthermore, it is seen that j is an increasing function of

the reduced variable $I/\bar{n}_m$.

Two of the three functions necessary to determine temperature from the isothermal energy balance have now been evaluated. The third and remaining function is ΔQ. While this function is not dominating, it does have a noticeable effect on the results and is important for evaluating the laser schemes to be discussed later. In steady-state and assuming the energy source model of A.11 with R=0, it follows that:

F.19 $$\Delta Q = -E_0 \int_0^1 \bar{S}^{(n)} d\xi$$

Then, eliminating the mass source term using the density equation D.1, an exact integral results:

F.20 $$\Delta Q = \Lambda_c \bar{E}_0 \sqrt{\frac{m}{M}} \left[\bar{\mu}_i \frac{\partial \bar{P}}{\partial \xi} + \frac{\bar{\mu}_i}{\mu_e} I_e \right]_0^1$$

Evaluating the pressure gradient at the walls as before yields:

F.21 $$\Delta Q \cong -\left(2\pi S_\rho \bar{D}_a \Lambda_c \bar{E}_0 \sqrt{\frac{m}{M}}\right) \bar{n}_m$$

For typical numbers*:

$$\Delta Q \cong -0.385_\rho \bar{n}_m$$

It is now possible to show how temperature and density are determined in a thermionic converter under the present model. First, let us consider the density-independent ionization rate constant case, i.e. $\rho = 1$. Under this assumption, the ignition temperature, τ_I, is a constant. Thus on a plot of temperature versus maximum density, $\bar{n}_m$ as shown in figure 3, the ignition temperature is a straight horizontal line. The ignition temperature is shown in this figure for two values of the collisional rate constant, C_T=0.31 and 0.46. These values will be discussed in chapters III and IV. The plot of the isothermal steady-state temperature, τ_E, on the same graph would however be a curve. This is also shown in figure 3 for three different levels of current, I=0.02, 0.5, and 0.7. The two lower currents are in the double-sheath regime while the higher one is in the single-sheath regime. Steady state solutions for both temperature and density can exist only at

*. $\Lambda_c = 1/3$; Da=3; Eo=30.17

crossing points of these curves, τ_E and τ_I. As is obvious from the above discussions, the steady-state solution at the crossings of these curves will be a stable solution only if:

$$\frac{\partial \tau_I}{\partial \bar{n}_m} > \frac{\partial \tau_E}{\partial \bar{n}_m}$$

This condition is satisfied for all crossing points shown in figure 3.

Let us turn to the case of the variable rate constant. Now, the ignition temperature, τ_I, varies with density according to the natural log behavior derived in the formulas above. A plot of the ignition temperature versus density, $\bar{n}m$, is shown in figure 4 for the case $\rho>1$. This plot is based on the ionization coefficients to be derived in chapter IV. As in figure 3, the isothermal steady state temperatures are also plotted on this graph for three different levels of current. The crossings between these graphs have quite a different character here than they did in figure 3. As the current decreases from I=0.5 to 0.02, the temperature is increasing. According to the isothermal analysis of section II.E, this means that the arc-drop increases with decreasing current. This is a cause for the faster-than-Boltzmann rise discussed earlier. In fact an additional arc-drop of 0.90 (110mV) occurs in this way.

Some other interesting effects occur also. For one, from this analysis, it is apparent that suppression of the emitter sheath obstruction is undesirable. This obstruction reduces thermal energy losses at the emitter and is thus beneficial. These calculations show that its suppression at I=0.5 would increase the arc-drop by about 0.5 (60 mV).

Another unexpected result is that energy addition to the plasma does not increase the electron temperature but rather lowers it. The effects of energy addition by laser ionization enhancement will be discussed in a later section. Direct heating of the electron translational mode can be considered here. Such heating means that there is a reduced need for plasma arc-drop to maintain the ignition temperature. As a consequence the density must rise. An increase in density, however, means that radiative loss is just slightly less important in the ionization process causing a small decline in the ignition temperature. As a consequence of this reduced temperature, the arc-drop is reduced. Under conditions tested presently though, this is not an overall energy efficient process.

In summary, a simple isothermal model has been developed which highlights the important physical processes and is sufficiently simple so as to allow solution by hand. This model was derived from the analysis in section II.E by finding expressions for R and j thereby closing the model. The model was also extended to allow for density dependent

ionization-rate constants. This led to conclusions that (1) the emitter sheath obstruction is beneficial since it reduces thermal energy losses, (2) energy addition to the plasma reduces the temperature, and (3) the faster-than-Boltzmann rise can be explained as being due to reduced ionization rate constants at lower densities.

II.G A Study of the Complete Energy Equation

The determination of the electron temperature distribution may be the most involved and complex part of the T.E.C. For operating efficiency, it also may be the most important part. While the ignited mode of operation has been actively researched for two decades, even just the general shape of this distribution is still controversial. One question has been the existence or not of 'hooks' in the temperature near the electrode walls. A hook is a rapid change in the electron temperature that occurs near one or the other of the electrodes. The calculation of A. T. Yen [8] was the first to indicate the possible existence of hooks. Since it is the temperatures near the walls which dominate the determination of arc-drop , the existence of such hooks is of significant practical import. The following year Lam produced an analysis that explained much about the behavior of temperature in T.E.C., and in particular, why hooks can exist. This theory also indicates why numerical schemes can run into difficulties solving the energy equation. These implications will be discussed in this section.

To review the Lam [9] theory, there are two concepts to be introduced. First, there is the thermal resistance of the plasma. Rather than measure distance in the plasma in centimeters, it is found more useful to measure it in terms of the thermal resistance. How this is done will be discussed below. The second concept is that of a pseudo-temperature distribution for which the effects of convection have been removed mathematically. This will also be discussed below.

A major feature of this analysis is that it locates which phenomena cause which effects. In particular, the cause of the temperature hooks will be found to be the ohmic and ambipolar arc-drops. These phenomena become large at near the walls because they are inversely proportional to the magnitude of the density. This theory shows the ambipolar arc-drop to emerge as a dominate process determining the shape of the temperature distribution. Notice that this occurs in contrast with the isothermal theory where the ambipolar arc-drop quietly cancelled out from the overall arc-drop equations.

To begin, consider thermal resistance. If K is the thermal conductivity, then 1/K is the thermal resistivity. In a distance $d\xi$, there is a thermal resistance $(1/K)d\xi$. Let η be the total thermal resistance between the emitter and a position ξ. Thus:

G.1
$$\eta = \int_0^{\xi} \frac{d\xi'}{K(\xi')}$$

Rather than consider the temperature as a function of the distance, $\bar{\xi}$, consider it as a function of the thermal resistance, η. With this idea, the energy equation D.2 can, assuming B.15, be rewritten:

$$G.2 \qquad \frac{3}{2}\bar{n}\frac{\partial \tau}{\partial \bar{t}} = \frac{\partial^2 \tau}{\partial \eta^2} - \frac{3}{2} I \frac{\partial \tau}{\partial \eta} + I\left(\frac{5}{2} L_e I + \frac{\partial \ln \bar{n}}{\partial \eta}\right)\tau$$

In this form many of the rapidly varying coefficients that appeared in the original energy equation are gone. Apart from the unsteady term the only explicit appearance in the equation of the thermal conductivity, K, is in a ratio with the electrical conductivity, $\bar{\sigma}$. This ratio is related to what is called in gas dynamics a Lewis number, Le, and generally varies little from a value of one for gases:

$$G.3 \qquad L_e = \frac{K}{\frac{5}{2}\bar{\sigma}\tau}$$

This equation is thus much better behaved and numerical solutions of this equation are more likely to be accurate.

It is possible to determine when hooks are likely to occur just be considering this equation and its boundary conditions. Written in the thermal resistance coordinate, the boundary conditions become:

$$G.4 \qquad \left.\frac{\partial \tau}{\partial \eta}\right|_0 = 2 I_E (\tau_0 - 1) - I(\chi_E - \tau_0/2)$$

$$G.5 \qquad \left.\frac{\partial \tau}{\partial \eta}\right|_1 = -I(\chi_c - \tau_1/2)$$

Since the temperature generally declines from the emitter to the collector, a hook is expected to exist if the boundary condition indicates a rising temperature leaving the emitter or a rise in the temperature as it approaches the collector. As can be seen from the above, this will occur on the emitter side when:

$$G.6 \qquad j < \frac{2(\tau_0 - 1)}{\chi_E - \tau_0/2} \qquad \text{WHERE} \quad j = I/I_E$$

Likewise, a hook will occur on the collector side when:

$$G7 \qquad \frac{\chi_c}{\tau_1} < \frac{1}{2}$$

The numerical computations, which will be discussed in greater detail later, appear to indicate that both emitter and collector hooks will commonly occur, though the emitter one is typically more pronounced.

While the transformed energy equation above is an improvement over the original form, it is still possible to make one more change to simplify it. While this change is

not necessary, it facilitates solution by analytical methods such as WKB. The explicit mathematical goal of this transformation is to eliminate the convective (first-derivative) term from the equation, leaving only a second derivative term and a term proportional to the transformed temperature. To do this a transformed temperature, G, is defined:

G.9 $$G = \tau e^{-\frac{2}{4} I \eta}$$

With this substituted into the energy equation and steady-state assumed, there follows:

G.9 $$0 = \frac{d^2 G}{d\eta^2} + \omega^2 G$$

Where: $$\omega^2 = I\left[I\left(\frac{5}{2}Le - \frac{9}{16}\right) + \frac{d\,\bar{n}}{d\eta}\right]$$

At this point one thing should be apparent: the above G-equation has an extremely simple form.

First, considering the general behavior of w^2 which is a function of position, note that on the emitter side of the T.E.C. where density is rising, w^2 is positive. This indicates that G has a sinusoidal character, and therefore the temperature has a growing sinusoidal behavior. Somewhere shortly after density peaks, w^2 will generally go through zero and become negative. This indicates that G will have an exponential type behavior with both growing and decaying components possible.

The goal of this work, as stated earlier, was to work to behavior of the temperature distribution as a function of a given density distribution. For a number of special density distributions, which look more or less realistic to some varying degree, it is possible to have exact analytic solutions of the temperature equation. Sinusoidal or parabolic type behavior could result respectively in Mathieu or Airy function type temperature distributions. If the density were about linear then w could be a constant and the temperature solution would be sinusoidal or exponential. The sample solution discussed in Lam[9] was based on a two-piece linear density distribution and this was shown to contain the essential features of the problem. It should be remembered, of course, that for a general density distribution the solution can be obtained by WKB approximation with a turning point.

A notable feature of this steady state energy equation is that there are some values of current for which there is no acceptable solution of temperature. In particular, there will be no solution unless the current level, and therefore w^2, is small enough that the following inequality is satisfied[9]:

$$\int_0^{\eta^*} w\,d\eta < \pi$$

Where η^* is defined as the location where w^2 becomes zero. Failure to satisfy this would result in unphysical negative temperatures.

This limitation has physical significance. It indicates that when the current is too large there is more heat generation in this region between $\eta=0$ and $\eta=\eta^*$ than can be conducted out. Thus there is no steady state solution, but rather an unsteady solution wherein the temperature grows rapidly. The question arises: what is generating this heat and why is it generated only in the specified region? the answer is that this is the heat generated by the ambipolar arc-drop. Such heat is generated only on the emitter side of the T.E.C. since, on the collector side, there is an ambipolar arc-rise not drop and this is actually causing a cooling not a heating.

II.H Laser Ionization Enhancement

In previous sections theories have been developed to explain thermionic converter behavior. The implication of these developments would seem to be that there are some fundamental limits to thermionic converter efficiency due to the ignition condition and the nature of the arc-drop. It is hoped presently to alter these limits by altering the ionization rate constants with laser radiation. As will be discussed in detail in later chapters, laser radiation can enhance ionization rate constants at a fixed temperature by a large factor. In fact, this factor is generally the order of a Boltzmann factor in the photon energy. Thus, laser ionization enhancement has an effect on T.E.C. performance similar to reducing the ionization potential of the atom. With this ionization enhancement it is hoped that density can be increased thereby increasing electrical conductivity and thus reducing the ohmic losses.

This scheme is quite different from other ionization enhancement schemes. In particular, laser ionization enhancement puts energy directly into ionization in an efficient manner. In fact, the energy cost of an ion produced by a laser enhanced T.E.C. plasma is generally the same as or less than if the ion was produced by collisional processes. Further, laser enhancement is a volume process. This contrasts with the various third electrode techniques.

There are several practical questions concerning laser ionization enhancement that should be discussed. One such question concerns the need for a source of laser light resonant with the atoms in the plasma. One such source could be a dye laser. A technique to develop a relatively efficient laser suitable for ionization enhancement is the subject of the next section, II.I. A second question concerns the absorption length for the laser light. Obviously, a plasma that is optically thick to the laser light prohibits absorption of such light in the volume of the plasma and is thus unacceptable. On the other hand, if the plasma is too optically thin, it may not be possible to absorb enough light to enhance the ionization. By checking the orders of magnitude it immediately becomes apparent that practically all optically allowed radiation involving the ground state are absorbed in extremely small distances. This does not affect the present discussion though since the ground state makes a relatively inefficient lower level for ionization enhancement anyway, as will be shown in later chapters. To obtain an absorption length that is not too short, the laser light must be absorbed by an excited level of the atom.

Using the isothermal theory, it is possible to analyze the effects of a reduced ignition temperature on T.E.C. operation at a given current level. From equation II.E.11, it was found that the isothermal arc-drop would be:

H.1 $$-V_d = \frac{2(\tau-1)}{j} - \Delta Q$$

For simplicity, consider only the high density regime wherein the variation of ignition temperature with density may be neglected. With laser ionization enhancement reducing the ignition temperature, the above equation indicates that the arc-drop would also decline provided that j did not also drop significantly. For the case of a single emitter sheath and Schottky neglected, j would not change at all. For a double-sheath, j will generally decline at least slightly when declines. Thus laser ionization enhancement will be especially effective in the single sheath regime.

Consider an example. For reasons to be presented in the next section, laser ionization enhancement resonant with the Cs 7s-7p transition is particularly interesting. This transition is infrared, $h\nu \approx 0.41eV$. The photon energy is thus much less than the Cesium ionization potential, 3.89eV. Nevertheless, a substantial increase in the ionization rate constant is found. For pd=10 torr-mill, irradiation on this transition frequency can reduce the ignition temperature by $\Delta\tau=0.08$ (120K) from $\tau=2.12$ (3200K). For the single sheath regime, and taking a typical value for j, say 0.66, this implies an arc-drop reduction of:

H.2 $$\Delta V_d \approx 0.25$$

For the double-sheath regime, again, it is necessary to evaluate the change in j for a given drop in temperature. This is done using equation II.E.13:

H.3 $$\tau = \frac{2I_E + I^2 + \Delta Q}{2I_E + I\ln\left(\frac{I_E}{I} - 1\right)}$$

As is seen in figure 4, this curve is very steep. As a result a small change in ignition temperature means only a very small change in density and thus in j. In the present example with the original j of 0.66, the final j will be 0.65. combining this with the arc-drop equation implies that laser excitation of the 7s-7p transition can reduce the arc-drop by:

H.4 $$\Delta V_d \approx 0.20$$

which is only slightly smaller than the reduction for the single sheath case.

The important question for any T.E.C. enhancement scheme is how the energy cost of operating the scheme compares with the energy saved by enhanced performance. As with the various proposals for third electrode and microwave enhanced converters, the answer is not immediately apparent. As will be shown in chapter V, ionization by absorption of laser radiation is a very efficient process. The combination of laser energy absorbed and electron energy lost in inelastic collisions needed to produce an ion is generally less than it would be without laser enhancement. However, the generation of laser light is not usually an efficient process. For laser ionization enhancement to be an energy producing process, the losses incurred during the generation of the laser light must be less than the gain in output of the T.E.C. The minimum laser production efficiency needed for this to be true can be estimated. For the 7s-7p transition and over the parameter range of interest, roughly two photons or 0.82eV of energy is absorbed for each ionization. Thus the required laser power, L, is:

$$L = 2\hbar\nu\,\hat{S}^{(n)} \qquad \text{WHERE } \hat{S}^{(n)} = \int_0^1 S^{(n)}\,d\xi \tag{II.5}$$

Suppose the laser production efficiency is Θ. Thus the power cost of producing the light is:

$$L/\Theta$$

For T.E.C. laser ionization enhancement to exhibit a net energy gain, it is required that:

$$I\,\Delta V_d > L/\Theta \tag{II.6}$$

Examination of the numbers for the 7s-7p transition indicate that the laser cannot be too inefficient. Most lasers however are very inefficient. The value of Θ indicated is 30% to 40%. To obtain such efficiency would require a special laser. A possible technique for creating such a laser will be discussed in the next section, II.I.

In sum, it is presently proposed that laser light can improve thermionic converter performance by enhancing the ionization rates. It is important to remember that the energy loss to ionization is typically a small fraction of the total energy loss in the converter. The majority of the T.E.C. energy loss occurs as heat transfer by the free electrons to the walls. This technique works by injecting energy directly into the ionization process. It is thus possible to operate the converter at lower free electron temperatures and thus at lower loss rates of heat to the walls. For the example of 7s-7p resonant laser light, the arc-drop was shown to be reduced, though by a small amount.

II.I The Cs Recombination Laser

The idea of plasma or recombination lasers is receiving much attention in the literature, e.g.[11,95,112-7]. This is because recombination lasers have the potential for tremendous power output, and some may operate at short wavelengths. A major challenge in this field is obtaining the necessary plasma cooling rates. This thesis presents the first prediction of a Cs I plasma recombination laser. It is shown not only that cesium is probably capable of recombination lasing, but that the cooling can be obtained quite conveniently in a thermionic converter type of plasma. The kinetics of recombination lasing are discussed in later chapters. The question of plasma cooling is analyzed in this section using isothermal theory.

The principle behind a plasma recombination laser is as follows. The plasma is initially at some high temperature. It is then suddenly cooled. There will then be rapid electron ion recombination. During this recombination, the excited levels of the species will be in disequilibrium. If it occurs that some excited level has a population sufficiently greater than a less excited level, lasing may be possible.

Many methods for cooling recombination lasers have been proposed[11]. They include gas dynamic expansion, elastic energy transfer to heavy particle diluents, and radiative energy loss. It has been noted before that cooling be obtained by conduction of heat to walls, but it is generally observed that this can be significant only for plasmas with very high surface to volume ratios. It is found presently that thermionic converters are such plasmas. In fact cooling of thermionic plasmas can take place quite rapidly. Furthermore this cooling can be obtained conveniently by just reducing the T.E.C. output current.

The predicted thermionic Cesium recombination laser has some peculiar features. First, most lasers use electricity as an input and produce heat as a byproduct. In the present scheme, the input energy is heat, and electricity is produced as a byproduct. Further, as will be shown in later chapters, the Cesium recombination laser can scale to higher electron densities and higher power densities because it is a collisional rather than a collisional-radiative recombination laser.

Simple theories of cooling will be presented in this section. The present results will be compared with numerical results in later chapters. The general behavior

of a recombination laser thermionic converter plasma dynamics can be illustrated in the isothermal model. Recalling the isothermal result for unsteady thermionic converters:

$$\text{I.1} \qquad \frac{3}{2}\hat{n}\frac{d\tau}{d\bar{t}} = -2I_E(\tau-1) + I^2R + \hat{S}^{(E)} - I\mathcal{M}_1\left(\frac{I_E}{I}-1\right)\tau$$

Where:

$$\hat{n} = \int_0^1 \bar{n}\, d\xi$$

$$\hat{S}^{(E)} = \int_0^1 \bar{S}^{(E)}\, d\xi$$

It is supposed that the T.E.C. is operating at steady-state at some current, I, and some temperature, $\tau(0)$. If the current were suddenly reduced, then the ohmic heating term, I^2R, and the ambipolar-sheath term would both drop. If the current were reduced sufficiently or actually set to zero, both these terms may be neglected. For this case the unsteady isothermal energy equation can be rewritten:

$$\text{I.2} \qquad \frac{3}{2}\hat{n}\frac{d\tau}{d\bar{t}} = -2I_E(\tau-1) + \hat{S}^{(E)}$$

Let us consider the two terms on the right-hand-side of the above equation. The first represents cooling by loss of hot electrons to the walls. It is generally of order one. The second term is the collisional source term. This is generally dominated by inelastic energy transfers. For present purposes this can be written as the sum of two processes. The first is the energy released by depopulating the atomic excited levels, and to a good approximation this can be modeled by a single atomic level of excitation energy E_{01} which has a density N_1^e in Boltzmann equilibrium with the ground state. The second process is the actual ionization-recombination heat release. Under present T.E.C. circumstances, this latter may actually be negligible as a heat source as this occurs on a longer time scale. Other loss mechanisms, such as the escape of radiation, are neglected. The energy source can thus be written:

$$\text{I.3} \qquad \hat{S}^{(E)} = -E_0\hat{S}^{(n)} - \bar{E}_{01}\frac{d\bar{N}_1^e}{d\bar{t}}$$

where:

$$\bar{E}_0 = E_0/kT_E$$

E_0 = THE IONIZATION POTENTIAL

$$\bar{E}_{01} = E_{01}/kT_E$$

$$\bar{N}_1^e = N_1^e/n_e = \left(N_0\frac{g_1}{g_0}e^{-E_{01}/\tau}\right)/n_e$$

and where g_0 and g_1 are the ground and excited level degeneracies, respectively. With such a source term the energy equation can be written:

$$\text{I.4} \qquad C_v\frac{d\tau}{d\bar{t}} = -2I_E(\tau-1) - \bar{E}_0\bar{S}^{(n)}$$

where:

$$C_v = \frac{3}{2}\hat{n} + \bar{E}_{01}\frac{d\bar{N}_1^B}{d\tau}$$

Again, since recombination occurs on a longer time scale than that for the relaxation of temperature, it is an adequate approximation to consider electron density constant during the decay of temperature. It also follows that the emitted current is approximately a constant even in the double-sheath regime. With these assumptions, the above energy equation can be solved by quadratures. With the initial condition of $\tau=\tau(0)$ at t=0, then:

$$\bar{t} = \frac{1}{2I_E}\int_{\tau(\bar{t})}^{\tau(0)} C_v \frac{d\tau'}{\tau'-1}$$

and hence:

$$\bar{t} = \frac{3}{4}\frac{\hat{n}}{I_E}\ln\frac{\tau(0)-1}{\tau(\bar{t})-1} + \frac{\bar{E}_{01}}{2I_E}\left[\bar{E}_{01}\bar{N}_1^B(1)\left\{E_i\left(\bar{E}_{01}\left(\frac{\tau(0)-1}{\tau(0)}\right)\right)-E_i\left(\bar{E}_{01}\frac{\tau(\bar{t})-1}{\tau(\bar{t})}\right)\right\}\right.$$

$$\left. + \bar{N}_1^B(\tau)-\bar{N}_1^B(1)\right]$$

where Ei(x) is the exponential integral:

$$E_i(x) = \int_{-\infty}^{x} e^y\frac{dy}{y}$$

Examination of the orders of magnitude indicates that the cooling of a T.E.C. occurs in two regimes. In both cases energy is lost dominantly by exchange of electrons with the cooler walls. The distinction between the two regimes is in from where the energy was lost. In the first regime it is the decay of excited atomic levels which dominate the release of energy. In the second regime, the excited atomic levels have a negligible population and the energy release is dominantly from the translational modes of the free electrons.

The relaxation for the first regime can be estimated. the initial energy stored in the excited levels is:

$$\bar{E}_{01}N_1^B(\tau(0))$$

Thus, this energy is lost to the walls in a characteristic time of:

$$\frac{\bar{E}_{01}\,\bar{N}_1^B(\tau(0))}{2I_E(\tau(0)-1)}$$

This time is exponentially sensitive to the initial temperature through the Boltzmann population function. For the conditions to be studied presently though, it is the order of one half of a microsecond.

After the excited state populations become small, the second regime occurs. This regime, dominated by the decay of the free electron translational modes, is generally much shorter. For this regime, the energy conservation equation becomes:

$$\frac{3}{2}\hat{n}\frac{d\tau}{d\bar{t}} = -2I_E(\tau-1)$$

Thus in this regime, the temperature decays on a time scale of:

$$\frac{\hat{n}}{I_E}$$

This is typically the order of twenty nanoseconds.

To summarize, it is found that when the current flow through a thermionic converter is suddenly reduced, the electron temperature will decay rapidly towards the wall temperature in, typically, less than one microsecond. During the initial stage of the decay, energy is transferred from the atomic excited states to the walls. After the excited populations are depleted, the free electron translational energy decays, again by loss to the walls. Following the decay, the free electron temperature remains roughly the same as the emitter wall temperature. As will be shown in later chapters this decay is sufficiently rapid to produce the required recombination lasing.

III Collisional Rate Constants

Reliable inelastic cross-sections are essential to much of atomic laser theory. While ionization-recombination rates may be forgiving to some large errors, laser calculations can be quite sensitive to rate constants for one or two transitions. Towards selecting rate constants and assessing the uncertainty in them, available experimental and theoretical information will be reviewed. The rates selected as most appropriate to this problem are due to Mansbach and Keck[51]. In section III.B, the formula they suggest is analyzed and improved.

The impact energies of present interest are low, generally much less than the binding energy of the target atom. The cross-sections at such impact energies are unfortunately much less well known than those for high impact energies. This is true from the viewpoints of both theory and experiment. As the experimental information available is quite limited, the use of theory to provide information on unmeasured cross-sections is essential. The theories available are based on widely differing physical approximations. As a result, some controversy can arise over the choice of cross-section values for this regime. The present discussion will focus on the physical significance of approximations made in the available theories and on which experiments the theories should be tested against.

Two criteria are particularly important when categorizing cross-section theories. First, over what range of collision parameters does the method yield reasonably accurate values? Secondly, is the method practical for calculating the large number of values that are needed for engineering application? While cross-sections have been studied for some time and many theories have been proposed, few can claim positive answers to both the questions over the conditions of present interest. Thus for example theories as diverse as close-coupling, Bethe-Born, and binary encounters may claim to meet one or the other of the above criteria, but they generally cannot meet both.

Classical approximations have proved quite useful in this field. This usefulness is both because of the relative simplicity of classical theories which allows their employment in practical engineering calculations and because of their success in producing fairly accurate estimates of cross-section values. This success is an indication of the close relationship between quantum mechanics and the classical approximation. They are of course related not

only through Ehrenfest's theorem but also, and for present purposes more importantly, through the similarity of classical mechanics to the WKB-Jeffreys approximation to the Schroedinger Equation. Thus despite such difficulties as lack of formal validity at low quantum numbers and uncertainty of correct low energy correspondence principles, classical dynamics appears to be a valuable first approximation.

Some numerical classical solutions have been performed, typically using Monte-Carlo integration techniques. These have been valuable for engineering calculations. Some limitations remain though. For one, the results have not been computed over as wide a range as desired. This thus has led to some uncomfortable extrapolations. Section III.B considers this question. Further the calculations have been done for hydrogenic atoms only. Extrapolation to such nonhydrogenic atoms such as Cesium is discussed in section III.A. While such uncertainties do remain, the progress that has been made over cross-section estimates used in earlier ionization-recombination calculations is quite significant.

III.A Summary of Available Theories

The theory of electron-atom inelastic collision cross-sections has received much attention over a long period of time. This subject has been well reviewed. Reviews of quantum theory include[66-78] and for classical theory[79-84]. With so many thorough reviews, the present discussion will be in the nature of a survey and avoid technical detail. For present purposes it is important to consider the types of models that have been developed and how they are interrelated. The Born approximation will be mentioned first along with some of the many models which are closely connected with it. Higher quantum mechanical approximations starting with distorted wave and leading to close coupling will be considered next. A different series of models based on the binary encounter concept is then discussed with both quantum and classical formulations cited. Following this, models will be discussed which attempt to combine the better features of two models. Lastly, some classical numerical solutions will be discussed. While this overview is necessarily incomplete, it serves to outline the types of methods that have been used and their usefulness for cross-sections of present interest.

Probably the best known quantum mechanical model is the Born approximation. This model considers the effects of the collision to be a perturbation on the otherwise independent motion of the incident electron and the atomic electron. This perturbation expansion is called the Born series. This subject is reviewed in[71]. The first term in this series is called the first Born, or simply the Born, approximation. Although the first Born is among the simplest quantum mechanical approximations its evaluation is still quite laborious.

The Born approximation is valid at very high impact energies. Because of its relative convenience, however, it is often evaluated at low energies and even near threshold. Furthermore, much effort has been devoted to improving its performance at these low energies. One group of such efforts has focused on applying indistinguishability considerations[20,21,44,76]. Other approaches to improving the Born approximation attempt to include some effects of the interaction potential in the lowest order approximation. An example is the Coulomb-projected Born approximation[22,23]. This includes the nuclear potential for the inelastically scattered electron. An different approach was developed by Glauber[24]. This allows for phase distortion of the incident electron as it passes

through the atom.

There are other approximations which simplify Born. Probably the best known of these is the Bethe-Born approximation which expands the interaction potential into multipole moments. This is valid when the inelastic cross-section is dominated by long-range collisions. This is true at very high impact energies. Evaluation of cross-sections in the Bethe-Born approximation is sufficiently simple that it is practical for use in engineering calculations. Unfortunately the values at low energies are not very accurate. They are generally much too large. Moreover, the functional dependencies are quite questionable when used at low energies. Bethe-Born cross-sections depend prominently on the dipole moment of the transition. This seems to be in strong disagreement with experiment over the parameter range of interest[49]. This dependence is also theoretically suspect since low energy collisions are dominated by short-range interactions for which multipole moment expansions are usually not useful. Some confirmation for this suspicion is provided by the Born approximation. Thus while the Born approximation does seem to prefer dipole connected transitions at large impact energies, the preference ceases close to threshold as seen in the calculations of [25]. As the dipole moment dependence is so often assumed in engineering calculations, this question as to their importance needs further investigation.

Because of its valuable simplicity, the Bethe-Born approximation has inspired many variants. One is the semi-classical model of Seaton[26]. This uses an impact parameter formulation which allows unphysically high transition probabilities to be located and corrected for in a somewhat ad hoc fashion. There is also a fully classical dipole moment interaction theory developed by Percival and Richards[45,46]. These and other theories have led to some semi-empirical formulas such as[47,48]. All work excellently over some ranges of parameters but conditions of present interest appear to be outside these ranges.

There are a series of approximations that are more complex than that of Born. The first of these is the distorted wave approximation which is similar to Born except that the lowest order approximation includes the effect of elastic scattering. By including more terms of the interaction potential, the strong coupling approximation is found. This can be interpreted as allowing the atomic electron to be in any linear combination of the initial and final levels, but in no other level at any time during the collision. Finally there is the close coupling approximation. This extends the strong coupling approximation by allowing the atomic electron to occupy additional atomic levels during the collision. The set of atomic levels that can be included is limited only by

computational requirements. This can be a fairly severe limitation, however. Close coupling has been used most successfully only in the lowest atomic energy levels and only when few open channels exist. Even under these conditions, to obtain convergence it is sometimes necessary to create pseudo-state functions and/or functions to simulate correlation effects. While it is of value to know of theories more advanced than Born, these, at least in their quantum formulation, are much more laborious to calculate and thus most likely impractical for application.

A completely different approach to inelastic collisions is exemplified by the many, varied, and often controversial binary encounter theories. While quantum mechanical versions of these theories are the subject of current research[63,64,65], this physical model predates the Schroedinger equation. It was first used to model atomic excitation by Thomson[27] in 1912. The basic concept of this approach is that the collision between the incident and atomic electron can be modeled neglecting the atomic core. This is thus a simple two-body coulomb interaction which is described by Rutherford scattering[28]. In the Thomson model the atomic electron is assumed to be initially at rest. This model is fairly successful at predicting ionization cross-sections. Several years later this model was improved by Thomas[29] to allow for motion of the atomic electron prior to the collision. Further additions to the theory were proposed to partially account for the presence of the nucleus. Thomas[29] proposed that the nucleus would have the effect of accelerating the incident electron prior to its encounter with the atomic electron. Webster[31] further proposed that the nucleus would also focus incident electrons. Both of these additions though are controversial[81].

With the introduction of quantum mechanics by Schroedinger in 1927, work in binary encounter theory lapsed until 1959 when Gryzinski[32] published his binary encounter theory and found agreement with experiment that was superior to many complex quantum mechanical calculations. This provoked a series of papers[33-43] and much discussion. As a result of this some uncertainties in the formulation of binary encounter theory became apparent, but its agreement with available experiments remained impressive nonetheless and comparable to many quantum mechanical results. Considering the simplicity with which binary encounter cross-sections can be calculated, the degree of agreement achieved with experiment was quite astonishing.

Binary encounter theories are probably the most widely used for engineering application. However as more information was found, it appeared that some of the agreement with experiment that binary encounter theory achieved was misleadingly reassuring. The problem was that most of the experimental data available was for a limited

variety of cross-sections. In particular, most experimental cross-sections were for excitation from the ground state. By the nature of atoms, this generally means that the energy transfer was of comparable size to the ionization potential. Binary encounter theory, it turns out, works quite well for such large energy transfers. When, however, the energy transfer is smaller these theories can give serious errors. This is illustrated in[49] by comparison with some recent experimental results. It is further confirmed by comparison with the classical exact solutions to be discussed later. Compared to the magnitude of this error, the differences between the various binary encounter theories is quite small.

Explanations have been advanced for the failure of binary encounters for these small energy transfer collisions. The most apparent problem is that binary encounter theories predict that large contributions to such cross-sections may occur from large impact parameter collisions for which binary encounters is an inadequate approximation because the nuclear potential shields the electrons from one another.

The success of binary encounters at large energy transfers and of dipole theories for small energy transfers has naturally led to symbiotic theories. Burgess[36] suggested an impact parameter scheme with small impact parameters treated by binary encounters and large ones by a semi-quantum dipole approximation. Vriens[37] suggested using momentum transfer to determine the crossover point. He proposed using binary encounters for large momentum transfer and a quantum theory, e.g. Born or Bethe, for small transfers. A fully classical treatment was developed by Percival[50] to combine dipole theory at large impact parameters with binary encounters at small ones and a smooth transition in between. These approximations have achieved some success but are limited by the importance of that region for which neither binary encounters nor dipole theories are valid.

One of the valuable features of the classical approximation is the ability to find exact solutions numerically. This has been done by several investigators. Mansbach and Keck[51], using the theory of classical phase space to reduce computation, calculated thermally averaged transition rates. Percival[50] has calculated cross-sections for atomic excitation at various impact energies. He used classical scaling laws to generalize his results. Other such calculations also exist but were done for limited parameter ranges, e.g.[52-55]. Both calculations averaged and summed over atomic angular momentum distributions. Since the Mansbach and Keck[51] calculation was thermally averaged and an empirical fit was provided, it has found more application to practical problems. Its agreement with experiment appears quite

good[49].

While these numerical computations have been performed over a wide range of parameters, their great value has led to a need for calculations over an even wider range. Extrapolation of the Mansbach and Keck[51] results is needed in ionization-recombination calculations and was used for comparison with experiment in[49]. While such extrapolation is easily done, theoretical analysis of the Mansbach and Keck empirical fit suggests that it is possible for large errors to result. This will be discussed further in section III.B.

Attempting to apply these theories to engineering calculations, an important gap emerges. There is limited information on nonhydrogenic effects. These effects take two main forms. First, the kinetic energy distribution of bound electrons in nonhydrogenic atoms is different and approximate theories have shown this to be an important effect[43,56]. Secondly and more importantly, the subshells of nonhydrogenic atoms often must be treated individually. This contrasts with hydrogenic atoms for which the subshells are approximately degenerate and thus their populations may be assumed to be related by statistical equilibrium as per theories such as[57]. For atoms with such large quantum defects as Cesium or other alkali metals that are commonly used in engineering, the assumption of approximate degeneracy is invalid over most important levels. Thus cross-sections for simultaneous energy and angular momentum are needed for nonhydrogenic atoms.

As this question of subshell to subshell cross-sections must be resolved before calculations can be performed, this has led to the use of some unsatisfying assumptions. One common approach has been to borrow theory from high impact energies, Bethe-Born theory and thus assume a dipole moment dependence. As discussed above however, this is highly questionable. Upon observation of the available experimental data and the near threshold behavior of theories such as Born, it appears that all final subshells of the same energy have cross-sections of similar magnitude. Present calculations thus assigned equal probability to such subshells. While this seems to be superior to the assumption of a dipole moment dependence, it is likely to be accurate to only a factor of two. The results of these assumptions are compared in later chapters.

There is one uncertainty that all classical theories have in common. That is the present ambiguity over correspondence principles for use under conditions of present interest. A number of such principles have been suggested and used successfully but not without controversy[81,58,59]. The ionization-recombination calculations presented in later chapters were performed under a variety of such principles and few qualitative

changes resulted. Where changes did occur, they are of course noted.

To summarize, a large number of cross-section theories have been developed over many years. There are quantum mechanical theories ranging from Born to close-coupling. There are classical mechanics theories ranging from impact parameter to Monte-Carlo numerical solutions. For the type of collision of present interest, it appears that only the classical Monte-Carlo calculations combine the required calculational simplicity with reasonable accuracy.

III.B Analysis of Mansbach-Keck Results

The Classical Monte-Carlo calculations of electron-atom inelastic collision rate constants performed by Mansbach and Keck are very useful. A consequence of this usefulness is the desire to extrapolate the results beyond their range of validity. To improve the accuracy of the Mansbach and Keck empirical fit both within and without its range of validity, it is presently analyzed on a theoretical basis. Some deficiencies are found and an improvement is suggested.

First it is shown how the inelastic electron atom cross-section can be found from the Mansbach and Keck thermal rate formula. While because of the simplicity of the Mansbach and Keck fit to the thermal rate constants this cross-section formula is necessarily simple, it is possible to examine the scaling properties of such a formula. This examination yields four discrepancies with available theory. It is then found that by altering one of the empirical constants in the Mansbach and Keck fit that two of these four discrepancies can be eliminated. This modified fit is then compared with the Mansbach and Keck Monte-Carlo data. Careful interpretation of their data indicates that most of the difference between their fit and the present suggested modification is due to a systematic error they made in analyzing their results. Further, eliminating from consideration some points for which the form of the fit is not expected to apply explains the small remaining difference. Finally, a classical scaling law is invoked to obtain the temperature dependence of the rate constants. This dependence will confirm what Mansbach and Keck inferred on limited computational evidence.

Mansbach and Keck considered energy transfer to a classical hydrogen atom from a bath of Maxwellian free electrons. The initial atomic energy is E_i and the final is E_f. The rate constant for transition from E_i to E_f per unit final energy is written $K(E_f,E_i,T_e)$. This thus has units of volume per time and per unit energy. The thermal rate is an average of the cross-section over the Maxwellian electron energy distribution. The cross-section for an impact energy E to cause a transition from energy E_i to E_f per unit final energy is denoted by $\sigma(E,E_f,E_i)$. Thus:

$$K(E_f,E_i,T_e) = \int_{\sqrt{2U/m}}^{\infty} \sigma(E,E_f,E_i)\, v\, f(v,T_e)\, dv$$

where $U=E_f-E_i$ is the threshold energy, v is the electron speed, $f(v,T_e)$ is the Maxwellian distribution, and m is the electron mass. $E=mv^2/2$ is the impact energy. For present

purposes it is more convenient to change the variable of integration from speed to impact energy. This results in the exactly equivalent form:

$$B.1 \qquad K(E_f, E_i, T_e) = \bar{v} \int_0^\infty \sigma(U+E', E_f, E_i) \frac{U+E'}{kT_e} e^{-\frac{U+E'}{kT_e}} \frac{dE'}{kT_e}$$

where E'=E-U is the impact energy above threshold, k is Boltzmann's constant, and $\bar{v}$ is the mean thermal speed of the free electrons.

Mansbach and Keck provided a formula for the rate constant K. To find the cross-section implied by such a formula, the above integral equation, B.1, will need to be solved. This is conveniently done by rewriting the above integral in terms of a Laplace transform. Thus:

$$B.2 \qquad K(E_f, E_i, T_e) = \frac{\bar{v}}{(kT_e)^2} e^{-\frac{U}{kT}} f\left(\frac{1}{kT_e}\right)$$

where $f(1/kT_e)$ is the Laplace transform of F(E'):

$$B.3 \qquad f\left(\frac{1}{kT_e}\right) = \int_0^\infty F(E') e^{-\frac{1}{kT_e}E'} dE' = \mathcal{L}\{F(E')\}$$

and where F is given by:

$$B.4 \qquad F(E') = \sigma(E+E', E_f, E_i)\,(U+E')$$

The solution of the integral equation can now be easily done. The Mansbach and Keck empirical formula for rate constant K for excitation is:

$$B.5 \qquad K(E_f, E_i, T_e) = a_1 \frac{\bar{v} r_T^2}{kT_e} \left(\frac{-E_i}{kT_e}\right)^{-a_2} e^{-\frac{U}{kT_e}}$$

where r_T is a Thomson radius defined by:

$$r_T = e^2/kT_e \quad ; \quad e^2 = 14.40\ eV\text{-}\mathring{A}$$

The quantities a1 and a2 are empirical constants which Mansbach and Keck choose to be:

$$B.6 \qquad a1=6.75 \quad ; \quad a2=2.33$$

Equating the expressions B.2 and B.5 shows that the Mansbach

and Keck fit implies that the function f is given by:

$$f\left(\frac{1}{kT}\right) = a_1 F^2 kT \left(-E_i/kT\right)^{-a_2}$$

Thus the Laplace transform f behaves as a power law. Such a transform is easily inverted to find F. It follows that the Mansbach and Keck implied cross-section is:

B.7 $$\sigma(E, E_f, E_i) = \frac{a_1 e^4}{\Gamma(\frac{1}{2}+a_2)} \left(-E_i\right)^{-a_2} \frac{(E-U)^{a_2-2}}{E}$$

Naturally, this formula applies only to impact energies above threshold, i.e., E>U. Below threshold, the cross-section must be zero.

This can now be examined in light of theoretical knowledge of such cross-sections. Such knowledge is available for large and small energy transfers U, and large and small impact energies E.

First for small energy transfers U, dipole theories, such as Bethe-Born or Percival[46], can be employed. The classical theory yields the ln(U)/U behavior. It can be seen however that the Mansbach and Keck implied cross-section does not follow this rule. According to the results of [50], though, this is not always a serious limitation. The region over which dipole theories apply seems to be quite small, restricted to impact energies at least the order of the atomic binding energy, -Ei, and energy transfers much less than that.

Secondly, the behavior at large energy transfers can be compared with the predictions of classical binary encounter theories which have been found applicable in this range[51,55]. For large energy transfers, this binary encounter theory predicts an inverse U squared dependence. This also disagrees with the Mansbach and Keck formula.

Thirdly, consider large impact energy. In this regime a 1/E dependence is expected. This is predicted by classical Binary encounters. (The ln(E)/E dependence of quantum theory can be found from classical theory if correspondence principles are carefully applied[81].) Again, this is at variance with the Mansbach and Keck fit.

Fourthly and finally, consider small impact energies. While this is a very important regime, it is also somewhat controversial. The well-known Wigner threshold theory implies a rise of the cross-section proportional to the square-root of the energy above threshold. Recent theory and experiment appear to indicate that this has a very limited range of validity. The Wigner theory assumes a smoothly varying integral of the wave-function. The limited

usefulness of the resulting cross-section law appears to be because the wave function is poorly behaved near threshold, given to resonances. Thus other sources must be consulted for practical threshold laws. The Monte-Carlo classical calculations of Percival[50] seem to imply a cross-section which is finite at threshold. This threshold law is in disagreement with the Mansbach and Keck fit.

Many experimental and quantum-mechanical results show cross-section which are not finite at threshold. It is however a well-known result of quantum cross-section theory[102] indicates that cross-sections may be effectively finite at threshold when the final state is nearly degenerate with some other state. Atomic states in classical mechanics are always degenerate. It is thus not surprising that Percival[50] should find classical cross-sections to be apparently finite at threshold.

Of these four objections to the Mansbach and Keck fit, two can be easily removed. These two are the last two which deal with the behavior as the impact energy E varies. It is seen that if the coefficient a_2 is changed to:

B.8 $$a_2 = 2$$

proper asymptotic behavior with respect to E results. At large impact energies, the cross-section decays like 1/E which is proper for a classical cross-section. Near threshold, the cross-section is finite which agrees with the Percival[50] Monte-Carlo computations. Below threshold, the formula B.7 does not apply and the cross-section is zero. With this change the Mansbach and Keck fit should be better suited to extrapolation.

It is beneficial to ask why, if the above suggested a is an improvement, did not the Mansbach and Keck empirical fit find it? The answer will be shown to be that there were systematic errors in the method of least squares fitting used by Mansbach and Keck. To find this answer, it is necessary to examine the organization of the Mansbach and Keck data. Mansbach and Keck counted transitions rates from a range of initial energies within some q/2 of the energy Ei to a range of final energies within q/2 of Ef. q varies from one half to twice kT_e. Thus Mansbach and Keck did not measure K but rather:

B.9 $$\underline{K}(E_f, E_i, T) = \int_{E_i - q/2}^{E_i + q/2} \int_{E_f - q/2}^{E_f + q/2} K(E_f, E_i, T)\, dE_f\, dE_i$$

To find K, Mansbach and Keck approximated the above integral by:

B.10 $$\underline{K}(E_f, E_i, T) \cong K(E_f, E_i, T) \cdot q^2$$

This introduced a systematic error of typically over 10% but sometimes up to 80%.

This approximation and the resulting error are unnecessary. Eliminating it, and re-doing the least-squares fit gives new values for the correlation coefficients:

B.11 $$\alpha_1 = 5.33 \quad ; \quad \alpha_2 = 2.109$$

This is closer to the theoretical suggestion above. Moreover, with the ill-suitedness of the formula for small binding energies and small energy transfers as found in comments 1 and 2 above, it is suggested that the three data points which most violate this region be eliminated from the least-squares fit process. These three are the ones with U of one half and an upper state binding energy less than three, both in units of kT_e. Having removed these points, the least squares fit can be performed again yielding:

B.12 $$\alpha_1 = 4.37 \quad ; \quad \alpha_2 = 2.005$$

This is now impressively close to the value of a2 expected from theory as above.

It is thus concluded that a better fit to the Monte-Carlo data of Mansbach and Keck is given by formula B.5 using coefficients B.12. For application to hydrogenic atoms, it is useful to apply the density of states correspondence principle to find the the rate constant for a transition from a principle quantum number l to a principle quantum number u:

B.13 $$K_{ul} = (9.6 \times 10^{-5} K^{\frac{1}{2}} cm^3/sec) T_e^{-\frac{1}{2}} \frac{l^4}{u^3} e^{-\frac{U}{kT_e}}$$

where again excitation, i.e. u>l, is considered. By detailed balance, the de-excitation rate from u to l would be:

B.14 $$K_{lu} = (9.6 \times 10^{-5} K^{\frac{1}{2}} cm^3/sec) T_e^{-\frac{1}{2}} \frac{l^6}{u^5}$$

According to some Monte-Carlo computer calculations, Mansbach and Keck found evidence that an integral of the rate constant K over atomic states varied insignificantly with respect to temperature, T. From this they concluded that the temperature dependence of their empirical fit was correct. By virtue of classical scaling laws, however, the temperature variation of the rate constant K can be determined exactly, and conforms to the Mansbach and Keck formula. This classical exact scaling is:

$$\sigma(E, E_f, E_i) = \alpha^3 \sigma(\alpha E, \alpha E_f, \alpha E_i)$$

This implies that K scales by:

$$K(E_f, E_i, T_e) = \alpha^{\frac{5}{2}} K(\alpha E_f, \alpha E_i, \alpha T)$$

which agrees with the Mansbach and Keck empirical results.

In summary, modifications to the results of Mansbach and Keck is proposed. This was done as follows. First, it was shown that their thermal rate constant empirical fit formula implies a cross-section fit. This fit is found by inverting a Laplace transform. With the theoretical information available, a modification of the empirical fit was suggested which gave it some of the correct asymptotic behaviors. This modification was verified by the Mansbach and Keck data as modified to remove systematic errors in its interpretation. The agreement was further improved as points which are expected to be influenced by long range collisions were removed. In the present thesis, both the original and the modified Mansbach and Keck formulas are employed.

IV Theory of Ionization-Recombination

The ionization-recombination process is essential to ignited mode thermionic energy conversion. It is well known that under conditions of present interest ionization and recombination occur through a multi-step process. The present chapter introduces the theory of how the rate constants for elementary processes combine to form the overall ionization-recombination rate constants. While the essentials of the theory of ionization-recombination have been known for nearly twenty years, some of the more subtle implications are sometimes unappreciated. Among these is the location of the rate-limiting steps, known as the 'bottleneck'. Detailed analysis shows its location to be contrary to some oft applied rules-of-thumb. The reasons for this will be explained qualitatively in this chapter, and analyzed quantitatively in the next. Also discussed are the conditions under which recombination lasing may occur and what role if any spontaneous radiation will play in generating the requisite population inversion. Further, there is a quasi-steady assumption often made in the conservation equations whose justification and limitations have commonly been arrived at intuitively. This assumption is analyzed presently and is found to work as expected in most cases, but not all cases. This chapter, while reviewing the theory of ionization-recombination, will address these questions.

In the first section to follow, the conservation equations for each of the atomic level populations will be set up. This will be a system of many ordinary differential equations. It will then be shown advantageous to introduce some reduced variables. Eigenvector analysis will indicate that a quasi-steady assumption is often accurate. The limitations on this assumption will be discussed and shown to be quite contrary to some previously published limitations. Finally some sample results of this theory will be discussed.

IV.A The Conservation Equations

As in other kinetic problems, conservation equations for each species present should be written. In the regime of ionization-recombination of present interest, the 'species' are atoms in each electronic state and ions. The present development follows Bates, Kingston, and McWhirter[13].

Discussions of ionization-recombination generally involve reactions such as the following three:

A.1 $$A_i + e \rightleftharpoons A^+ + e + e$$

A.2 $$A_i + h\nu \rightleftharpoons A^+ + e$$

A.3 $$A_i + A_j \rightleftharpoons A_2^+ + e$$

Here Ai is an atom in some excited state i. Aj is another atomic state. A+ is an atomic ion and A2+ is a molecular ion. e is an electron and hv is a photon. Of the three reactions above, the third is molecular ionization-recombination. The cross-section for this reaction and similar molecular reactions are quite uncertain which makes them difficult to treat. Fortunately there is as yet no conclusive evidence that they are important*. The second reaction above is radiative ionization-recombination. For electron densities of present interest, this is known to be negligible. It is the first of the reactions above, ionization-recombination by electron impact, that is believed to be the fastest under T.E.C. conditions.

In a kinetic sense however, none of the above reactions is important. The important, that is rate limiting, step involves not ionization nor recombination but rather the production and destruction of the atomic states which will be ionized or were formed by recombination. Even though the vast majority of the atoms may be in the ground state, it is the high excited levels which dominantly participate in the actual ionization and recombination reactions. The rate limiting steps thus involve transitions between the ground state and these excited levels. This is generally a multi-step process for which collisional and radiative transitions must be considered:

A.4 $$A_i + e \rightleftharpoons A_j + e$$

A.5 $$A_i + h\nu \rightleftharpoons A_j$$

* However, see[97].

To study these, conservation equations for the atomic levels are written. In phenomenological form:

$$\text{A.6} \qquad \frac{\partial N_i}{\partial t} = \{\text{collisions}\}i + \{\text{radiation}\}i + \{\text{external}\}i$$

for all levels i

where t refers to time and Ni is the population density of level i at some point in space. The following paragraphs discuss the terms on the right hand side.

In the conservation equations, advantage is taken of three approximations. It is assumed that under thermionic converter conditions molecules play a negligible role and that ions exist only in their ground state. The latter assumption is quite accurate at these temperatures. The former, however, is a matter of controversy but must be made until quantitative information on the relevant molecular cross-sections is established . Spatial diffusion of these species is also neglected as this is generally much slower than the inelastic collision rates.

There are four types of radiative processes that may play a role: (1) spontaneous emission, (2) stimulated emission, (3) absorption, (4) radiative ionization, and (5) radiative recombination. Under T.E.C. conditions, radiative ionization and recombination are quite small since at these electron densities collisional ionization and three body recombination dominate[11]. This leaves processes (1), (2), and (3). They are simplified further by dividing the atomic levels into two types. This first is the levels whose absorption length is so small that all spontaneously emitted radiation is reabsorbed. For such levels the spontaneous radiation coefficient can be replaced by an effective coefficient of zero. The absorption then need not be considered explicitly. Under T.E.C. conditions, transitions into the ground state fall into this category. The other group of transitions are those for which re-absorption of radiation can be neglected. Generally all transitions into excited levels fall into this latter category. The exception however is when a transition is subjected to intense radiation as might be produced by some external source or generated by laser action, then absorption and stimulated emission of this radiation must be considered explicitly.

There are four types of inelastic collisional processes which must generally be considered: (1) excitation from one atomic level to another, (2) the reverse process, de-excitation, (3) direct ionization, i.e. collisions that result in an electron and ion being formed, (4) direct collisional three-body recombination. It will be apparent

later that it is quite rare when these processes can be completely neglected. All are explicitly included in the present theory and calculations.

With the above approximations, the conservation equations can be written:

$$\frac{dN_i}{dt} = n_e \sum_{j=0}^{e-1} (K_{ij} N_j - K_{ji} N_i) + n_e (K_{ie} n_e^2 - K_{ei} N_i) + \sum_{j>i} A_{ij} N_j - \sum_{j<i} A_{ji} N_i \qquad A.7$$

where Ni and Nj are the population densities of levels i and j, Kji is the collisional rate constant for a transition from level i to level j, Kij is the reverse rate constant, Aji is the Einstein A-coefficient, as modified for possible trapping.

The conservation equation for the free electron density can also be written:

$$\frac{dn_e}{dt} = n_e \sum_{j=0}^{e-1} K_{ej} N_j - n_e \sum_{j=0}^{e-1} K_{je} n_e^2 \qquad A.8$$

The first summation above represents the actual ionization rate. The second represents the actual recombination rate. Both of these rates are quite large and much cancellation occurs between the two summations. This is a result of the approximate local thermodynamic equilibrium between the free electrons and the highly excited levels. When the words ionization rate and recombination rate are used in practice, though, they do not refer to the terms in the above equation. They refer rather to the terms on the right hand side above which scale as an elementary single-step ionization or recombination reaction would. This will be elaborated upon later.

Estimating the relative sizes of the terms in the above system of conservation equations is a natural first step for studying the system. It is common to focus attention on the relative magnitudes of excitation and de-excitation terms. This question is often answered with one of two contradictory arguments. The first is to conclude that de-excitation can be neglected as the populations of upper levels are always much smaller than those of lower levels. The other is to conclude the excitation can be neglected since its rate constants are typically much smaller than that for the reverse process. While there are some fields of study where one or the other of these conclusions may be valid, generally neither of these is good to even an order of magnitude for the present system even during extremes of strong ionization or recombination. To emphasize this and also provide a systematic method for estimating the relative sizes of terms in the above system, it is convenient to introduce some well-known[13,85] reduced variables. First, define a reference Boltzmann population for each atomic

level:

$$A.9 \qquad N_i^B(T) = N_{ref} \frac{g_i}{g_0} e^{-E_i/kT}$$

Where Ei is the binding energy of level i, g_i is the degeneracy of level i, and Nref is an arbitrary constant. With this a reduced population is defined:

$$A.10 \qquad \nu_i = N_i / N_i^B$$

A reduced electron density is defined similarly based on $n_s(T)$, the Saha electron density corresponding to the chosen Nref:

$$A.11 \qquad \nu_e = n_e^2 / n_s^2$$

In thermodynamic equilibrium, the magnitudes of all the reduced populations are equal. Thus the variation in these populations gives a measure of the disequilibrium.

To accompany the reduced populations, reduced rate constants are defined:

$$A.12 \qquad \begin{aligned} W_{ij} &= K_{ij} N_j^B \\ W_{ie} &= K_{ie} n_s^2 \\ \alpha_{ij} &= A_{ij} N_j \end{aligned}$$

The forward reduced collisional rate constants, Wij, are equal to reverse reduced collisional rate constants, Wji. This is by virtue of macroscopic detailed balance.

As a result of this symmetry, analogies can be made between this system and an electrical circuit or fluid mechanical system of pipes. Rewriting the conservation equations in the reduced variables:

$$A.13 \qquad \frac{d[N_i^B \nu_i]}{dt} = n_e \sum_{j=0}^{e} W_{ij}(\nu_j - \nu_i) + \sum_{j>i} \alpha_{ij} \nu_j - \sum_{j<i} \alpha_{ji} \nu_i$$

To clarify the analogy, let us consider a single term. The collisional net transfer rate into level i from j is:

$$A.14 \qquad K_{ij} N_j - K_{ji} N_i = W_{ij}(\nu_j - \nu_i)$$

This is similar to an electrical Ohm's Law. (The fluid mechanical analogy will be discussed in the next paragraph.) The current in a resistor is a net transfer rate. It is proportional to the difference on voltages at the resistors ends. The reduced populations can be seen to be analogous to voltages. The constant of proportionality between the current and the voltage difference for a resistor is its conductance. The reduced rate constant, Wij, is thus analogous a resistor's conductance. The collisional terms in the conservation equations can thus be drawn as a network of resistors interconnecting the levels which are represented as terminals. This concept is illustrated in figure 5. Further discussion of the electrical analogy can be found in Bates[14].

The collisional terms in the atomic level conservation equations can also be thought of in a fluid mechanical analogy. Referring back to equation A.14, an analogy between the collisional net transfer rate and the mass flow through a pipe can be made. The mass flow through a pipe is proportional to the difference in pressures across the ends of the pipe. The reduced populations can thus be seen to be analogous to pressures. In fluid mechanics the constant of proportionality is a function of the size and shape of the pipe and also the kinematic viscosity of the fluid. Here the constant of proportionality is the reduced rate constant Wij. The collisional terms of the conservation equations can thus be represented by a network of pipes which meet at terminals representing the atomic levels. This is shown schematically in figure 5, though using electrical notation.

In chapter V, it will be shown how the circuit of figure 5 reduces to that of figure 6.

In addition to the above analogies, there are two more important advantages of the reduced variables. One is that it is possible to determine the direction of the net collisional transition flux between two levels just by looking at a graph of the reduced populations. The direction is always from higher reduced populations to lower reduced populations. Such information cannot be so simply deduced from a graph of ordinary dimensional populations. Secondly, reduced populations have the advantage of being more slowly varying as temperatures change than dimensional populations. This makes interpolation between tabulated values simpler.

These analogies can be extended further to include more than just the collisional terms. The time derivative of the level densities can be represented by water storage towers in the fluid analogy or capacitors in the electrical system. Unless the radiation field is in black body equilibrium at the same temperature as the free electrons, the radiation terms have no simple analogies.

To summarize, a system of simultaneous ordinary differential equations has been stated which describes the ionization-recombination process of atoms subjected to inelastic collisions with electrons and various radiative processes. Each equation described the conservation of number densities of the excited levels of the atom and of the ion or free electron density. Reduced variables were introduced to create symmetry between forward and reverse rate constants. It was shown that the collisional and unsteady terms are analogous to electrical and fluid systems. While these equations can be solved as they stand, the results of eigenvector analysis discussed in the next section will provide much simplification.

IV.B Eigenvector Analysis and the Quasi-Steady Theory

The implications of the conservation equations developed in the previous section are not obvious. It is found however that an approximate analysis can lead to some important physical insights. The dynamics of the atomic level conservation equations can be greatly simplified using an eigenvalue analysis. As is typical of many reactive systems, the atomic level conservation equations include phenomena which are characterized by widely disparate time scales. For present purposes only the most slowly varying of these need be considered. This approach leads to what is known as the quasi-steady assumption. Under this approximation, simple formulas characterize the ionization and recombination results as well as determine the excited state populations. As a result the time history of these variables is explained.

The quasi-steady assumption has been used at least implicitly for many decades as in for example[12]. It was explicitly discussed and used on the atomic level conservation equations of the form discussed in section IV.A by Bates, Kingston, and McWhirter[13]. Published justifications of this assumption have tended to be intuitive in nature. The invocation of eigenvector analysis, as is done presently, provides a rigorous basis for it. The implications of this are mentioned herein. An important result of this analysis is the ability to assess the limits of validity of the quasi-steady assumption. It is found in one case that the limit of validity is the opposite of that commonly suggested in the literature.

To obtain the simplification, the atomic level conservation equations are rewritten. Separating positive from negative collisional and radiative terms, write:

$$\text{B.1} \quad \frac{dN_i}{dT} = \{\text{in}\}i - \{\text{out}\}i + \{\text{external}\}i$$

where:

$$\{\text{in}\}i = n_e \sum_{j \neq i} W_{ij} N_j + \sum_{j>i} A_{ij} N_j$$

$$\{\text{out}\}i = n_e \sum_{j \neq i} W_{ji} N_i + \sum_{j<i} A_{ji} N_i$$

The unsteady behavior of such an equation can be described

by eigenvectors. The more common heuristic approach will be described here with its limitations noted. It is observed that for i belonging to the excited levels:

B.2 $$\frac{dN_i}{dt} \ll \{out\}i$$

When this is the case, equation B.1 can be valid only if:

B.3 $$\{out\}i \cong \{in\}i + \{external\}i$$

where this approximation is known as the quasi-steady approximation. Since the collisional terms on the right hand side of B.2 grow linearly with electron density, it is often stated in the literature that this inequality will be valid for sufficiently large electron density. This, as will be discussed later, is not the complete story. This approximation will be shown to be invalid for large electron density. Assuming that quasi-steady is valid, the solution to the equations can be seen to have the form:

B.4 $$\nu_i = V_i \nu_e + V_i' \nu_0$$

Where v_i' and v_i are functions of the electron temperature and, if radiation is significant, also the electron density.

The quasi-steady assumption applies to the conservation equations for the excited levels. The conservation equations for the free electrons and the ground state still remain to be considered. These equations, rewritten using the quasi-steady excited level populations, are:

B.5
$$\frac{dn_e}{dt} = n_e\left[\sum_{j\neq e} W_{ej} V_j'\right]\nu_0 - n_e\left[\sum_{j\neq e} W_{je}(1-V_j)\right]\nu_e$$
$$\frac{dN_0}{dt} = n_e\left[\sum_{j\neq 0} W_{0j}(1-V_j') - \frac{\sum_{j\neq 0} a_{0j} V_j'}{n_e}\right]\nu_0 + n_e\left[\sum_{j\neq 0} W_{0j} V_j + \frac{\sum_{j\neq 0} a_{0j} V_j}{n_e}\right]\nu_e$$

As a further consequence of the quasi-steady assumption, it can be shown that the coefficients of the reduced ground and free electron populations in the each of the above equations are the same as in the other. These are thus written:

B.6 $$-\frac{dn_e}{dt} = \frac{dN_0}{dt} = n_e(R\nu_e - I\nu_0)$$

Where these coefficients are now identified as the effective ionization and recombination coefficients. It is interesting to note that the actual ionization and recombination rates do not correspond to the terms in the above equation. They are given by the terms in equation A.8 which are quite different.

The ionization and recombination coefficients are often written without benefit of reduced variables. In this form:

B.7 $$-\frac{dn_e}{dt} = \frac{dN_0}{dt} = \beta n_e^3 - \alpha n_e N_0$$

where: $$\beta = R/n_s^2$$

and: $$\alpha = I/N_{REF}$$

At this point the limitations of the quasi-steady approximation can be discussed. Knowing the form of the ionization-recombination rates from B.6 and the excited level population from B.4, it is possible to return to B.2 and consider its validity. It is seen that in recombining plasmas, the excited state populations are proportional to the cube of the electron density. By contrast, the term {out}i rises no faster than linearly with large electron density. Thus from B.2, the quasi-steady approximation will fail for large electron densities. With eigenvector analysis, this limit can be quantified. It is found that for the quasi-steady approximation to be valid in Cs, the electron density must be much less than some number n* where n* is a function of the electron temperature T:

T (K)	n* (cm-3)
1500	8 (15)
2000	1 (16)
2500	3 (16)
3000	7 (16)

A second limitation of the quasi-steady approximation is that if the electron temperature changes suddenly, an adjustment time is required for the new quasi-steady state to be reached. This time, as found from eigenvector analysis, is typically the order of 0.1 microseconds or less under T.E.C. conditions.

When the electron density is high enough that collisions dominate over radiation, some interesting and well known symmetry properties exist. This is due to the reduced rate constants being symmetric for this case and thus the Boltzmann distribution is a solution of the conservation equations. First, there is a relation between the excited state population coefficients. thus:

B.9 $$V_i' = 1 - V_i$$

A second relation, between the reduced ionization and

recombination rate coefficients, indicates that steady state occurs when the free electrons have a Saha density with respect to the ground state:

B.10 $$I = R$$

Again these equations hold only when all the reduced rate coefficients are symmetric. Under typical T.E.C. conditions, this occurs only when the effect of radiation is negligible with respect collisions. This is typically true for $n \gtrsim 1(14)$ cm-3.

To summarize, it is found that the excited level populations can be determined by approximately quasi-steady conservation equations. These populations are thus functions of the ground state density, the electron density, the electron temperature, and the elementary rate constants. By virtue of the quasi-steady approximation, they are not functions of time history of these variables but only of their present values. Expressions were also written for the effective ionization and recombination rate constants. The conditions for validity of the quasi-steady approximation were found using eigenvector analysis. It was explained why the quasi-steady assumption may fail at high electron densities.

IV.C Some Quasi-steady Ionization-Recombination Results

In the this section, the results of some calculations using the quasi-steady ionization-recombination theory just stated will be discussed. This will illustrate the general features of ionization-recombination behavior without additional abstraction. The theory developed in the next chapter will further explain the results. Results both with and without the effects of laser irradiation will be considered.

Calculation of the quasi-steady ionization and recombination behavior has been performed presently for Cesium. Such calculations have been performed before for Cesium[85,87], as well as for other atoms[e.g.13,93,98,99,100]. The present calculations in Cs have the advantage of over ten years of development of collisional rate constants. As discussed in chapter III, recent theory and experiment indicate that cross-sections from binary encounter theory, used by Norcross and Stone[85], or from Bethe-Born theory, used by Abramov[87], have large errors.

The present results are collisional-radiative computations involving over thirty-seven levels. These levels and the radiative rate constants are as tabulated by Norcross and Stone[85]. Resonance radiation is assumed completely trapped. Doublets and other nearly degenerate orbitals were each compressed to single levels. A Grotrian diagram for this scheme of levels is shown in figure 34.

Tabulated results of these calculations appear in figures 8 to 32. These cover the range of electron temperatures from 1500 to 4500K in 250K steps and of electron densities from 1(12) to 1(15) cm-3 in logarithmic steps. (The tables indicate powers of ten using the computer E-notation.) Figures 8 through 12 show the ionization and recombination rate constants in various forms. Figures 13 through 32 can be used to determine excited state populations. In each of these, a column represents the results for some electron density and the rows for the indicated electron temperatures. Figures 34 through 39 show graphs of excited state populations for various conditions and some different rate constant theories. These and more results will be discussed herein.

As discussed in the last section, two coefficients are needed to determine the excited state populations. These are v and v'. As per equation B.4, the v coefficient indicates how strongly the level population is affected by

the reduced free electron population and the v' coefficient indicates how strongly the population depends on the ground state density. Generally, low lying levels have large v' coefficients and small v coefficients. Conversely high lying levels have large v coefficients while having small v' coefficients. This means low lying levels may be nearly in equilibrium with the ground state population while high levels may be nearly in equilibrium with the free electrons. With respect to the high lying levels and their use in experimental measurements, more will be said later. The transition range between such low levels and high levels is called the bottleneck. When collisions dominate, as at high electron densities, the bottleneck is located among levels with binding energies of about 3.5 times the electron temperature, as found earlier by Mansbach and Keck[51].

An important point to note is that there is generally a local thermal equilibrium between the ground state and the first excited level. This is because this level is below the bottleneck as verified by figures 13 and 14. This is contrary to what incautious application of a common 'rule of thumb' might imply. Many would say that since this transition has such a large energy gap that it would be 'slow.' Also transitions among higher levels in the atom which often have smaller energy spacing would be relatively 'fast.' This would indicate the the first excited state would be in equilibrium with levels above it which would be in equilibrium with the free electrons. Only the ground state would not be in such equilibrium. Such models have been called block-of-excited-states models. The reasoning behind them is as follows. Let us consider the ground to first excited state transition and, for example, the first to second excited transitions:

C1 $Cs(6s) + e \rightarrow Cs(6p) + e$

C.2 $Cs(6p) + e \rightarrow Cs(5d) + e$

To make the first reaction above go, the free electron needs an impact energy of over 1.43eV while in the second reaction only 0.37eV is needed. For Boltzmann distributed electron energies and the temperatures of interest, the former electrons are much rarer than the later. By 'rule of thumb' analysis, this observation is used to indicate that the first reaction is likely to be much slower than the second.

The above 'rule of thumb' reasoning fails because it misses a fundamental if subtle point about reactions among excited states. This point is that the populations of different excited states differ greatly. Looking again at the above reactions, it is apparent that in thermal equilibrium the collision frequency of 6s atoms with 1.43eV electrons is going to be higher than for 0.37eV electrons and 6p atoms since the former are at a lower total energy

level. The actual relative reaction rates are the opposite of the 'rule of thumb' predictions.

For the quite highly excited levels, the same type of reasoning can be applied. However, as the energy differences between these levels are small while their degeneracies are rapidly rising, this means that the transition rates start to increase in the highly excited levels eventually becoming fast enough that a local equilibrium is established between these levels and the free electrons.

The experimental determination of electron temperature from measurements of highly excited level populations must be done with caution however. While a sufficiently high level will be in equilibrium with the free electrons, the number of such levels and their experimental visibility may vary. First, these levels are defined by:

C.3 $$\nu_i \cong \nu_e$$

which means that they have populations in equilibrium with the free electrons. Using the results of section B and equation B.4 in particular, it is seen that this condition is satisfied only if the following two criteria are met:

C.4 $$\nu_i \cong 1$$

C.5 $$\nu_e \gg \frac{\nu_i'}{\nu_i}\nu_0$$

The first of these is met by a generally plentiful number of levels above the bottleneck. The second condition is more stringent and not always appreciated. This is because electron densities in experiments are often well below Saha so that criterion C.5 becomes hard to satisfy. This is illustrated in figure 39 where the populations of excited Cesium levels is plotted against their binding energy for a ground state density of 1(16) cm-3, an electron temperature of 3000K, and various electron densities. For an electron density of 1(15) cm-3, which is very close to Saha, a Boltzmann line is seen indicating the correct electron temperature. For lower electron densities, the highly excited level populations indicate a distinctly wrong temperature because condition C.5 is failed.

Experimentally, an additional complication occurs: even if a level is sufficiently highly excited that it meets both criterion, it may not be experimentally observable. this is due to the significant electron densities typical of thermionic converter conditions. The radiation from such levels is reduced and finally disappears for sufficiently high levels because of Stark broadening as explained by Inglis and Teller[101].

In any event, the region between the levels in near equilibrium with the ground state and the upper levels in near equilibrium with the free electrons there is a transition known as the 'bottleneck.' It is this region whose slow rates dominate the ionization-recombination rate constants. This region exists even if radiation were negligible. The existence of a collisional bottle-neck in the excited states of the atom has been apparent since detailed solutions of the simultaneous system of equations such as in Bates, Kingston, and McWhirter[13], became possible twenty years ago. Confusions about this point though have been perpetuated by interpretations of a paper by Byron, Stabler, and Bortz[15].

Let us turn attention now to the recombination rate constants. By dimensional analysis on Newton's laws of motion for an electron plus classical hydrogen atom system, it is found that the recombination rate may be written:

C.6 $$\beta = C_T \bar{v}_e r_T^5$$

Where: $$\bar{v}_e = \sqrt{8kT_e/\pi m}$$

$$r_T^2 = e^2/kT_e$$

And C_T is a constant. This formula, which correlates experimental and theoretical data very well, was found using different reasoning by Thomson[16], although his assumptions would today be of questionable validity. The quantity C_T can vary only if radiation or quantum effects are included invalidating Newton's laws.

Surveying various determinations of C_T, it is found to be of order one as expected from the dimensional analysis. Many of the experimental determinations have such large scatter, as seen in e.g. [19,51], that while this order of magnitude is verified, nothing more can be deduced. A more recent experiment, by Sayer et. al.[19], claims to use improved measurements of electron temperature and thus have superior consistency and accuracy. They found values of C_T between 0.2 and 0.3. This is a factor of five to ten less than some previous experiments. Theoretical values tend to lie between these two. Use of Mansbach and Keck rate constants, as is done presently, yields a value of about 0.46. The calculations of Norcross and Stone[85] give results in the range of 0.4 to 0.7 between 1500K and 3000K. The theory of Sayer and Pascale[86] implies a value of 0.37. Abramov[87] calculated values ranging from 1.3 to 4 which are large because he used Bethe-Born cross-sections. In the T.E.C. calculations to be presented in Chapter VI, values of 0.31 and 0.46 were tried. There was little difference in the overall results.

Examining now how C_T varies when radiative or quantum effects become important, the results of the present calculations for this quantity are shown in figure 8. First consider the result for high electron density, say 1(15) cm-3, for which collisions dominate. If the atom were classical, C_T would be a constant in this region for all temperatures. The fact that Cesium is not classical but does in fact have discrete levels is seen to have little effect. C_T varies only from a low of .45 to a high of .48 over the entire temperature range. As density declines, radiation becomes more important and C_T does vary. It becomes larger. How much larger depends on the temperature. At low temperatures, the bottleneck is in higher levels where radiation is weaker and the the increase in C_T is smaller than for higher temperatures.

By detailed balance, the theory of Thomson[16] can also be used to predict ionization rate constants. Thus one writes:

$$\text{C.7} \qquad \alpha = \frac{n_s^2}{N_{ref}} \frac{C_T \bar{U}_e k_T^5}{\rho_0}$$

n_s is the Saha density and is exponentially sensitive to temperature. A correction factor ρ_0 has been introduced. If collisions dominate, then detailed balance is valid and ρ_0 would have to equal one. If the loss of spontaneous radiation occurs, ρ_0 will be greater than one. This factor is determined also from the solution of atomic level conservation equations described earlier. When ionization and recombination are in balance, ρ_0 takes on a special significance. When this balance occurs, it can be seen from equation B.6 that:

$$\text{C.8} \qquad \nu_e = \nu_0 / \rho_0$$

Thus ρ_0 determines how far below Saha the electron density will be when the balance exists. ρ_0 is tabulated in figure 11. It is seen that a substantial departure from Saha occurs at low densities. Curiously, ρ_0 is only weakly a function of temperature.

The entire nondimensional constant of C.7, C_T/ρ_0, is shown in figure 12. A substantial reduction from the collision dominated values is seen at low densities. Additionally, the dimensional ionization rate constant, α, and the dimensional recombination rate constant, β, are tabulated in figures 10 and 11 respectively.

The special application of the ionization-recombination theory which is of interest in the present thesis is the determination of the nature of the interaction of resonant radiation and the excited levels of a recombining or ionizing atom, particularly of Cesium . The case of a

strongly recombining plasma will be discussed first. For sufficiently strong recombination, terms involving ν_o can be neglected. When this is true, it follows that:

C.4 $$\nu_i \cong V_i \nu_e$$

C.5 $$\frac{dn_o}{dt} \cong -n_e R \nu_e$$

Under these conditions it is quite possible that there may be population inversions among the atomic excited levels. This means that:

C.6 $$\frac{N_l}{g_l} < \frac{N_u}{g_u}$$

Where l and u are atomic levels with u higher than l. Naturally, if transitions between these two levels are optically allowed and the difference in there populations is greater than the threshold inversion then laser action is possible. As the above equations indicate, two levels will invert if the reduced population coefficients satisfy the inequality:

C.7 $$\frac{V_u}{V_l} > e^{\frac{h\nu}{kT_e}}$$

If spontaneous radiation is negligible, then all the quantities in the above equation are functions only of temperature. If the inequality is satisfied the two levels will invert for large enough ν_e. Otherwise, they will not invert no matter how large ν_e.

A sample population distribution for Cesium under this condition of strong recombination is shown in figure 34. This is a semi-log plot of level population against level energy for and atomic density of 1(16) cm-3, an electron density of 1(14) cm-3, and an electron temperature of 1500K. There is a clear population inversion between the 7p and 7s levels. This graph was made using Mansbach and Keck collisional rate constants. The same type of results occur using various binary encounter theories. This is illustrated in figure 35 which shows Cesium populations under the same conditions as in figure 34 but computed using Stabler[34] theory collisional rates. Although the reasons not to apply dipole moment rules to collisional cross-sections were discussed in chapter III, some calculations have been performed using them and the result seems to be that the 7p-7s inversion disappears. Thus for example, Norcross and Stone[85] did this and obtained no inversion. Also calculations have been done presently using Bethe-Born rates which use these rules and the 7p-7s inversion also disappeared, as shown in figure 36. Note however that the Bethe-Born rates predict another inversion instead, a 7s-5d (optically forbidden) inversion.

Additional calculations have been performed using Gryzinski[42] collisional rates. This is a variation of binary encounter type rates and was also discussed in chapter III. These are the same rates as used by Norcross and Stone, except dipole moment rules were not applied. Assuming ν_e / ν_0 sufficiently large and an electron temperature of 1500K, the excited state populations are plotted in figure 37 for various electron densities. Again a 7p-7s inversion is seen. More of the effects of recombination lasing can be explained in the next chapter.

More population inversions are sometimes predicted to exist in the higher levels of Cesium. Some of these can be seen in the figure 34. Oettinger[17] has found some experimental evidence that such inversions may exist. Unfortunately, theoretical prediction of such inversions is sensitive to the particular rate constants used in the calculations. Different rate constant theories predict different inversions. This being the case, such inversions are not amenable to theoretical study at the present time and shall not considered here any further.

If the recombining plasma discussed above were put in a laser cavity, it is predicted that laser action may occur. Calculations indicating the effects of such radiation on the excited state kinetics have been performed. Since this inversion is so far above threshold, it is a good approximation that the laser action saturates the transition. The population distribution both without radiation and with radiation of sufficient intensity to saturate the transition is shown in figure 38. This data was obtained using the same rate constants and conditions as figure 37. In addition to altering the excited state distributions, the presence of laser radiation changes the recombination rate of the plasma. This change in Cesium for the 7p-7s transition is small.

Laser radiation can produce profound changes in the ionization process. Under normal discharge conditions, i.e. when the plasma is not rapidly recombining, there are no population inversions. Thus when laser radiation is introduced,there will be a net absorption of such and thus a net excitation of the atomic levels. When the radiation is chosen to be resonant with the proper levels, this can result in tremendous increases in the ionization rate constant. This increase can be like lowering the ionization potential of the atom by the amount of the photon energy. This will be elaborated upon in chapter V. Further, if the radiation were chosen resonant with a transition that straddled the bottleneck, then the increase in the ionization rate is given nearly by the net absorption rate of photons, as predicted in the theory of Oettinger and Dewey [18].

The present theory differs from the theories employed in the opto-galvanic literature[103,106,110]. Herein the complete set of simultaneous equations governing the atomic level populations were written and solved. Although limited by the accuracy of the inelastic collision cross-section data, these results are expected to be quantitative.

To summarize, this section has presented results of numerical computations on the excited state populations and ionization-recombination rate constants of a Cesium plasma. The bottleneck was found to be in the excited levels even in the collisional dominated regime. This was explained by a more detailed examination of chemical rules of thumb for excited state kinetics. Recombination rate constants were computed and found to be in good agreement with recent experiments. It was found that for low temperatures and moderately high electron densities there was a population inversion in the Cs excited levels. This prediction survived through calculations employing a variety of elementary rate constants. A calculation under lasing conditions was performed. The inverse process of laser ionization enhancement was also studied. By this method, large increases in the ionization rate are possible. All these computational results will be further explained by the analysis presented in the following chapter.

V Analysis of Ionization-Recombination and, the Equivalent Circuit Concept

While it is possible to solve the ionization-recombination problem on modern computers using the techniques of the last chapter, the results are not always self-explanatory. The results for recombination lasing and ionization enhancement in particular are unintuitive. Why the results of such computations behave as they do and how they can be optimized is not always clear. Because of such conceptual difficulties, it would be advantageous to reduce the system of conservation equations to new equations wherein the interactions among the various levels were represented more simply. Herein such a simplification is found for the collisional terms. Furthermore this simplification is obtained without loss of quantitative accuracy.

Many processes have been suggested to affect ionization-recombination rates in thermionic converter conditions. Examples include possible resonant molecule-cesium inelastic collisions, wall deactivation of excited atoms, atomic impurities, and resonant absorption or emission of laser light. The present simplified conservation equations can be easily applied to such questions. As will be apparent, calculations which would otherwise require use of large modern computers can be performed 'on the back of an envelope' using this technique.

Many of the previously published approximate models of ionization-recombination can be obtained from the present model by specialization of the coefficients. Among these are the block of excited states[88], bottleneck[15], one-quantum[89], diffusion[90,91], and Mansbach-Keck[51] models. The regions of validity of these models can be assessed.

The form of the present simplification is easily understood in terms of the electrical or fluid mechanical analogies discussed in chapter IV. The present theory will transform the atomic circuit of figure 5 to the relatively simpler circuit of figure 6. The analogy, we remember, related collisional transfer rates to fluid flow through pipes or to electrical current flow through resistors. The atomic level populations became analogous to fluid pressures or electrical voltages. This was introduced after expression IV.A.14 in the previous chapter. This reduction to a circuit nearly as simple as that for the one-quantum model will be applied to many sample situations.

V.A Equivalent Circuit Derivation

The conservation equations shall presently be simplified to their equivalent circuit form. This will start by using the separable form of the collisional transition rate constants that was discussed in a previous chapter. With such rates, the conservation equations will be manipulated. The result will the equivalent circuit, as shown in figure 6, and simple expressions for the values of the new resistors in the equivalent circuit.

The present simplification deals with the collisional terms of the conservation equations. It is thus convenient to denote the other effects, radiation, unsteady, or external, all together as a single symbol. The conservation equation for each level i is written:

A.1 $$0 = \sum_j W_{ij} (\nu_j - \nu_i) + S_i$$

The first term represents the net collisional transfer rate into level i. This is a completely general equation as the source term, Si is left arbitrary. Thus Si can include any effects a researcher may wish to add such as, radiation resonant collision rates, radiation, resonant inelastic collisions, and/or unsteady effects. Even corrections for presumed non-separable features of the electron-atom collision rates could be so included. The present theory will make no assumption concerning the magnitude of the terms Si.

In chapter III, the collisional rate constants were discussed. The ones which were selected as having the greatest experimental and theoretical support were written mathematically in a separable form. Advantage will be taken of this form. In the separable form, the collisional rate constants are written as a product of a function of the lower level and a function of the upper level. Thus:

A.2 $$W_{ij} = \begin{cases} L_i U_j & i \le j \\ L_j U_i & i > j \end{cases}$$

Substituting the separable rates into the conservation equation, there results:

A.3 $$\nu_i = \Omega_i \left(U_i \sum_{j<i} L_j \nu_j + L_i \sum_{j>i} U_j \nu_j + S_i \right)$$

Where $$\Omega_i = \left(U_i \sum_{j \le i} L_j + L_i \sum_{j > i} U_j \right)^{-1}$$

This new quantity has the units of a reciprocal rate constant. That makes it analogous to an electical resistor.

Taking the difference between this equation for level i and the equation for level (i-1), and after performing some algebraic manipulation, it results that:

A.4 $$V_i - V_{i-1} = R_i J_i + \Omega_i S_i - \Omega_{i-1} S_{i-1}$$

where two new terms, Ri and Ji, are introduced. The function of the collisional rate constants Ri is defined by:

A.5 $$R_i = \Omega_i \Omega_{i-1} \left(L_i U_{i-1} - L_{i-1} U_i \right)$$

And where the other new quantity Ji is defined by:

A.6 $$J_i = \left(\sum_{j<i} L_j \right) \left(\sum_{j \ge i} U_j V_j \right) - \left(\sum_{j \ge i} U_j \right) \left(\sum_{j<i} L_j V_j \right)$$

This is an unknown as it depends on the unknown populations. The physical significance of Ji is apparent when it is rewritten as:

A.7 $$J_i = \sum_{j<i} \sum_{k \ge i} W_{jk} \left(V_k - V_j \right)$$

Thus Ji is the net collisional flow rate from levels i and above to all levels below i. This makes Ji analogous to an electrical current or fluid mass flow. In the absence of other effects, Ji is the net recombination rate.

While the values of the resistances Ri and Ω_i can be easily calculated, the current Ji is still unknown as it involves all the unknown population variables in its definition. This difficulty can be remedied. In the general case, an expression for Ji can be found by studying the quantity $(J_i - J_{i-1})$. After some algebra it is found that:

A.8 $$J_{i-1} - J_i = S_i$$

Thus, it follows:

A.9 $$J_i = \sum_{j>i} S_j$$

With this information, it becomes possible to interpret equation A.4 in the electrical and/or fluid mechanical analogies. It says that the difference in voltage between i and i-1 is the sum of the voltage drops across three resistors[*]. The first is the resistor Ri which has the current Ji flowing through it. The latter two are the resistors i and i-1 which have currents Si and -Si-1 respectively. It can be seen that this corresponds to the circuit as sketched in figure 6.

At this point it is possible to write down a complete solution for the populations as a function of the source terms. This is done by applying A.9 to A.4 and simplifying. Thus:

A.10 $$V_i = V_e + \Omega_i S_i - \Omega_e S_e - \sum_{j>i} R_{ij} S_j$$

Where the quantity Rij is defined as the sum of all R resistances between levels i and j:

A.11 $$R_{ij} = \begin{cases} \sum_{k=i+1}^{j} R_k & j>i \\ R_{ji} & j<i \end{cases} .$$

To illustrate the use of this theory, some examples will be discussed. First, the solution of the simplest collisional ionization-recombination problem will be performed. This will be followed by two numerical examples of the calculation of the equivalent circuit resistances.

Comparison of the quasi-steady conservation equations for collisional ionization-recombination in section IV.A with the equation A.1 of this section shows that the source terms are given by:

$$S_0 = -(1/n_e)\frac{dN_0}{dt}$$

A.12 $$S_i = 0 \qquad 0<i<e$$

$$S_e = -\frac{1}{n_e}\frac{dn_e}{dt}$$

*. Students of fluid mechanics should substitute the word pressure for voltage and so forth according to the explanation of the analogies as given in section IV.A.

From this and A.8 it follows that the current Ji is independent of i. Thus define J by:

A.13 $$J = J_i \qquad 0 < i < e$$

It follows that:

A.14 $$J = S_e = -S_0$$

Using the solution A.10, the quasi-steady populations can be written:

A.15
$$V_i = V_e - J(R_{ie} + S_e)$$
$$V_0 = V_e - J(\Omega_0 + R_{0e} + S_e)$$

Thus the net recombination rate can be written:

A.16 $$J = \frac{V_e - V_0}{\Omega_0 + R_{0e} + S_e}$$

This is just the difference in voltages between ground and continuum divided by the sum of the resistances between them. Thus for this case the ionization and recombination coefficients are found to be:

A.17 $$I = R = \frac{1}{\Omega_0 + R_{0e} + S_e}$$

They are of course equal because the present model has no radiation. Cases involving various types of radiation will be discussed in later sections.

A couple of simple numerical examples will show how the resistances are calculated. First, consider the (unphysical) case where all the collisional transition rate constants are equal. Thus:

$$W_{ij} = 1 \qquad \text{for all } i,j$$

This can be rewritten in separable rate form as:

$$L_i = U_i = 1 \qquad \text{for all } i$$

It follows immediately that the resistances are given by:

$$R_{ij} = 0 \qquad \Omega_i = 1/N$$

Where N is the number of levels in the system. In the quasi-steady collisional ionization-recombination problem, this distribution of resistances would mean the all the excited levels would have the same reduced populations and this population would be the average of the ground and continuum populations.

As a second numerical example, consider a system with six levels. Suppose the separable rate constants are as in the table:

i=	0	1	2	3	e
Li=	1	2	3	4	5
Ui=	5	4	3	2	1

From this it follows that the resistances are:

i =	0	1	2	3	e
R_i =		1/60	1/108	1/108	1/60
Ω_i =	1/15	1/24	1/27	1/24	1/15

In this case the reduced populations of the excited levels would change monotonically between the ground and continuum levels.

To summarize, the general atomic level conservation equations have been manipulated so as to be reduced to a much simpler system for analyzing collisional transition. If N is the number of levels in the system, each original conservation equation involved N(N-1)/2 resistors, one for each distinct pair of levels. Under the assumption of separable rates, this was reduced to an equivalent circuit involving only 2N-1 resistors. This is often orders of magnitude simpler. As will be shown in the following sections, calculations that would have involved large modern computers can be reduced to back-of-an-envelope type simplicity.

V.B Distribution of Resistance and Limiting Cases

The behavior of the resistances in the equivalent circuit will be discussed. The be the distribution of resistance for the Mansbach-Keck collision rate constants will be compared with the assumed distribution of resistances used in a variety of well-known ionization-recombination models. These models, such as the one-quantum, diffusion, bottleneck, and block-of-excited-states, are of at least qualitative value for some ranges of parameters. The degree of quantitative accuracy can be assessed by comparison with the equivalent circuit resistances.

The equivalent circuit resistances, Ri and Ωi, in Cesium and at various temperatures are tabulated in figures 41 through 51. These cover the temperature range of 500K to 20,000K and give Ωi, Ri, Rie for 37 Cesium levels.

In the block-of-excited-states model it is presumed that the collision rate constants for transitions between excited levels are very large while rate constants for transitions between ground and the excited levels is rate limiting. This approximation is similar to the 'rule of thumb' discussed in section IV.C. To compare this model with the Mansbach-Keck rate constants, it shall be analyzed using equivalent circuit theory. The rate constants for this model are given in separable form by:

$$U_i = W_{oi} \quad ; \quad L_i = \begin{cases} \infty & i > 0 \\ 1 & i = 0 \end{cases}$$

From this it follows that the equivalent circuit resistances are given by:

$$\Omega_i = 0 \qquad i \geq 1$$

$$R_i = 0 \qquad i \geq 2$$

$$\Omega_{01} + R_1 = \frac{1}{\sum_{j=1} W_{oj}}$$

This is as one would expect: the resistances among the excited states are zero in the block-of-excited-states model. Only the resistance between the ground and first excited states is finite. Comparing this with the tables of resistances, it is seen that this is rarely a valid approximation under conditions of present interest.

In another model, it is assumed that the rate limiting transitions occur in the excited levels. This is usually case. For mathematical simplicity it is further assumed that the rate limiting processes are so sharply defined that they occur across just one level. Let that level be k*. This is called the bottleneck and the following model is called the bottleneck model[15]. All rate constants for transitions between levels which are either both above k* or both below k* are considered fast. The separable rate constants that correspond to this model are given by:

Lj large for $j \geq k^*$

Uj large for $j < k^*$

The remaining Lj and Uj are defined by:

$L_i \cdot U_j = W_{ij}$ for $i < k^* \leq j$

It follows that the equivalent circuit resistances are given by:

$$\mathcal{R}_i = 0$$

$$R_i = 0 \qquad i \neq k^*$$

$$R_{k^*} = 1/\left(\sum_{i<k^*\leq j} W_{ij}\right)$$

This implies a two tiered population structure. Levels above and below the bottleneck are each in local thermodynamic equilibrium. Thus:

$$\nu_i = \begin{cases} \nu_e & i \geq k^* \\ \nu_0 & i < k^* \end{cases}$$

Even though the actual bottleneck is not as sharp as in this model, qualitatively correct behavior can often be predicted in this approximation. The above two models are similar in that both assume large rates in some region(s) of the atom so that the resistances are negligible almost everywhere. The difference is that the block-of-excited-states model assumed the important resistance to be between the ground and first excited states while the bottleneck model postulated that the important resistance was somewhere among the excited levels. The following model differs from both of the above by not a priori assuming fast rates anywhere among the atomic levels.

Early work on inelastic collisions indicated that the cross-sections were strongly dependent on the energy gap between the levels, with transitions between closely spaced levels much more likely than less closely spaced levels.

This leads to an approximation in which transitions are neglected unless they occur between adjacent levels. This is called the one-quantum model and has received considerable attention in the literature. While it is now known that the approximation used to develop this model is not quantitative, the resulting model is often useful and instructive. While one quantum rate constants can be incorporated into the separable rate form many ways, the following system has the virtue of simplicity. If the separable rate constants are given by:

$$L_i = X^{i+1}$$

$$U_i = a_i X^{-i}$$

where the a are constants and X is an arbitrary large number, then these rate constants display one-quantum behavior in the limit of large X. It is apparent that the rate constant between adjacent levels is given by:

$$W_{i-1,i} = a_i$$

As x approaches infinity, all other rate constants go to zero, as they should in the one quantum approximation. In this limit, it follows that the resistances are given by:

$$Ri = 1 / W_{i,i-1} \quad ; \quad \mathcal{R}_i = 0$$

Thus a consequence of the one-quantum model is that the resistances $\mathcal{R}_i$ are all zero. As can be seen from the tables, this is not always a good approximation.

The above models have all made assumptions about the relative sizes of collisional rate constants for various transitions. An alternative approach is to make assumptions about the levels themselves. In particular, it has been found to be advantageous in some instances to neglect the discrete nature of the levels and assume rather that the atom has a continuum of bound levels, as a classical atom would . Two applications of this approximation will be mentioned. The simpler is the diffusion model which results from applying the atomic levels continuum approximation to the one-quantum model. The other is the Mansbach and Keck[51] model. This model starts with the full system of separable rates and develops the resistances Rij under the atomic level continuum approximation. Their model is similar to the present equivalent circuit model with the additional level continuum approximation. There are distinct differences though in the treatment of the resistances $\mathcal{R}_i$, and source terms Si are not considered by Mansbach and Keck. Also when the continuum model is found

as a limit of the present theory, it becomes apparent that the Mansbach and Keck model contains a small error due to neglecting a delta function term in the conservation equations. this delta function arises from the atomic level continuum limit of the term SO. Further for their model as extended to include spontaneous radiation, there is an error due to ignoring the resistances $\mathcal{R}_i$.

This concludes the review of simplified ionization-recombination theories. It is shown that each of them can be formulated as some limit of the present equivalent circuit theory. This re-formulation has allowed the limits of qualitative and quantitative accuracy for these models to be assessed by comparison with the actual resistances as given by equivalent circuit theory.

V.C Sensitivity Analysis

For systems of many simultaneous equations, determination of their sensitivity to changes in the value of parameters or introduction of new effects is often a tedious process. The simplicity of equivalent circuit theory however allows the this to be done for the ionization-recombination process quite easily. Several examples will illustrate this. First, sensitivity to changes in the collisional rate constant for the ground to first excited state will be considered. Next the importance of resonance radiation loss will be analyzed. This will be followed by a discussion of the effects of de-activation by heavy particle collisions. While this nowhere near exhausts the list of possible effects that one might want to include for one or another reasons, these discussions will illustrate application of equivalent circuit theory to such problems.

It is sometimes suggested that there may be circumstances under which separable rate constants may not be adequate. It might for example be suggested that such rate constants should fail for the Cesium 6s-6p transition because it is strongly resonant. Write this 6s-6p rate constant as a sum of that given by some scheme of separable rates and a correction that will account for the supposed special nature of 6s-6p. Thus:

C.1 $$W_{01} = L_0 U_1 + Q_{01}$$

With this, it follows that the source terms are given by:

$$S_e = -\frac{1}{n_e}\frac{dn_e}{dt} = J$$

C.2 $$S_1 = Q_{01}(\nu_0 - \nu_1)$$

$$S_0 = -J - Q_{01}(\nu_0 - \nu_1)$$

This can be solved to give the net recombination rate:

C.3 $$J = \frac{\nu_e - \nu_0}{\Sigma_0 + R_{0e} + \Sigma_e - \frac{(\Sigma_0 + R_{01})^2 Q_{01}}{1 + (\Sigma_0 + R_{01} + \Sigma_e) Q_{01}}}$$

By examining the tables of resistance, it is seen that even if the correction Q_{01} were to go to infinity, its effect

would be negligible on the ionization or recombination rates for conditions of interest in thermionic conversion. This is of course because the 6s-6p rate is fast to begin with, and thus kinetically unimportant.

Cesium has a large radiative rate for the resonance 6s-6p transition. While most of this radiation is trapped, the effect of that which escapes will be analyzed. Defining a reduced radiative rate constant:

C.4 $$a_{01} = \epsilon N_1^{v} A_{01}$$

where A01 is the Einstein A-coefficient and ϵ is the escape factor. For this case, the source terms are written:

C.5 $$S_e = -\frac{1}{n_e}\frac{dn_e}{dt} \equiv J$$
$$S_1 = -a_{01}\nu_1/n_e$$
$$S_0 = -\frac{1}{n_e}\frac{dN_0}{dt} + a_{01}\nu_1 = -J + a_{01}\nu_1/n_e$$

It follows that the net recombination rate is given by:

C.6 $$J = \frac{\left[1 + \frac{a_{01}(\Omega_0+R_{01})}{n_e+a_{01}\Omega_1}\right]\nu_e - \nu_0}{\Omega_0+R_{0e}+\Omega_e + (R_{1e}+\Omega_e)\frac{a_{01}(\Omega_0+R_1)}{n_e+a_{01}\Omega_1}}$$

The coefficient of ν_e is the recombination rate constant while the coefficient of ν_0 is the ionization rate constant. Assuming a one per cent escape of this radiation as is typical for thermionic converters, the loss of resonance radiation does not affect the recombination rate constant significantly for Cesium , though it may affect the ionization rate constant at low electron densities.

Another process that may occur is the quenching of excited atoms by collision with some heavy particle. It has been suggested that this may be used to help clear the lower levels in a recombination laser [17]. Without pursuing the possibility of lasing, The analysis of such heavy particle interactions will be set up to indicate the important parameters. It has sometimes been suggested that such heavy particles as noble gases be included in the thermionic plasma to improve the current transport processes. This analysis will also indicate when such additional gases may alter the ionization-recombination kinetics. There is a significant amount of data available on quenching cross-sections for first excited levels of atoms. For nitrogen-cesium collisions there is data on quenching of the first two excited levels. The effect of quenching collisions on the first two excited levels will be

considered. Antonov, Korchevoi, and Lukashenko[92] estimated damping cross-sections of Cs 6p and 5d levels by collision with molecular Nitrogen. The 6p cross-section was found to be 6.0(-15) cm2. While the 5d cross-section was larger, 6.6(-15)cm2, it will be shown to be typically less important.

Writing the quenching coefficients for 6p and 5d as a and b respectively,

$$a = Q_{6p}\,\bar{v}_r\,N^0_{6p}\,N_N/n_e$$

$$b = Q_{5d}\,\bar{v}_r\,N^0_{5d}\,N_N/n_e$$

where $\bar{v}_r$ is the mean relative speed of Nitrogen and Cesium, and N_N is the molecular Nitrogen density. The source terms are:

$$S_e = -\frac{1}{n_e}\frac{dn_e}{dt} = J$$

$$S_2 = -b\,N_2$$

$$S_1 = -a\,N_1$$

$$S_0 = -J + a\,N_1 + b\,N_2$$

The corresponding excitation terms for the molecular collisions are neglected due to the low temperature of neutrals. From this it follows that the 5d population is given by:

$$N_2 = \frac{N_e - (R_{2e}+S_e)\,J}{1+b\,\Sigma_2}$$

The 6p population is:

$$N_1 = \frac{1+\frac{b R_{12}}{1+b\Sigma_2}}{1+a\Sigma_1}\,N_e - \frac{R_{1e}+S_e+\frac{b R_{12}}{1+b\Sigma_2}(R_{2e}+S_e)}{1+a\Sigma_1}\,J$$

Lastly the net recombination rate is:

$$J = \frac{\left[1+\frac{a(R_{01}+S_0)}{1+a\Sigma_1}\left(1+\frac{b R_{12}}{1+b\Sigma_2}\right)+\frac{b(R_{02}+S_0)}{1+b\Sigma_2}\right]N_e - N_0}{\Sigma_0 + R_{0e}+S_e+\frac{a(\Sigma_0+R_{01})}{1+a\Sigma_1}\left[R_{1e}+S_e+\frac{b R_{12}}{1+b\Sigma_2}(R_{2e}+S_e)\right]+\frac{b(R_{02}+S_0)}{1+b\Sigma_2}(R_{2e}+S_e)}$$

Using the Antonov et al. cross-sections, it is found that the N2-Cs(6p) collisions are at least an order of magnitude more important than the 5d collisions.

It has been shown here that a wide variety of effects can be easily analyzed using equivalent circuit theory. Specifically, resonance collisions, resonance radiation, and

molecular deactivation were considered as examples. The simple algebra required in these analyses contrasts with the large computational efforts that would be required without the equivalent circuit.

Commonly, sensitivity analysis is limited to determining merely a partial derivative of some result with respect to a parameter given numerical values for all the parameters. The present theory found the behavior of the result over the whole possible range of the changing parameter. This was done moreover in a general analysis that was not restricted to given numerical values of all the remaining parameters. These results are thus far more useful.

V.D Computation Techniques

One of the features of equivalent circuit theory is the ease with which solutions can be computed. If N levels are under consideration, the populations and rate constants can be computed in time proportional to N for collisional recombination. For collisional-radiative problems, computation can be performed in time proportional to N squared. This contrasts greatly with the order of N cubed needed for the usual solution by Gaussian elimination. The procedures for these calculations will be outlined here.

For both the collisional and collisional-radiative problems the equivalent circuit resistances must be calculated. First the sums

$$A_i = \sum_{j=0}^{i} L_j$$

$$B_i = \sum_{j=i+1}^{e} U_j$$

Are calculated for successive i. This requires O(N) operations. With these sums, the resistances can be calculated:

$$\mathcal{R}_i = \frac{1}{U_i A_i + L_i B_i}$$

$$R_i = \mathcal{R}_i - \mathcal{R}_{i-1}\left(L_i U_{i-1} - L_{i-1} U_i\right)$$

This again requires only O(N) operations and provides all the numbers necessary for solution of the collisional ionization-recombination problem.

If spontaneous radiation is included, more calculations are necessary. The spontaneous radiation source terms are:

$$S_i = \frac{1}{n_e}\left[\sum_{j=i}^{e} a_{ij} \nu_j - \sum_{j=0}^{i-1} a_{ji} \nu_i\right]$$

Note that the source term for each level i depends only on the level populations of that and higher levels. This fact can be used to advantage. Calculations start at the free electron level and proceed to lower levels via the population difference equation V.A.4 and the current equation V.A.9. In this way, only O(N squared) operations are needed to complete the calculation.

In summary, it has been shown how computation times of ionization-recombination problems can be reduced by what is typically one or more orders of magnitude using equivalent circuit techniques. Comparison with usual Gaussian

techniques will also show a large reduction in necessary computer storage. These reductions could be very important if such ionization-recombination calculations were necessary at, say, every grid cell of some larger numerical problem.

V.E Highly Excited Levels

The system of atomic level conservation equations should, in principle, include one equation for each atomic level. As there are a very large number of atomic levels, in particular highly excited levels, this can cause computational difficulties. Many ionization-recombination calculations have simply truncated the number of levels under consideration and sometimes altering the direct ionization and recombination coefficients to account for the missing levels. It is still often necessary to include up to one hundred levels in such calculations. Sometimes researchers have approximated the highly excited levels with a level continuum and then solved an integral equation for them simultaneously with the system of equations for the discrete levels. Burgess and Summers[93] used a system of interpolation to reduce the numbers of equations involved for these levels. With equivalent circuit theory applied to the highly excited levels, however, a much simpler approach results. It is found that the effect of the highly excited levels on the remaining excplicitly considered levels can be represented by effective rate coefficients. These coefficients are of two types. The first is effective direct ionization and recombination coefficients. Such effective rate constants was anticipated by previous direct ionization and recombination rate constant fudging schemes. The second type are effective inter-level rate constants. These are conceptually new.

Suppose m is the highest excited level to be considered discretely. The goal of the present analysis is to eliminate the terms in the conservation equations involving all levels higher than m in favor of terms involving lower level populations as well as the free electron population. The conservation equation for any such lower level i is written now as:

$$E.1 \qquad 0 = \sum_{j=0}^{m} W_{ij}(\nu_j - \nu_i) + W_{ei}(\nu_e - \nu_i) + H_i + S_i$$

where Hi is the net transfer rate into any level i of the discrete levels from the highly excited levels:

$$E.2 \qquad H_i = \sum_{k=m+1}^{e} W_{ik}(\nu_k - \nu_i)$$

The present goal is to express Hi in terms of the free electron population and the lower level populations thus eliminating the highly excited levels altogether from conservation equation E.1. This is done using the present

separable rate-equivalent circuit theory. While other processes such as radiative recombination could be included without much complication, assume the simple, and for present conditions accurate, model that only electron-atom collisions are important for the highly excited levels. From equation V.A.10 the populations of the highly excited levels are:

$$E.3 \qquad \nu_k = \nu_e - R_{ke} J$$

where J is an unknown that must be determined. With J evaluated at level m using the definition V.A.7, and eliminating the highly excited level populations as above, it follows that:

$$E.4 \qquad J = \frac{A_m \nu_e - \sum_{j=0}^{m} L_j \nu_j}{1 + A_m \Lambda_m} B_m$$

where:

$$\Lambda_m = \sum_{k>m} U_k R_{ke}$$

and where Am and Bm are defined by D.1. With this substituted into the net transfer rate, the final result is:

$$E.5 \qquad \dot{H}_i = \hat{W}_{ei} (\nu_e - \nu_i) + \sum_{j=0}^{m} \hat{W}_{ij} (\nu_j - \nu_i)$$

where the rate constants Wej and Wij are defined by:

$$E.6 \qquad \hat{W}_{ej} = \frac{L_j}{1 + A_m \Lambda_m} \sum_{k=m+1}^{e} U_k$$

$$\hat{W}_{ij} = \frac{L_i B_m}{1 + \Lambda_m A_m} L_j \Lambda_m$$

Substituting the above expression for Hi into the conservation equation E.1, it is found:

$$E.7 \qquad 0 = \sum_{j=0}^{m} (W_{ij} + \hat{W}_{ij})(\nu_j - \nu_i) + (W_{ei} + \hat{W}_{ei})(\nu_e - \nu_i) + S_i$$

The goal of eliminating the highly excited levels from this conservation equation has thus been achieved.

The above equation can be interpreted as follows. The above equation indicates that the net transfer between the highly excited levels and any other lower level j can be replaced by effective net transfer rates between j and the continuum and between j and other levels m and below. The coefficient involving j and the continuum can be thought of as an effective ionization-recombination rate constant. It represents 'indirect' ionization-recombination caused by

transfers passing from j or the continuum through the highly excited levels eventually to its continuum or j destination. The formula above gives a systematic method for calculating such effective coefficients replacing earlier approximate schemes. The coefficients involving j and other levels k m indicate a new phenomenon. They are additional effective rate constants for transitions between the discrete levels. This indicates that transfers between two levels j and k can occur not just directly but also indirectly, passing through the highly excited levels. Such effective rate constants had not been included in earlier approximate schemes.

Essential to the present model is the assumption that the highly excited levels are quasi-steady. Because of the small populations and fast transition rates of these levels, this is generally a very accurate assumption. Also because the populations of these levels are so small, energy storage in them can be neglected.

Thus, an analytic scheme, exact within the context of separable rates, has been found which reduces the system of conservation equations to a finite number. This eliminates the need to solve integral equations for such levels, or to retain very large numbers of equations in the system. This can greatly reduce precision and computational time requirements that can be associated with solving up to one hundred or more simultaneous equations. This scheme introduced effective ionization-recombination rate constants and a new type of effective inter-level transfer coefficient.

V.F Spontaneous Radiation

The loss of spontaneous radiation from the plasma can significantly alter the plasma dynamics. While escape of such radiation is a power loss mechanism, the more important effect is often the alteration of the ionization and recombination rate coefficients. These coefficients become dependent on the electron density and Saha detailed balance relations may fail by one or more orders of magnitude. Simple analytic models given here will explain this behavior.

The nature of these effects can be well illustrated by supposing that there is just one radiative transition. This will be from an upper level u to a lower level 1. The source terms for this situation are given by:

$$S_e = \frac{1}{n_e}\frac{dn_e}{dt} \equiv J$$

$$S_u = -\frac{1}{n_e} a V_u$$

$$S_l = \frac{1}{n_e} a V_a$$

$$S_o = -\frac{1}{n_e}\frac{dN_o}{dt} = -J$$

Applying these source terms to the equivalent circuit, the equations may be solved. The net recombination flux is seen to be:

$$J = \frac{V_e}{\Omega_o + R_{oe} + \Omega_e - \frac{a R_{ou}(\Omega_o + R_{ou})}{n_e + a(R_{ou} + \Omega_u)}} - \frac{V_o}{\Omega_o + R_{oe} + \Omega_e + \frac{a R_{ou}(R_{ue} + \Omega_e)}{n_e + a\Omega_u}}$$

The recombination rate constant increases with the loss of spontaneous radiation while the ionization rate constant decreases. Moreover it is apparent that the importance of such radiation to either coefficient depends on the positioning of the upper level on the resistance ladder. If level u is below the bottleneck, then:

$$\Omega_o + R_{ou} \ll R_{ue} + \Omega_e$$

and the radiation will never have a significant effect on the recombination rate. It may however have a dominating effect on ionization. Conversely, if level u is well above the bottleneck, such radiation would have its dominant effect on the recombination rate and possibly only a small effect on ionization.

If the electron density were large enough that radiation had negligible effect, the reduced ground and continuum populations would have the same value in steady state, indicating Saha equilibrium. When spontaneous radiation is important, however, Saha equilibrium will not be achieved. The actual steady state values are found by setting J to zero. Thus from the above equation:

$$\nu_e = \frac{\nu_0}{1 + \frac{a R_{gu}}{n_e + a s_u}}$$

The steady state electron density becomes smaller and smaller as the contribution of radiation increases.

The above model indicates how the excited level populations and ionization-recombination rates behave as the contribution of spontaneous radiation increases. For most purposes, the above one-radiative-transition model is only qualitative. Greater accuracy is achieved by including more transitions but, this is done at the expense of simplicity.

V.G Laser Ionization Enhancement

The possibility of increasing ionization in a plasma by subjecting it to radiation resonant with excited atomic levels is of importance. Under some conditions this may be used as an experimental technique[94,103-111]. It may yield schemes for improved thermionic energy conversion[18]. The behavior of such radiation enhancement will be considered using the tools of equivalent circuit analysis.

Under consideration here are the consequences of letting some radiation, probably of narrow bandwidth, impinge on a plasma. If the frequency corresponds to a transition between two levels of the atom, such radiation may be significantly absorbed and can alter the ionization-recombination kinetics. The two levels that the radiation is resonant with will probably be both excited levels as radiation connecting with the ground state often may have short absorption lengths and be unable to penetrate into the bulk of the plasma. This is currently the case for thermionic converters. This light need not necessarily have a short wavelength. It will be shown that even infrared light can have major effects on the ionization of Cesium.

For collisional ionization-recombination subjected to radiation enhancement, the equivalent circuit analysis proceeds to a simple and powerful result. Suppose the laser radiation were to be absorbed by a transition between a lower level l and an upper level u. The source terms for this situation are:

$$S_e = -\frac{1}{n_e}\frac{dn_e}{dt} = J \qquad S_u = A/n_e \qquad \text{G.1}$$

$$S_l = -A/n_e \qquad S_o = -\frac{1}{n_e} dN_o/dt = -J \qquad \text{G.2}$$

Where A is the net rate of photon absorption. By applying Kirchhoff's laws and the principle of linear superposition it is quickly found that the voltage drop between the continuum and ground is:

$$V_e - V_o = (S_o + R_{oe} + S_e) J + \frac{A}{n_e} R_{lu} \qquad \text{G.3}$$

Solving this for the net ionization rate yields:

$$\frac{dn_e}{dt} = n_e \frac{V_o - V_e}{S_o + R_{oe} + S_e} + \epsilon A \qquad \text{G.4}$$

Where: $$\epsilon = \frac{R_{lu}}{S_0 + R_{le} + S_e}$$

Thus the increase in the ionization rate over the unenhanced case is directly proportional to the net photon absorption rate. For every photon absorbed, ϵ electrons will be ionized.

A previously published formula can be derived as a special case of this. A special case can be considered for which the radiative transition spans the bottleneck. This means:

G.5 $$R_{lu} \approx S_0 + R_{le} + S_e$$

Which leads to the approximation:

G.6 $$\epsilon \approx 1$$

With this last approximation substituted into the equation G.4, the model of Oettinger and Dewey[18] is found.

An important practical parameter for this process is the energy efficiency. This shall be defined as the ratio of the light energy that must be absorbed to ionize an additional atom to the atomic ionization potential. Thus:

G.7 $$\eta = \frac{h\nu/\epsilon}{E_0}$$

It is apparent from this formula that the efficiency so defined need not be less than one. By choosing a transition l-u in the midst of the bottleneck it is easy to obtain efficiencies greater than one. The additional energy, of course, is supplied by the inelastic collisions of atoms with the free electrons.

The net absorption rate of photons can be related to the radiation intensity by examining the level l and u populations. The quantity A is given by:

G.8 $$A = I\sigma\left(N_l - \frac{g_l}{g_u} N_u\right)$$

where I is the intensity, σ is the absorption cross-section, and g_l and g_u are the atomic level degeneracies. Upon solving the equivalent circuit equations, this is written:

G.9 $$A = \frac{I\sigma \Delta N^0}{1 + I/I_{SAT}}$$

Where ΔN^0 is the population difference if no radiation were present:

$$\Delta N^0 = N_l^0\left[\frac{(R_{le}+S_e)\nu_0 + (R_{el}+S_0)\nu_e}{S_0 + R_{le} + S_e}\right] - \frac{g_l}{g_u} N_u^0\left[\frac{(R_{ue}+S_e)\nu_0 + (R_{eu}+S_0)\nu_e}{S_0 + R_{le} + S_e}\right]$$

And the saturation intensity is given by:

$$I_{SAT} = \frac{\nu_e}{\sigma N_0^B \{ \epsilon(\alpha_0 + R_{0R}) + \alpha_e + [\alpha_u + \epsilon(R_{ue} + \alpha_e)] e^{-h\nu/kT_e} \}}$$

By examining the magnitudes of these terms from the tables of resistances, it is apparent that absorption of radiation can tremendously increase the ionization rate. Further, it does so in an energy efficient manner. This efficiency can be unintuitively large: each additional ionization may occur even if the absorbed photon energy is less than the atomic ionization potential. Kinetic analysis also yielded a relation between laser intensity and the net absorption rate. It was found that the full enhancement effect can be obtained even at quite practical low intensities.

It should be remembered that even though the results of the present section are quite simple, they do constitute a complete solution of the quasi-steady collisional ionization-recombination problem. This contrasts with previous theories of the optogalvanic effect[103,106,110].

V.H The Recombination Laser

Recombining plasmas have great potential as a laser or light amplification medium. The possibility that excited state kinetics in recombination can cause population inversions has received much attention in the literature e.g. Gudzenko, Shelepin, Yakovlenko[11], Silfvast et. al.[112-117], and Campbell, Jahn, von Jaskowsky, and Clark[95]. This is both because of the higher power densities available in plasmas, as opposed to solids, liquids, or gases, and because, in some systems, ultraviolet lasing may be achievable. Herein the recombination kinetics of such plasmas will be considered. Use of equivalent circuit concepts allows a simple but general analysis.

The principle of recombination or plasma lasers is as follows. Starting with a hot plasma, the temperature is suddenly lowered. At the new lower temperature the electrons and ions rapidly recombine. This causes dis-equilibrium among the excited levels and population inversions may often occur. Thus, provided with a suitable optical cavity, lasing can result.

The questions to be answered here are when the recombination kinetics allow a population inversion to be established and how much power can be produced. A population inversion is defined by:

H.1 $$N_\ell < \frac{g_\ell}{g_u} N_u$$

In the form of reduced variables this becomes:

H.2 $$\frac{\nu_u}{\nu_\ell} > e^{h\nu/kT_e}$$

This inequality is most likely to be satisfied only when the electron density is much larger than its equilibrium value. As was discussed previously, for sufficiently large electron density the ground state contributions to the excited state populations may be neglected yielding:

H.3 $$\frac{V_u}{V_\ell} > e^{h\nu/kT_e}$$

Where again vl and vu are the free electron quasi-steady population coefficients. Assuming collisional recombination, these coefficients can be expressed in terms of the equivalent circuit resistances so that the inequality simplifies to:

H.4 $$\frac{R_0 + R_{ou}}{R_0 + R_{o\ell}} > e^{h\nu/kT}$$

It is possible that this condition for purely collisional recombination lasing may be satisfied. In other words, it is not always necessary to have additional mechanisms to depopulate the lower level, such as spontaneous radiation or heavy particle collisions.

Such an inversion is predicted to occur in Cesium. The 7p-7s transition is found to be invertible at low temperatures, e.g. 1500K. This is an infrared transition. As the 7p level is a doublet, lasing is predicted on two lines, 3330 and 3411 cm-1. Threshold inversions for this laser, as is typical of electronic lasers, is the order of 1(7) to 1(8) cm-3[96]. These are very small compared with the population densities under consideration here. It is thus reasonable to assume that the transition saturates. In this case the laser efficiency approaches a constant. It is useful to be able to describe the efficiency of a plasma laser. A variety of efficiencies could be defined that would depend on the plasma dynamics. Here an efficiency is defined to reflect the recombination kinetics. This efficiency, let it be called the photon efficiency, is the ratio of the rate at which laser photons are produced divided by the net recombination rate. Thus:

$$\phi = \frac{-A}{dn_e/dt}$$

where A is as defined in the previous section. This number depends on the light intensity in the laser cavity. This number is O(1/3) for the Cs 7p-7s laser predicted here.

The energy efficiency of the recombination laser may be defined as the ratio of the photon energy out to the to the total energy available, i.e., the energy released by recombination. This is simply the product of the quantum efficiency and the photon efficiency.

The power output that can be produced by plasma lasers is quite large. Neglecting distributed losses, the laser power output is the net rate at which photons are produced times the photon energy. Thus:

$$P = h\nu \phi \frac{dn_e}{dt}$$

This is strongly dependent on the electron density. Upon substituting some typical numbers, output powers of one watt per cc to possibly one kilowatt per cc can be produced in a plasma under thermionic converter conditions.

The total laser output energy per pulse can also be estimated. Assuming all electrons recombine and produce photons each, the energy output is:

$$\epsilon h\nu \phi n_e$$

Under thermionic converter conditions, this number is fairly modest, on the order of say tens of millijoules. This is consistent with the energy in ionization in thermionic converters being a small fraction of the overall energies involved. While the thermionic laser may produce very large powers, these powers last only a short time, maybe a few microseconds.

The above formulas assume that spontaneous radiation loss is negligible. If spontaneous radiation loss were included in the model, the laser performance may either be improved or reduced. Spontaneous radiation between levels both above the lasing levels would improve performance by increasing the recombination rate. Loss of spontaneous radiation from a transition between two levels both below the laser levels also increases performance. This is because it helps clear the lower laser level. In fact such radiation reduces the resistance ratio requirements for the purely collisional laser (V.H.4). Unfortunately the remaining type of spontaneous radiation loss, that from a transition which straddles the laser levels, reduces laser performance. This is because it depopulates the upper level and populates the lower level. The Cs 7p-7s inversion suffers from such radiation. It cannot maintain the inversion at electron densities below about 1(13) cm-3.

To summarize, employing equivalent circuit theory, the efficiency, power output, and energy output of recombination lasers can be characterized. A Cesium 7p-7s population inversion is predicted. This is expected to have a photon efficiency of about one third. The criterion for obtaining a purely collisional recombination laser was established in terms of equivalent circuit resistances, and the effects of spontaneous radiation were discussed.

VI Unsteady and Steady Numerical Solutions of Thermionic Converter Plasmadynamics

Although one dimensional, numerical solutions of the thermionic converter plasma equations challenge even modern computers. A new computer program is developed here to solve the thermionic converter plasma equations. The present method uses a relaxation or unsteady formulation. This contrasts with the shooting schemes that have been used previously. Special differencing techniques developed for this study have increased accuracy while decreasing computational requirements. The results of these computations will be discussed for the normal and laser enhanced ignited mode operation as well as the unsteady recombination laser mode. The results of these computations confirm the trends predicted by the simple ignition-isothermal theory discussed earlier.

The computer program that has been developed is capable of including a wide variety of effects. These include microwave electron heating and thermal diffusion. The present study, however, concentrates on the faster-than-Boltzmann rise, proposed laser enhanced ionization mode and the possibility of a thermionic plasma recombination laser.

For steady-state T.E.C. operation, a detailed account of the source of the arc-drops is given. This is done from two points of view: (1) an energy balance, and (2) Kirchhoff's Law. For the various modes of operation studied, the information from these viewpoints is organized in the form of short tables. From these, it is apparent that most of the arc-drop is due to plasma heat losses at the electrodes and that the sheaths play a major role in adjusting the plasma to different operating conditions. This confirms the predictions of chapter II.

VI.A Formulation and Methods

The equations solved and the method for solving them are discussed here. The numerical method benefited from tests against special case exact solutions and these will be described. The numerical method used presently is quite general and may be modified to include many additional effects if so desired.

There are a number of reasons why computational solution of thermionic conversion has been so difficult. One is that in either spatial direction, there are error terms which tend to grow exponentially. Secondly, the problem is a boundary value problem, and the interactions among the boundary conditions make it very difficult to obtain shooting algorithms that converge. Since the present method involves no shooting, neither of these problems occur.

The differential equations solved are those of section II.D in the form with ion current neglected. There are thus two parabolic quasilinear differential equations to be solved. One is for temperature and the other is for density. There is an additional equation to determine the arc-drop. This is the integral equation developed in section II.E, equation II.E. . These equations differ from those used by Yen[8] who neglected diffusion by temperature gradient in comparison with diffusion by density gradient and obtained convergence by assuming a thermal conductivity five times the physical value. The present study obtained convergence without making assumptions about the thermal conductivity. Further, more recent work[9] indicates that the neglect of temperature gradients near the walls is not valid.

The time dependent form of these equations is programmed. Solution proceeds by updating the variables in time using the a predictor-corrector method described in[60]. Since this is a diffusion dominated problem, the time step must be no greater than the order of the square of the spatial distance between mesh points. This implies that the major source of errors will be from spatial not temporal differencing.

Analytical tests of the numerical method proved valuable. Testing of the present method against the special case analytical solutions of the energy equation [9] revealed that special care should be taken when differencing the terms in the energy equation. This is due to the rapidly varying thermal conductivity. Taking advantage of

the information gained in these tests has greatly reduced computational requirements. As yet, no other numerical scheme has been tested against such analytical solutions.

The main result of the comparison with the Lam[9] theory has been that careful numerical treatment of the thermal conductivity term is very important. This term is:

$$\frac{\partial}{\partial \xi} K \frac{\partial \tau}{\partial \xi} \qquad \left(\frac{\partial}{\partial x} k_e \frac{\partial T}{\partial x}\right)$$

By normal differencing techniques one would approximate this as:

$$\left(\frac{K_i + K_{i+1}}{2}\right)\frac{\tau_{i+1} - \tau_i}{\Delta \xi} - \left(\frac{K_{i-1} + K_i}{2}\right)\frac{\tau_i - \tau_{i-1}}{\Delta \xi}$$

which is accurate through second order. This formal accuracy however is misleading. According to [9], the derivatives of temperature with respect to x or ξ are nearly singular near the walls of a small knudsen number converter. In such a case Taylor series expansions are of limited use and thus neither is 'second order accuracy.' Following[9], the solution to this is found to be a change of variables. Using the thermal resistance coordinate η, the derivatives of temperature become well behaved. To take advantage of this, the thermal conductivity term re-written in the mathematically equivalent form:

$$\frac{1}{K} \frac{\partial^2 \tau}{\partial \eta^2}$$

By expanding τ in a Taylor series and using the values of temperature at locations i-1, i, 1+1, the second derivative is found to be:

$$\frac{1}{K_i}\left[\frac{\tau_{i+1} - \tau_i}{\Delta \eta_{i+1}} - \frac{\tau_i - \tau_{i-1}}{\Delta \eta_i}\right]$$

where $\Delta \eta_i$ can be found to sufficient accuracy by assuming a linear variation in thermal conductivity between mesh points. Thus:

$$\Delta \eta_i = \int_{\xi_{i-1}}^{\xi_i} \frac{d\xi}{K} = \frac{\Delta \xi}{K_i - K_{i-1}} \ln \frac{K_i}{K_{i-1}}$$

Using this method of differencing, an order of magnitude fewer mesh points were needed.

The first derivative of temperature was likewise differenced using the η coordinate:

$$\frac{\partial \tau}{\partial \eta} \approx \frac{\Delta \eta_i \frac{\tau_{i+1} - \tau_i}{\Delta \eta_{i+1}} + \Delta \eta_{i+1} \frac{\tau_i - \tau_{i-1}}{\Delta \eta_i}}{\Delta \eta_i + \Delta \eta_{i+1}}$$

Mesh points were also placed at the walls*. Thus no differencing was required to find the first derivatives at the walls. These were found from the boundary conditions using the values of temperature and density at the walls. The second derivative of temperature is thus found:

$$\frac{1}{K}\frac{\partial^2 T}{\partial \eta^2}\bigg|_{\xi_0} \approx \frac{1}{K_0}\,\frac{T_2 - T_1 - \frac{\partial T}{\partial \eta}\big|_{\xi_0}\Delta\eta_1}{\Delta\eta_1^2/2}$$

where point 1 is on the wall and point 2 is next to the wall. This is accurate to first-order.

The remaining differencing techniques used are common. These are documented in the program listing of Appendix A. The program is written in the PL1 language and was run on Princeton's IBM 3033 computer.

---

* Actually, of course, they were not located precisely at the wall but rather at the plasma-sheath interface where the sheath is accurately assumed to have negligible thickness.

VI.B Ignited Mode Operation

Thermionic converter performance will first be considered under steady conditions, with and without laser enhancement. Most attention will be focused on operation below the knee. The difference between the classical-kinetics similarity operation and real kinetics behavior will be emphasized. The prediction of the faster-than-Boltzmann voltage rise will be discussed. This section uses terminology defined earlier in II.E. Laser enhanced performance is then considered. Finally, rapid cooling of the electrons is demonstrated and found sufficient for possible recombination lasing.

The operating conditions chosen to be studied herein correspond to a pressure-distance product of pd=10 torr-mil. Further, the pressure was taken to be one torr and thus d was ten mill (0.254 mm). The ion-atom momentum transfer cross-section was 1(-14) cm2 and the electron-atom cross-section was assumed to be one third of that. The Richardson current was chosen to be 20 Amps/cm2 which corresponds to a Richardson density of 1(13) cm-3. The emitter temperature was 1500K. The collector temperature was 1000K. These are fairly typical operating parameters for thermionic converters.

Referring to the nondimensionalization of section II.D, the above stated conditions imply that the parameter Kn is given be 0.061 while the characteristic time, t_*, is 0.017 microseconds. The electron density was scaled by the reference quantity 1(14) cm-3. The nondimensional current I is given by the actual current J divided by 24 Amps/cm2. The nondimensional Richardson current is thus 0.81. Actual temperatures are divided by 1500K to obtain the nondimensional temperature τ.

To simplify the interpretation of these results, some approximations have been made. As the ionization fraction under conditions of present interest is low, electron-ion momentum transfer collisions have been neglected. Ion emission from the emitter and all emission from the collector are neglected. The effect of radiation on the energy balance is neglected. As the region above the knee of the current voltage curve is not of major interest here, the Schottky effect is ignored. The thermal diffusion ratio is neglected. Again, these simplifications are made to clarify the results. There is no reason why future studies should not or could not include such effects if they were of interest.

For the chosen converter parameters, recombination is generally negligible at the knee and below. If also the ionization rate constant is assumed independent of density, i.e. radiation loss neglected, then the collisional-kinetics similarity holds. The temperature distribution becomes independent of the current level in this regime. The density is linearly proportional to the current. The density rises to a maximum value of about twice I, both non-dimensional. The temperatures are near 3000K. The temperature distribution has hooks at the emitter and collector. This distribution of versus is shown as the lower graph of figure 50.

A notable feature is the small size of the collector sheath height. It is χ_c=0.15 (=0.02eV) or less than a tenth of the electron temperature at the collector sheath edge. Such a small sheath height would invalidate approximations made in the sheath theory. It would also indicate that the plasma flow near the collector had a significant Mach number calling into question some of the plasma approximations. Yen [8] found similarly low collector sheath heights using an entirely different numerical method.

In the collisional kinetics similarity regime, the arc-drop vd is a constant. this means that the current voltage curve rises like a Boltzmann curve. The responsibility for the arc-drop can be divided among the energy losses at the emitter, at the collector, and to ionization-recombination as discussed in section II.E. Computations show that ionization-recombination contributes only 0.53 (0.07eV) to the arc-drop. The thermal energy exchange between the emitter and the plasma in net adds energy to the plasma thereby reducing the arc-drop by 0.83 (0.11eV). The major responsibility for the arc-drop rests on thermal energy loss at the collector amounting to an arc-drop of 3.6 (0.47eV). This gives a total arc-drop of -vd=3.3 (0.43eV). In an alternative view, the arc-drop can be characterized according to where in the plasma it occurs. In this way, most of the arc-drop, 2.4 (0.31eV), is due to the difference between emitter and collector sheath heights. Only 0.93 (0.12eV) occurs in the plasma itself.

All this information about the sources of the arc-drop can be organized. As found in section VI.E, there are two ways of accounting for the arc-drop. One looks at it from an energy conservation point of view and locates the energy sources and sinks. This is manifested by equation II.E.7. The other is to look at it from the point of view of Kirchhoff's law, that is, add the arc-drops from one side to the other. As in double-entry accounting, this can be written in two columns which must sum to the same total. In symbolic form:

T.E.C. voltage accounting

Energy Conservation			Kirchhoff's Law	
gain from emission		$2/j$		
less emitter plasma loss	$-2(1/j-1)/\gamma$		collector sheath	χ_c
less collector plasma loss	-2γ		less emitter sheath	$-\chi_E$
plus volume source		$\Delta Q/I$	plasma gain	$\Delta\chi_p$
total:	v_d	V_a	total: v_d	V_d

Applying this the the specific case just discussed:

T.E.C. voltage accounting

Energy Conservation			Kirchhoff's Law	
gain from emission		3.01		
less emitter plasma loss	-2.18		collector sheath	0.18
less collector plasma loss	-3.62		less emitter sheath	-2.57
plus volume source		-0.53	plasma gain	-0.93
total:	v_d	-3.33	total: v_d	-3.33

From this, it is seen that the major energy loss is the electron flow into the collector. The major voltage drop is the emitter sheath. The total above, v , is the difference between the voltage at the top of the collector sheath and at the top of the emitter sheath. With the assumed Richardson current, this implies an electrode to electrode voltage difference, v , which is lessened by the amount of the double sheath rise, $\Delta\hat{\chi}$, yielding an overall voltage drop of -3.25. The vacuum ideal voltage rise for this case is v =0.41 and thus the real converter is 3.74 (0.48 V) less than this. Because of the classical-kinetics similarity, the values in the table above remain unchanged throughout the double-sheath regime.

These results compare well with the isothermal-ignition theory presented in sections II.E and II.F. This theory predicted a temperature of 2.21 (3300K) while the numerical results indicate that the electron temerature varies from a peak of 2.22 on the emitter side to a minimum at the collector of 1.81 (2700K). This theory predicted an ionization voltage loss, $\Delta Q/I$, of 0.48 while the computer solution gave a value of 0.53. The nonisothermal computer solution gave a superior voltage performance, v_d=-3.33 against -3.58 for isothermal theory. This improved performance is principally because isothermal theory overestimates the electron energy loss rate at the collector. The maximum density predicted by isothermal theory was 0.6 (6(13) cm-3) and this is similar the computed result of 0.9 (9(13) cm-3).

Under the present assumptions, the collisional ionization kinetics similarity solution will fail for one of two reasons as current is increased. Both of these happen because the density rises with rising current. For one, this failure can occur if the density rises to a level for which recombination becomes important. It could also fail if the plasma density rises to a level where the double-sheath is suppressed. Which failure occurs first depends on the relative sizes of the Saha density at the ignition temperature and the emitter Richardson density. At the pressure-spacing product, pd, chosen for the present study, the double-sheath is suppressed first. This occurs at I=.54 (13 A/cm2). Above this the arc-drop rises rapidly, the sheath heights rise, and ion current eventually becomes more important. For a sample case of I=0.7 (17 Amps/cm2), the voltage accounting is:

T.E.C. voltage accounting

Energy Conservation		Kirchhoff's Law	
gain from emission	2.34		
less emitter plasma loss	-0.78	collector sheath	3.57
less collector plasma loss	-3.74	less emitter sheath	-9.11
plus volume source	-2.87	plasma gain	0.49
total: v_ℓ	-5.05	total: v_ℓ	-5.05

Again, this is for the case where collisional kinetics is assumed and c_T=0.31. It is seen that there are major changes between this single sheath case and the preceding double sheath case. First, the ionization voltage drop has increased six-fold and is now a major portion of the overall arc-drop. Secondly, the sheath drops are much larger. In fact, if they were any larger, ion current would become important. The total voltage difference is -5.05 (0.65 V). The vacuum ideal voltage difference is 0.15 (0.02 V) and thus the actual drop is poorer by 5.21 (0.67 V). These numbers agree well with the trends given by isothermal theory as before The major difference however is that isothermal theory underestimates the density by a factor of two in this case. As a result it underpredicts the ionization voltage loss. As this term is a significant part of the energy loss in this single sheath regime the predicted voltage difference, v_ℓ, is too small, being -4.4 versus -5.05 as shown above.

The above calculations were all done with collisional kinetics for ionization-recombination. If (real) collisional-radiative kinetics are used some different behavior results. First, the similarity behavior ceases. As discussed earlier, as the current decreases, the density decreases, the ignition temperature rises, and thus the arc-drop rises. This causes the faster than Boltzmann rise

of the current voltage characteristic. This manifests itself through decreased energy inflow at the emitter and increased energy loss at the collector. This appears both as increased sheath loss and increased plasma drop.

This effect appeared in the numerical calculations done using real ionization and recombination rate constants as described in chapter IV. Again consider the case of I=0.5. With real collisional-radiative kinetics, the voltage accounts become:

T.E.C. voltage accounting

Energy Conservation		Kirchhoff's Law	
gain from emission	3.02		
less emitter plasma loss	-2.15	collector sheath	0.17
less collector plasma loss	-3.53	less emitter sheath	-2.50
plus volume source	-0.55	plasma gain	-0.89
total: v_ℓ	-3.21	total: v_ℓ	-3.21

This case has a voltage drop 3.54 (0.46 V) greater than the vacuum ideal case. Now, as the current level is reduced, the ignition temperature rises and reduced performance is found. For the case I=0.02, again with real kinetics, there results:

T.E.C. voltage accounting

Energy Conservation		Kirchhoff's Law	
gain from emission	2.94		
less emitter plasma loss	-2.24	collector sheath	0.35
less collector plasma loss	-3.97	less emitter sheath	-2.94
plus volume source	-0.54	plasma gain	-1.22
total: v_ℓ	-3.81	total: v_ℓ	-3.81

This voltage drop is 4.20 (0.54 V) greater than the vacuum ideal voltage. This is seen to arise from increased energy outflows from the plasma to the walls as well as reduced energy inflow from emission at the emitter. The sheath heights and the plasma voltage drops are all larger.

All these results compare well with the isothermal-ignition theory predictions. For I=0.5, the predicted temperature was 2.16 (3240K) while in the computed solution the temperature ranged from 2.18 to 1.77. The predicted voltage difference, v_ℓ=-3.46, was larger the the actual drop of -3.21 due to overestimation of the collector temperature in the isothermal model. As the current is reduced from I=0.5 to I=0.02, the isothermal predicted

temperature rises greatly to a value of 2.54 (3800K). The numerical temperatures were close to this prediction, having a maximum of 2.46 and a minimum of 1.98. The predicted arc-drop was 4.56 (0.59 V), again larger than the numerical calculation of -3.81 for the same reason as before.

Thus, the faster-than-Boltzmann rise predicted in chapter II is verified in the numerical calculation. While the two dimensional effects to which this rise is commonly attributed may or may not be significant, they are not the only possible cause. The rise is explained presently by the deterioration of ionization rates at lower electron densities, and the magnitude of this effect is the same order as seen experimentally. Note though, that additional effects may also contribute to this rise but have been ignored here. For one, radiation power loss, commonly neglected as small at high electron densities, can have an observable effect at the low electron densities discussed here. Secondly, as the density decreases further, non-Maxwellian electron energy distribution effects start to play a role. Again, these are all effects which degrade performance and become significant at lower electron densities.

The performance of laser enhanced thermionic conversion can be analyzed with the present computer program. The important factor to be considered here is how much additional power would a laser enhanced thermionic converter produced over an unenhanced converter, and how does this power compare with the laser input power used. The question of how efficiently the laser light can be produced will be considered subsequently.

One laser enhancement frequency is considered here. This corresponds to the Cs 7s-7p infrared transition. It is supposed that the thermionic plasma is subjected to strong radiation on this wavelength. From the ionization-recombination theory discussed in chapter IV, new rate constants are calculated and employed in the present plasma solution.

The counter-intuitive result of isothermal theory for laser enhancement is confirmed. The act of injecting laser energy into the plasma lowers the electron temperature. Since it lowers the electron temperature, it lowers the arc-drop.

For numerical study of 7s-7p enhancement, it was chosen to study a current near the knee, I=0.5. With the enhancement, the temperature dropped about 0.09 (120K) while the density rose about 7 per cent. The temperature distributions with and without the enhancement are shown in figure 53. The density distributions with and without enhancement are displayed in figure 54. The overall effect that this had on the arc-drop is shown in the voltage

accounts for the enhanced converter:

T.E.C. voltage accounting

Energy Conservation		Kirchhoff's Law	
gain from emission	3.06		
less emitter plasma loss	-2.16	collector sheath	0.28
less collector plasma loss	-3.35	less emitter sheath	-2.34
plus volume source	-0.49	plasma gain	-0.87
total: v_ℓ	-2.94	total: v_ℓ	-2.94

Comparing this with the results given previously for the unenhanced case, a reduction of the energy loss at the collector is seen. There is also a slight reduction in the ionization energy loss. Further, the collector sheath height has increased while the emitter sheath height has dropped. Overall, v_ℓ has declined by .19 (24 mV) and the total arc-drop, v_T, declines by about the same amount. To obtain this arc-drop some laser power had to be supplied. This power is appropriately measured by the size of the voltage drop through which the output current of the thermionic converter would need to pass in order to create it. This voltage drop is called the Rasor equivalent drop. The Rasor equivalent drop for the laser power supplied to the plasma is 0.03 (8 mV). Thus three times as much power is produced by laser enhancement as is consumed by it. This unfortunately means that the production of the laser light need to be fairly efficient

No common laser would be sufficiently efficient to make this an overall energy producing process. For this purpose, however, an uncommon laser has been designed. Unlike common lasers which use electricity and produce heat as a byproduct, the presently proposed laser uses heat and produces electricity as a byproduct. The principal behind this laser is to use a thermionic converter operating at some high current level and suddenly reduce the current. When this happens the electron temperature is quickly decreased so that strong recombination occurs and a recombination laser becomes possible. A system of thermionic converters can thus be imagined wherein some would be acting as recombination lasers while others would be benefiting from laser enhanced operation.

The overall efficiency of this recombination laser will be determined by factors other than the characteristics of the laser. As was discussed in chapter II the laser power is only a small fraction of the power into ionization. Further, the power into ionization is a fraction of the other powers involved. Thus the efficiency of a recombination laser using an unsteady thermionic converter will be determined by the behavior of an unsteady thermionic

converter and not the behavior of the laser. The efficiency of an unsteady thermionic energy conversion cycle is a topic of current research and not addressed here.

To demonstrate that an unsteady thermionic converter can produce conditions under which recombination lasing is possible, a time dependent simulation of T.E.C. performance was computed. In the sample case chosen, the thermionic converter is initially in steady state at a current of I=0.5. This is reduced to I=0.1 and held constant. It is found, as expected, that the temperature drops much more rapidly than the density. Also, the temperature drops to a level very close to the emitter wall temperature. This is illustrated by the plot of centerline, $\bar{x}$=0.5, temperature and density versus time shown in figure 55. According to the results of chapter IV, most of the plasma is suitable for recombination lasing during this decay. A sample population distribution of the atomic levels in Cesium for a time 0.5 microseconds after the current decreases is shown in figure 56. A 7p-7s population inversion is indicated. Thus the ability of an unsteady thermionic converter to produce the conditions necessary for recombination lasing is confirmed. A difficulty in the computation occurs at 3.1 microseconds after the current is reduced. This is seen in figure 57 where the sheath heights are plotted against time. The emitter sheath height is seen to decline initially, reach a minimum at 0.5 microseconds and then rise. The collector sheath height behaves differently. It quickly rises to a peak after the current is dropped and then declines steadily. It is still steadily declining when it reaches zero signifying that the electron density at the collector plasma-sheath interface is insufficient to supply to required current without invalidating the underlying assumptions of the differential equations developed in chapter II. Thus further computation cannot be performed within the context of the present physical model.

In summary, computational solution of the thermionic converter plasma equations has been presented herein for steady and unsteady operation. These results give density and temperature distributions within the thermionic converter as well as the overall current-voltage characteristics . The faster-than-Boltzmann rise predicted in Chapter II has been verified. Overall, the results agree quite well with the trends predicted by simple ignition-isothermal theory. Further, laser ionization enhancement of thermionic converter operation has been verified. The ability of unsteady thermionic converter operation to generate the condition necessary for recombination lasing is confirmed.

VII Summary and Conclusion

Many aspects of thermionic energy conversion are examined in the preceding chapters. The ionization and recombination kinetics of Cesium are studied and computed. A new result, the equivalent circuit, was obtained. The effects of ionization and recombination kinetics on thermionic converter plasma dynamics are considered using two methods. A simple isothermal model is developed in Chapter II. This explains thermionic behavior and predicts trends. To verify such predictions, a numerical computer code is developed which is capable of solving for unsteady as well as steady thermionic converter behavior. All these techniques are applied to the study of laser ionization enhancement and the possibility of a Cesium thermionic recombination laser.

Towards a maximizing physical insight while minimizing unnecessary mathematical complications, a simple isothermal model is developed. This model which combines simplicity with closure highlights the physical features on the thermionic converter plasmadynamics. A number of interesting results were obtained. For one, the double sheath obstruction at the emitter was found to be beneficial to thermionic performance. This is a result of the obstruction's reducing thermal losses. Secondly, energy addition to the plasma is shown to reduce the electron temperature. The main features of this model are the generalized ignition condition, II.F.6, the energy balance condition, II.E.13, and the arc drop equation, II.E.11. As discussed in section II.F, this model can be closed and solved graphically.

One of the immediate implications of the isothermal model is that the faster than Boltzmann rise of the current voltage characteristic can be explained in a one-dimensional model. This was shown to be due to lower ionization rate constants that exist at lower electron densities due to increased radiative loss.

Because of the importance of elementary electron-atom inelastic collision cross-sections on the overall ionization-recombination rate constants, these were studied. As summarized in Chapter III, it is found that cross-section theories used in earlier calculations had serious flaws. Using recent experimental evidence, a different set of cross-sections was chosen. Thus an improved set of Cesium ionization and recombination rate coefficients could be computed and were tabulated.

The effects of the complete system of electron-atom inelastic collisions on the ionization-recombination problem are shown to reduce to a system nearly as simple as the well-known "one-quantum" approximation. This reduction is shown to be exact for collisional rates of the type chosen in Chapter III. The reduced system is illustrated in terms of an equivalent circuit in figure 6. As a consequence the effects of other processes such as recombination lasing, resonant atom-atom collisions, and resonant radiation enhanced ionization can be analyzed simply, analytically, and quantitatively. A number of well-known ionization-recombination approximations are limiting cases of this theory. These include the one-quantum, diffusion, bottleneck, and Mansbach-Keck models as well as others discussed in section V.B. The resonant radiation ionization enhancement process is analyzed and it is shown why large enhancements are possible. A simple expression for the photon efficiency of this process is derived in section V.G. A Cesium recombination laser is predicted and the magnitudes for the population inversion and the laser efficiency are derived.

To verify the trends predicted by isothermal theory, a finite difference computer program is constructed. It is capable of solving for both unsteady and steady thermionic converter behavior including possible laser ionization enhancement or atomic recombination lasing. This method of solution contrasts with previously used marching or shooting schemes which suffer from exponentially growing error terms.

The contrast between the results of the complex computer program and the simple isothermal theory is great. The predicted trends from both approaches agreed for the cases studied herein. It is tempting to conclude that the complications of a complete numerical solution of the governing differential equations is unnecessary since isothermal theory works nearly as well. However, there is as yet no method for estimating the error in the isothermal approximation. Lacking such an estimate, isothermal theory cannot stand on its own. It does remain useful as an explanatory tool.

Using the above developments, a proposal to improve thermionic converter performance using laser radiation is considered. In this proposed scheme, laser radiation impinging on a thermionic plasma enhances the ionization process. The consequences of this are that the ignition temperature is reduced and that implies that the ohmic losses will decline since less heating is required to maintain the new lower electron temperature. For the ohmic losses to decline, the density will need to rise. The reduced electron temperature means a reduced arc-drop and thus superior performance. A source for such radiation may possibly a Cesium recombination laser operating in a different thermionic converter.

It appears that such a system may be energy efficient overall. Laser ionization enhancement was found to be quite energy effective, as discussed in sections II.H, V.G, and VI.B. The increase in electrical power output is at least twice the laser power input. It was also found that the necessary laser light could be produced during unsteady operation of a thermionic converter, as considered in II.I, V.H, and VI.B. This laser is infrared with a photon energy of 0.41 eV. The efficiency of this laser, which operates on the Cesium 7p-7s transition, could not be established under the present physical model. Ionization enhancement on the 7p-7s frequency unfortunately saturates when the reduction on the arc-drop is only the order of ten millivolts. This effect is likely too small to be of commercial importance.

Although the effect of the 7p-7s laser studied is not large, these studies do indicate however that laser enhancement has a great potential for reducing or eliminating the plasma arc-drop. To realize such gains, higher frequency resonant laser sources are needed. Thus further studies should be directed towards finding superior laser sources.

REFERENCES

1. S.W. Angrist, Direct Energy Conversion, Allyn and Bacon (1976), Chapter 6

2. G.N. Hatsopoulos and E.P. Gyftopoulos, Thermionic Energy Conversion, Volume I and II, MIT Press: Cambridge (1979)

4. B. Ya. Moizhes and G.E. Pikus (eds.), Thermionic Converters and Low-Temperature Plasmas

4. F.G. Baksht and V.G. Yur'ev, Sov. Phys. Tech. Phys., 21 531 (1976)

5. S.H. Lam, Annual Progress Report, DOE contract AT(11-1)-2533 (1975)

6. S.H. Lam, Annual Progress Report, DOE contract AT(11-1)-2533 (1976)

7. A.T. Yen, A Theory of Thermionic Energy Converter with Variable Plasma Electron Temperature, Masters thesis, Princeton University (1978)

8. J. Lawless and S.H. Lam, Annual Progress Report, DOE contract AT(11-1)-2533 (1978)

9. S.H. Lam, paper 5D2, IEEE International Conference on Plasma Science, Montreal Canada (1979)

10. D.R. Wilkins and E.P. Gyftopoulos, J. Appl. Phys., 37 3533 (1966)

11. L.I. Gudzenko, L.A. Shelepin, and S.I. Yakovlenko, Sov. Phys.-Usp. 17 848 (1975)

12. S.T. Belyaev and G.I. Budker, Plasma Physics and the Problem of Controlled Thermonuclear Reactions, 3 41 (1958)

13. D.R. Bates, A.E. Kingston and R.W.P. McWhirter, Proc. Roy. Soc. A267 297 (1962)

14. D.R. Bates, Proc. Roy. Soc. A 337 15 (1974)

15. S. Byron, R.C. Stabler and P.I. Bortz, Phys. Rev. Letters 8 376 (1962)

16. J.J. Thomson, Phil. Mag. 44 337 (1924)

17. P.E. Oettinger, paper 2C8, IEEE International

Conference on Plasma Science, Monterey California (1978)

18. P.E. Oettinger and C.F. Dewey, AIAA Journal 8 880 (1970)

19. B. Sayer, J.C. Jeannet, J. Lozingot, and J. Berlande, Phys. Rev. 8 3012 (1973)

20. J.R. Oppenheimer, Phys. Rev. 32 361 (1928)

21. K.L. Bell and B.L. Moiseiwitsch, Proc. Royal Soc. A276 346 (1963)

22. S. Geltman, J. Phys. B 4 1288 (1971)

23. J.A. Schaub-Shauer and A.D. Stauffer, J. Phys. B 13 1457 (1980)

24. R.J. Glauber, in Lectures in Theoretical Physics, (W.E. Brittin, ed.) Interscience: New York (1959)

25. G.C. McCoyd, S.N. Milford, and J.J. Wahl, Phys. Rev. 119 149 (1960)

26. M.J. Seaton, Proc. Phys. Soc. 79 1105 (1962)

27. J.J. Thomson, Phil. Mag. 23 449 (1912)

28. E. Rutherford, Phil. Mag. 21 669 (1911)

29. L.H. Thomas, Proc. Cambridge Phil. Soc. 23 714 (1927), and 23 829 (1927)

30. E.J. Williams, Nature 119 489 (1927)

31. D.L. Webster, W.W. Hansen, F.B. Duveneck, Phys. Rev. 43 839 (1933)

32. M. Gryzinski, Phys. Rev. 115 374 (1959)

33. I.V. Ochkur and A.M. Petrun'kin, Opt. Spectr. 14 457 (1963)

34. R.C. Stabler, Phys. Rev. 133 A1268 (1964)

35. A. Burgess, Proc. Symp. Atomic Collision Processes in PLasmas, Culham (1964)

36. A. Burgess, in Atomic Collision Processes (M.R.C. McDowell, ed.) (1963)

37. L. Vriens, Phys. Rev. 141 88 (1966)

38. L. Vriens, Proc. Phys. Soc. 89 13 (1966)

39. M.R.C. McDowell, Proc. Phys. Soc. 89 23 (1966)

40. R. Abrines, I.C. Percival, and N.A. Valentine, Proc. Phys. Soc. 88 885, (1966)

41. M. Gryzinski, in Atomic Collision Processes, (M.R.C. McDowell, ed.) (1964)

42. M. Gryzinski, Phys. Rev. 138 A305,A322,A336 (1965)

43. B.B. Robinson, Phys. Rev. 140 A764 (1965)

44. I.V. Ochkur, Soviet Physics JETP 18 503 (1964)

45. I.C. Percival and D. Richards, Proc. Phys. Soc. 92 311 (1967)

46. I.C. Percival, J. Phys. B 6 2236 (1973)

47. L.C. Johnson, Astrophys. J., 174 227 (1972)

48. C.S. Gee, I.C. Percival, J.G. Lodge, and D. Richards, Mon. Not. R. astr. Soc. 175 209 (1976)

49. F. Devos, J. Boulmer, J.F. Delpech, J. Physique 40 215 (1979)

50. I.C. Percival, J. Phys. B 6 93 (1973)

51. P. Mansbach and J. Keck, Phys. Rev. 181 279 (1969)

52. M.S. Dimitrijevic and P.V. Grujic, J. Phys. B 12 1873 (1979)

53. P.V. Grujic, J. Phys. B 6 286 (1973)

54. V.F. Brattsev and V.I. Ochkur, Zh. E. Teor. Fiz. 52 955 (1967)

55. R. Abrines, I.C. Percival, and N.A. Valentine, Proc. Phys. Soc. 89 515 (1966)

56. J.A. Kunc, J. Phys. B 13 587 (1980)

57. I.C. Percival and D. Richards, J. Phys. B 12 2051 (1979)

58. M. Gryzinski, J. Kunc and M. Zgorzelski, J. Phys. B 6 2292 (1973)

59. D.R. Bates and R. Snyder, J. Phys. B 6 L159 (1973)

60. K. Meintjes, Ph.D. Thesis, Princeton University, (1980)

61. R.B. Bernstein, Advances in Atomic and Molecular Physics 15 167 (1979)

62. K. Binder, Topics in Current Physics 7 1 (1978)

63. R. Akerib and S. Borowitz, Phys. Rev. 122 1177 (1961)

64. L. Vainshtein, L. Presnyakov, I. Sobel'man, Soviet Physics JETP 18 1383 (1964)

65. R. Srivastava and D. K. Rai, J. Phys. B 11 309 (1978)

66. M.J. Seaton, p375 in Atomic and Molecular Processes (D.R. Bates, ed.) (1962)

67. N.F. Mott and H.S.W. Massey, The Theory of Atomic Collisions (1965)

68. R. Peterkop and V. Ya Veldre, Advances in Atomic and Molecular Physics, 2 264 (1966)

69. H.S.W. Massey, E.H.S. Burhop, and H.B. Gilbody, Electronic and Ionic Impact Phenomena, 2nd edition (1974)

70. S. Geltman, Topics in Atomic collision Theory, Academic Press:New York (1969)

71. A.R. Holt and B.L. Moiseiwitsch, Advances in Atomic and Molecular Physics, 4 143 (1968)

72. R.K. Nesbet, Advances in Atomic and Molecular Physics, 13 315 (1977)

73. B.L. Moiseiwitsch, Reports on Progress in Physics, 40 843 (1977)

74. M.R.H. Rudge, Advances in Atomic and Molecular Physics, 9 48 (1973)

75. M.K. Gaylitis, Soviet Physics-Usp. 18 600 (1976)

76. D.G. Truhlar, D.G. Cartwright and A. Kupperman, Phys. Rev. 175 113 (1968)

77. B.L. Moiseiwitsch, p.471 in Atoms, Molecules, and Lasers, International Atomic Energy Agency, (1974)

78. P.G. Burke, p.525 in Atoms, Molecules, and Lasers, International Atomic Energy Agency, (1974)

79. J.C. Keck, Advances in Chemical Physics, 13 85 (1967)

80. J.C. Keck, Advances in Atomic and Molecular Physics, 8

39 (1972)

81. I.C. Percival and D. Richards, Advances in Atomic and Molecular Physics, 11 2 (1975)

82. A. Burgess and I.C. Percival, Advances in Atomic and Molecular Physics, 4 109 (1968)

83. D.R. Bates, Physics Reports 35 307 (1978)

84. B. Makin and J.C. Keck, p.510 in Atomic Collision Processes, (M.R.C. McDowell, ed.) (1964)

85. D.W. Norcross and P.M. Stone, J. Quant. Spectrosc. Radiat. Transfer, 8 655 (1968)

86. B. Sayer and J. Pascale, C.R. Acad. Sci. (Paris) 273 453 (1971)

87. V.A. Abramov, High Temperature, 3 18 (1965) 88. L.M. Biberman and K.N. Ul'yanov, Opt i Spektr 16 395 (1964)

89. V.S. Vorob'ev, Sov. Phys. JETP, 24 218 (1967)

90. L.P. Pitaevskii, Sov. Phys. JETP 15 919 (1962)

91. A.V. Gurevich and L.P. Pitaevskii, Sov. Phys. JETP 19 870 (1964)

92. E.E. Antonov, IU. P. Korchevoi, and V.I. Lukashenko, High Temperature 14 1032 (1977)

93. A. Burgess and H.P. Summers, Mon. Not. Roy. Astr. Soc. 174 345 (1976)

94. R.M. Measures, J. Applied Physics 39 5232 (1968)

95. E.M. Campbell, R.G. Jahn, W.F. von Jaskowsky, and K.E. Clark, Appl. Phys. Lett. 30 575 (1977)

96. A. Corney, Atomic and Laser Spectroscopy, Oxford University Press: New York (1977)

97. B. Laskowski, paper 2E7, IEEE International Conference on PLasma Science, Madison Wisconsin, May 1980

98. L.C. Johnson and E. Hinnov, J. Quant. Spec. Rad. Trans., 13 333 (1973)

99. H.W. Drawin and F. Emard, Z. Physik 270 59 (1974)

100. T. Fujimoto, J. Quant. Spec. Rad. Trans. 21 439 (1979)

101. D.R. Inglis and E. Teller, Astrophys. J., 90 439 (1939)

102. M. Gailitis, and R. Damburg, Proc. Phys. Soc. 82 192 (1963)

103. D.M. Pepper, IEEE J. Q. El., 14 971 (1978)

104. F.M. Penning, Physica(Ultrecht), 8 137 (1928)

105. R.B. Green, R.A. Keller, G.G. Luther, P.K. Schenck, and J.C. Travis, Appl. Physics Lett. 29 727 (1976)

106. J.E. Lawler, Phys. Rev. A, 22 1025 (1980)

107. K.C. Smyth, R.A. Keller, and F.F. Crim, Chem. Phys. Lett., 55 473 (1978)

108. E.F. Zalewski, R.A. Keller, and R. Engleman, Jr., J. Chem. Phys., 70 1015 (1979)

109. R.A. Keller, R. Engleman, Jr., and E.F. Zalewski, J. Opt. Soc. Am., 69 738 (1979)

110. G. Erez, S. Lavi, and E. Miron, IEEE J. Q. El., 15 1328 (1979)

111. R.A. Keller, and E.F. Zalewski, Appl. Optics, 19 3301 (1980)

112. W.T. Silfvast, L.H. Szeto, and O.R. Wood II, Appl. Physics Lett. 31 334 (1977)

113. W.T. Silfvast, L.H. Szeto, and O.R. Wood II, Appl. Physics Lett. 33 936 (1978)

114. W.T. Silfvast, L.H. Szeto, and O.R. Wood II, Appl. Physics Lett. 34 213 (1979)

115. W.T. Silfvast, L.H. Szeto, and O.R. Wood II, J. Appl. Phys., 50 7921 (1979)

116. W.T. Silfvast, L.H. Szeto, and O.R. Wood II, Appl. Physics Lett. 36 500 (1980)

117. W.T. Silfvast, L.H. Szeto, and O.R. Wood II, Appl. Physics Lett. 36 615 (1980)

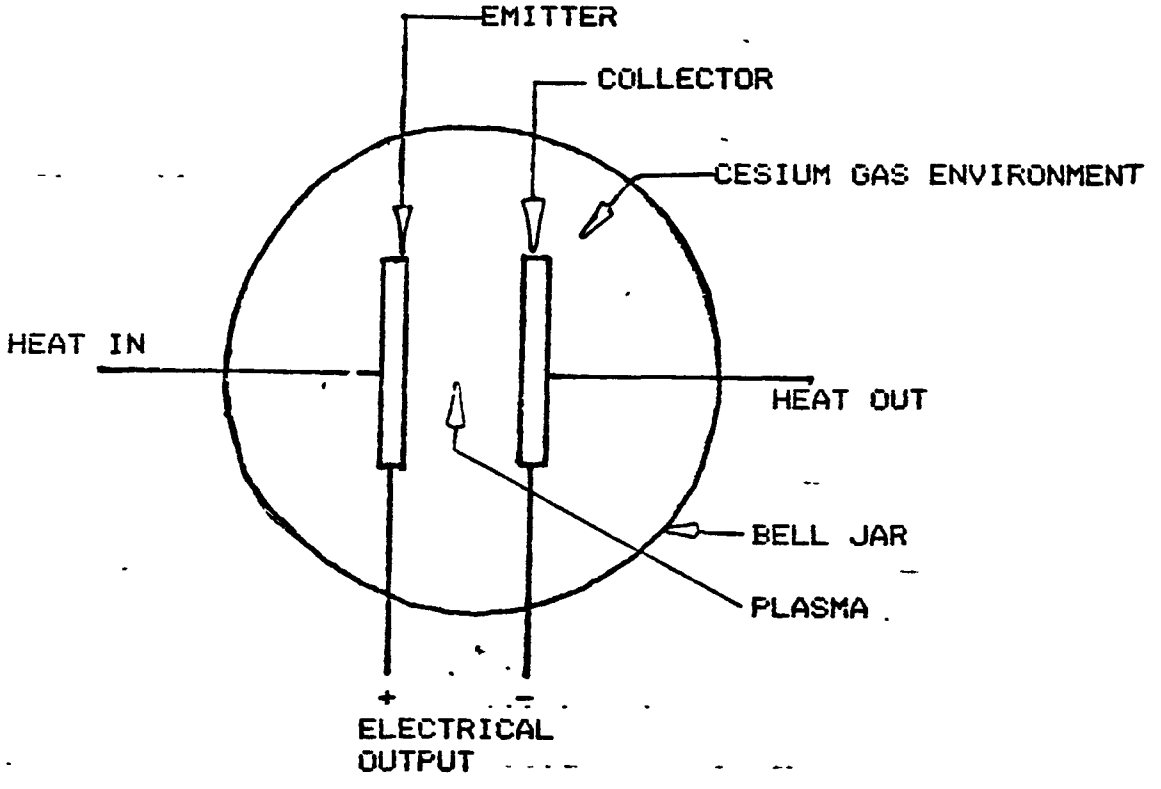

Figure 1: This diagram (not to scale) illustrates the components of a thermionic converter. Shown are two electrodes, the emitter and collector. They are subjected to a Cesuim gas environment in a bell jar. Heat is supplied to the emitter which emits electrons thermionically. In the narrow gap between the emitter and collector these electrons are transported through a plasma to the collector. In part, the electrons are transporting heat which is rejected from the collector as shown. The traversal of electrons also indicates that a current is flowing. Due to the work function difference between the electrodes, this current shows up as a power output. The electrodes are typically one square centimeter in area but less than one millimeter apart.

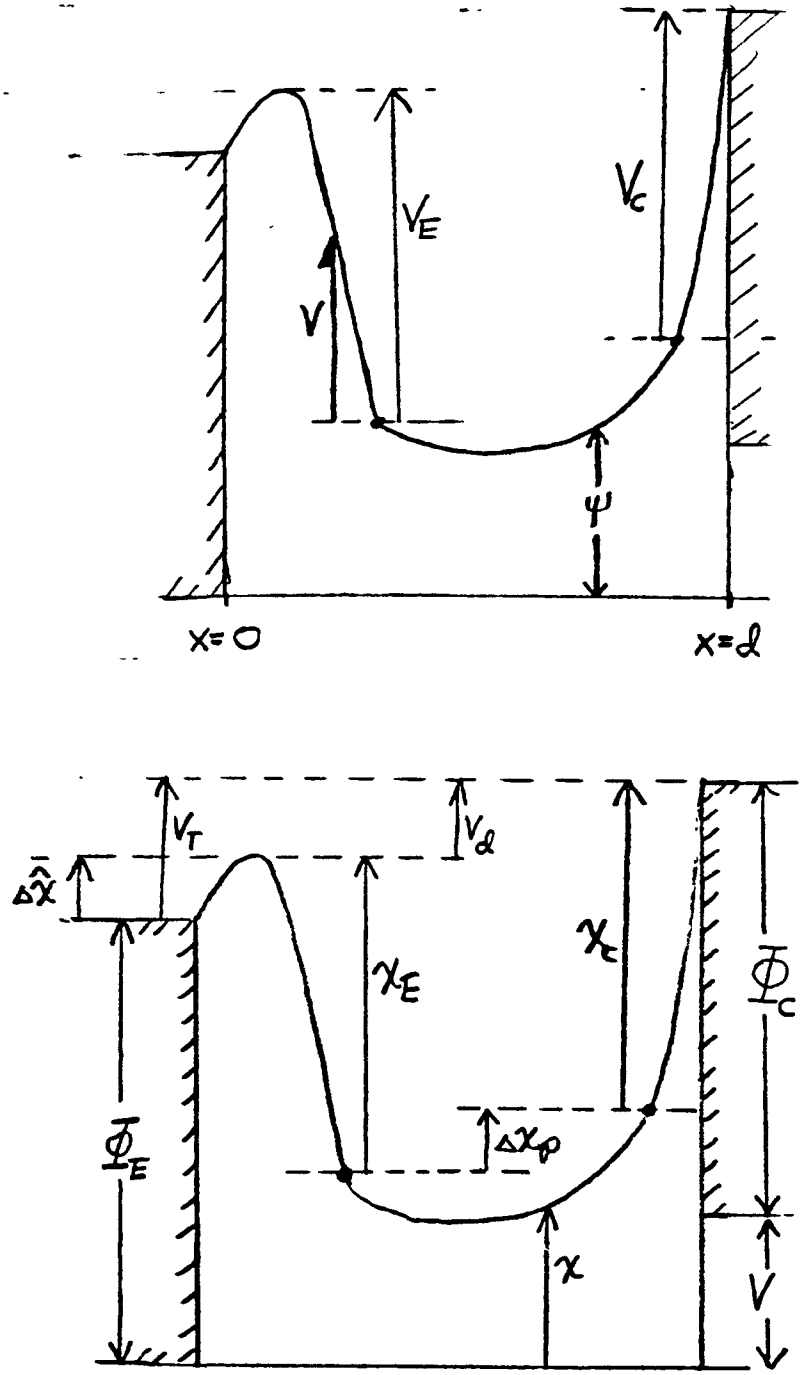

Figure 2: Shown are the voltages in a thermionic converter. The upper diagram gives the voltages in the dimensional form while the lower diagrams contains their nondimensional counterparts.

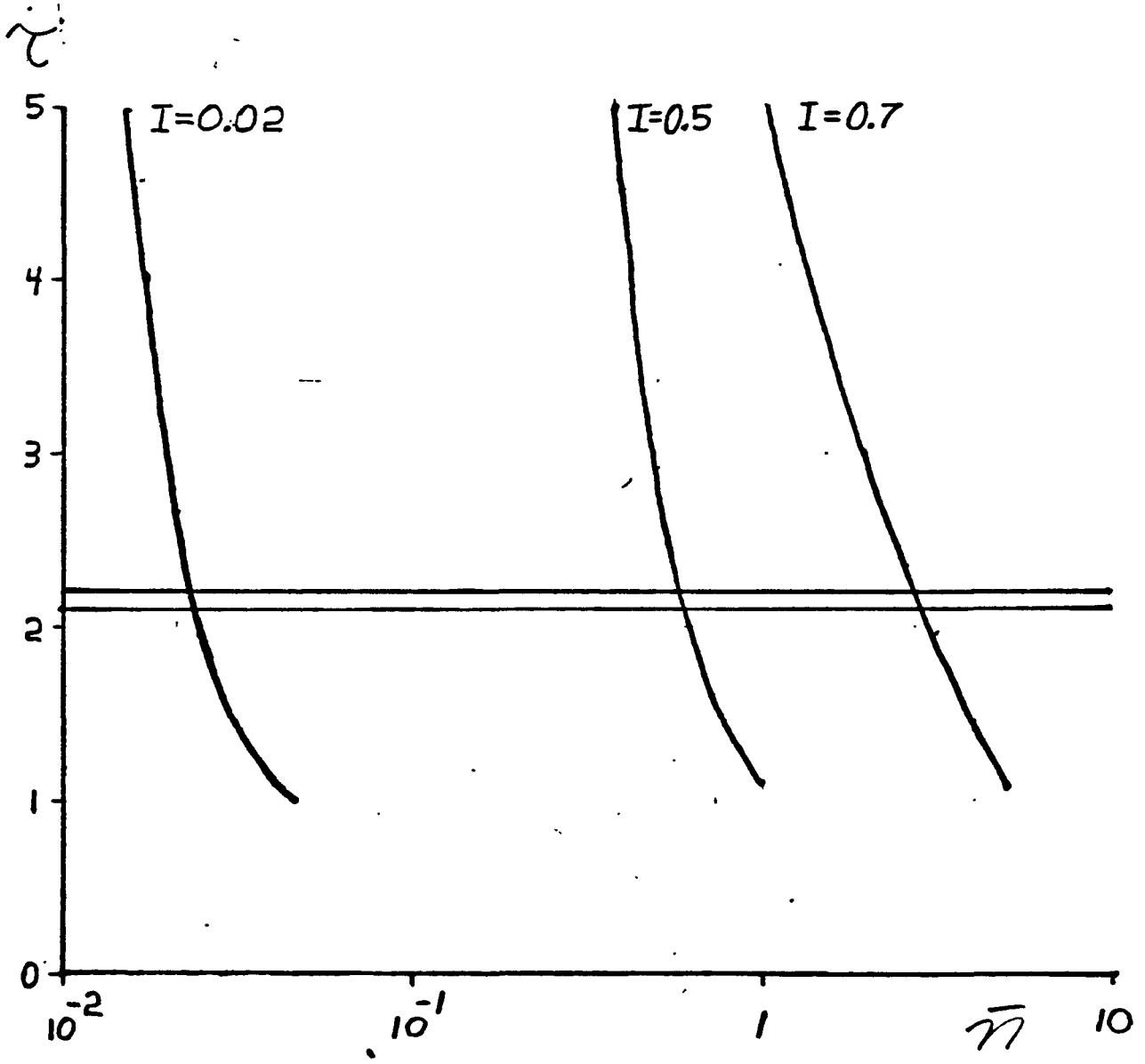

Figure 3: Shown are plots of ignition temperature and energy balance temperature against maximum electron density in units of 1(14) cm-3. For this plot of ignition temperature, collisional kinetics were assumed. The lower line for the ignition temperature was computed using C =0.46. The upper assumed a value of 0.31. The energy balance temperature is shown for three current levels, I=0.02, 0.5, and 0.7. This figure is discussed in section II.F.

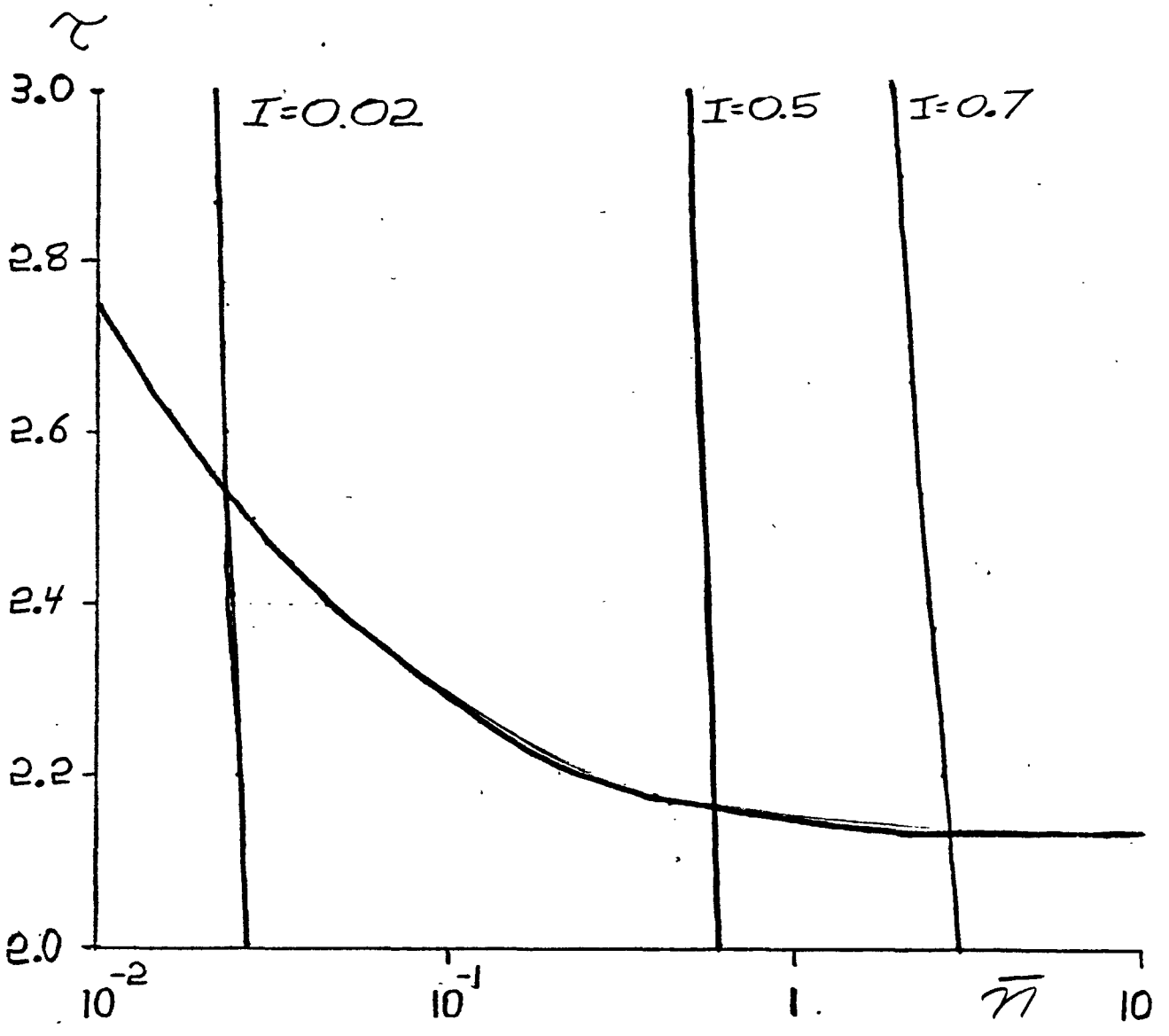

Figure 4: Shown are plots of ignition temperature and energy balance temperature against maximum electron density in units of 1(14) cm-3. For this plot of ignition temperature, collisional-radiative kinetics were assumed. The energy balance temperature is shown for three current levels, I=0.02, 0.5, and 0.7. This figure is discussed in section II.F.

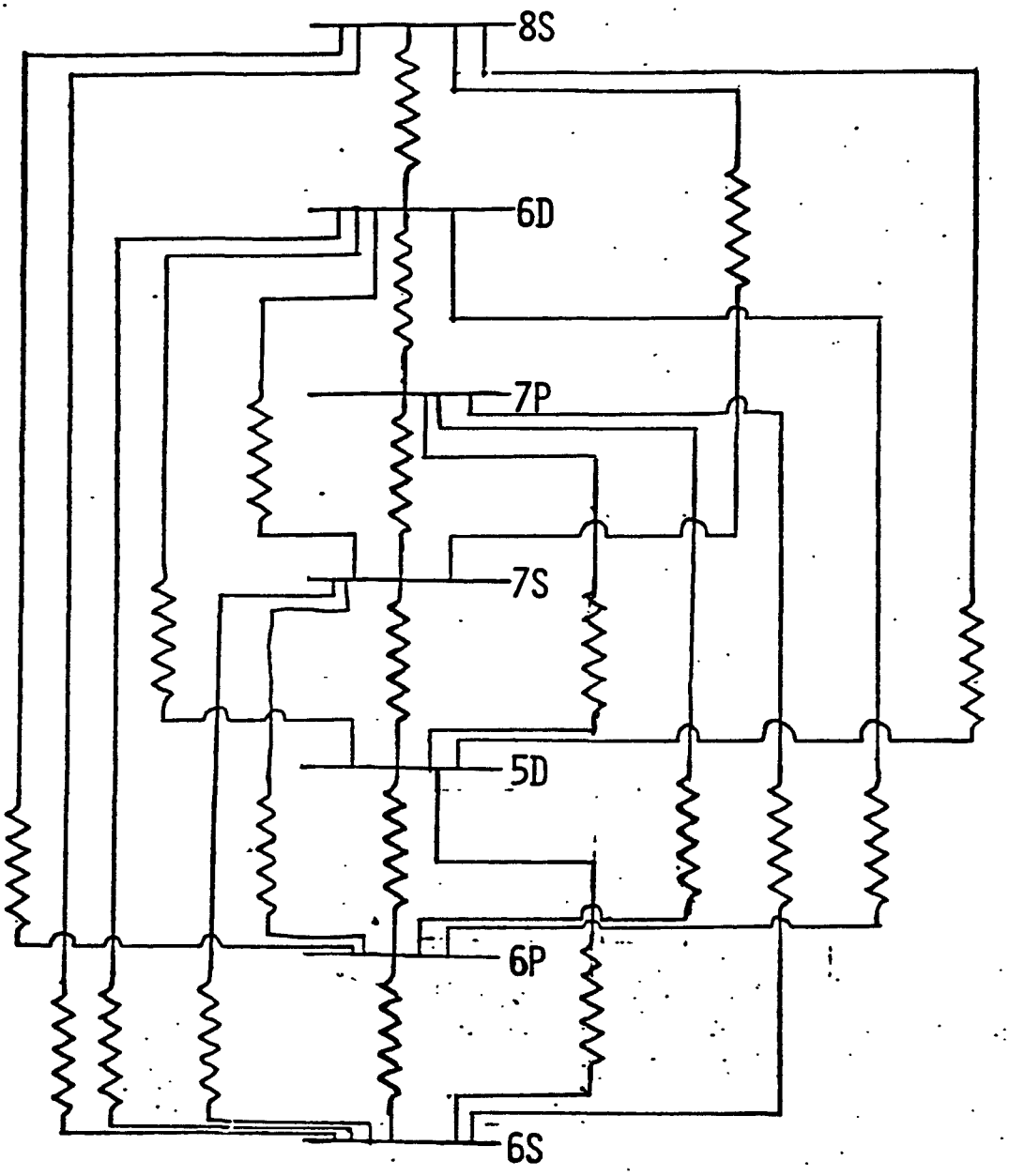

Figure 5: The circuit for collisional transitions between atomic levels is shown. This diagram has been simplified by including only those resistors that interconnect the first seven atomic levels of Cesium. Thus, each level should have resistors connecting with all higher levels in addition to the levels shown. In chapter V, a theory is developed which simplifies this circuit to the one shown in figure 6. This diagram is drawn using the notation of electrical circuits as per the analogy discussed in chapter IV.

EQUIVALENT CIRCUIT

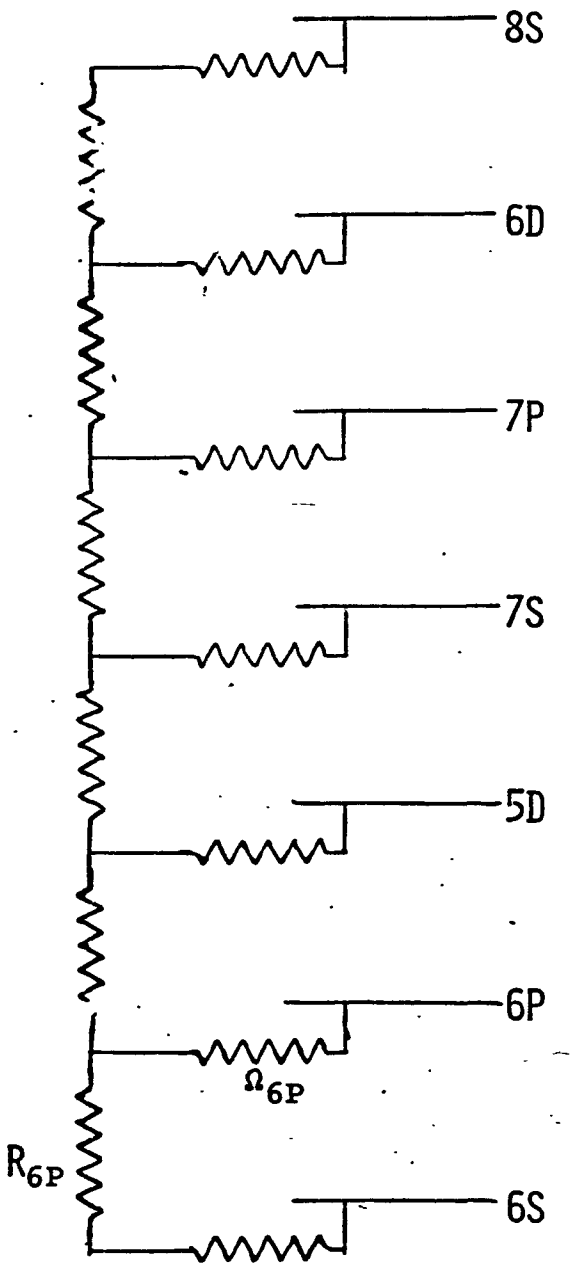

Figure 6: The equivalent circuit for collisional transitions between atomic levels is shown. This is based on the theory developed in chapter V.

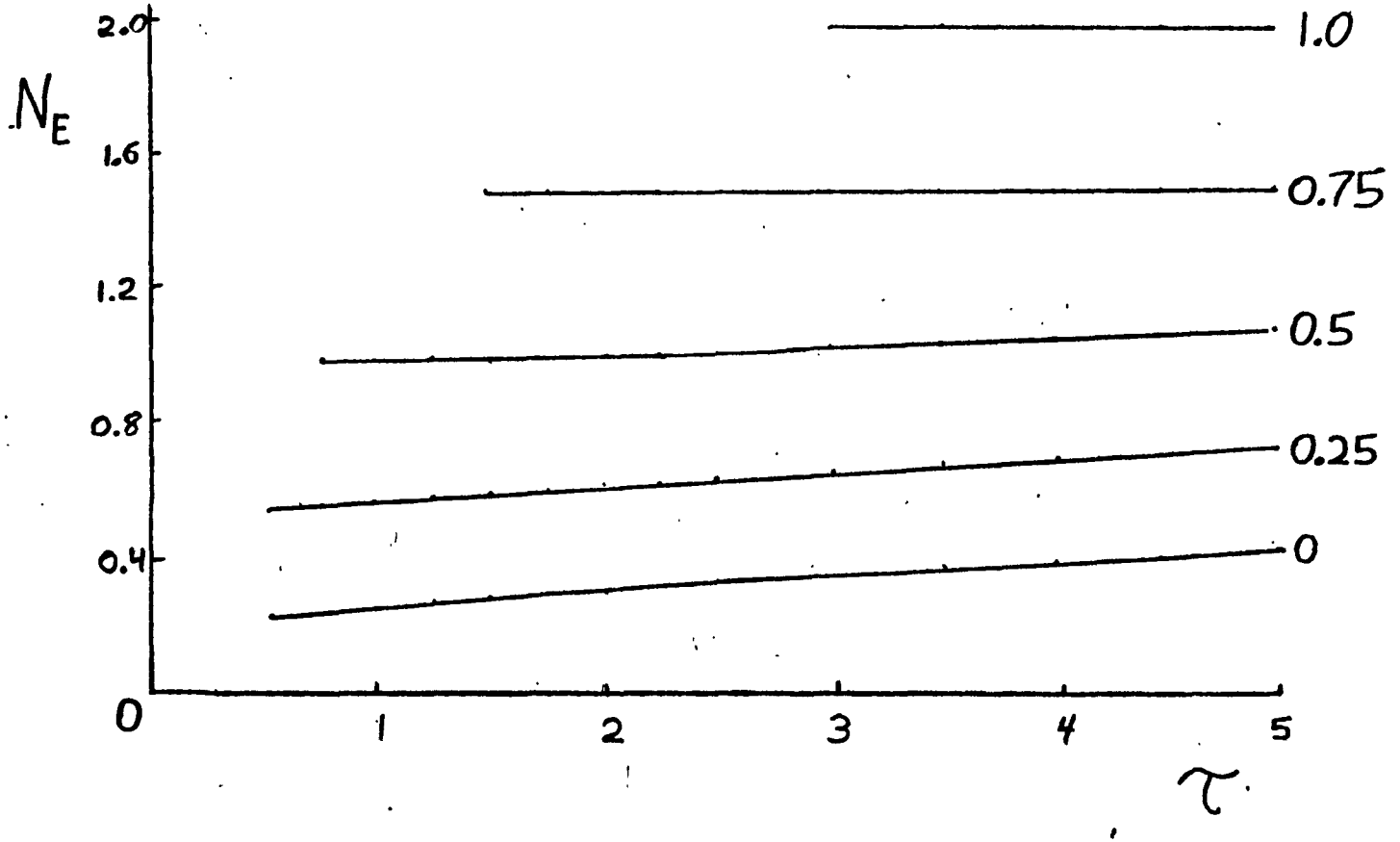

Figure 7: The ratio of the emitted number density to the plasma number density at the sheath edge is plotted against temperature with various values of a current related quantity, IK /n , as a parameter. The graph is plotted for all values of the parameter between 0 and 1 with increments of 0.25. Since all plots are nearly horizontal, it is seen that the emitted density is only a weak function of plasma electron temperature. These are the results of iterative solutions of the equations of the sheath theory of Lam[5].

	1.0E12	2.2E12	4.6E12	1.0E13	2.2E13	4.6E13	1.0E14	2.2E14	4.6E14	1.0E15
1500	0.86	0.70	0.60	0.54	0.50	0.47	0.46	0.46	0.45	0.45
1750	1.03	0.81	0.67	0.58	0.52	0.49	0.47	0.46	0.46	0.46
2000	1.24	0.95	0.75	0.63	0.55	0.51	0.48	0.47	0.46	0.46
2250	1.48	1.10	0.85	0.69	0.59	0.53	0.49	0.48	0.47	0.46
2500	1.75	1.27	0.95	0.75	0.62	0.55	0.50	0.48	0.47	0.47
2750	2.07	1.46	1.07	0.82	0.66	0.57	0.52	0.49	0.48	0.47
3000	2.41	1.67	1.19	0.88	0.69	0.59	0.53	0.50	0.49	0.48
3250	2.79	1.89	1.31	0.95	0.73	0.60	0.54	0.51	0.49	0.48
3500	3.20	2.12	1.44	1.01	0.76	0.62	0.54	0.51	0.49	0.48
3750	3.64	2.36	1.56	1.07	0.78	0.63	0.55	0.51	0.49	0.48
4000	4.10	2.60	1.67	1.12	0.80	0.63	0.55	0.51	0.49	0.48
4250	4.57	2.84	1.78	1.16	0.82	0.64	0.55	0.51	0.49	0.48
4500	5.05	3.07	1.88	1.19	0.83	0.64	0.55	0.50	0.48	0.47

FIGURE 8: THE THOMSON RECOMBINATION RATE COEFFICIENT IS SHOWN FOR ELECTRON TEMPERATURES RANGING FROM 1500K TO 4500K AND FOR ELECTRON DENSITIES FROM 1.0E12 TO 1.0E15 CM-3 IN LOGARITHMIC STEPS. THIS TABLE IS THE RESULT OF A COLLISIONAL-RADIATIVE CALCULATION FOR CESIUM INVOLVING 37 DISCRETE LEVELS AND EMPLOYING MANSBACH-KECK COLLISIONAL RATE CONSTANTS. THIS TABLE IS DISCUSSED IN SECTION IV.C OF THE TEXT.

TABLE .110

	1.0E12	2.2E12	4.6E12	1.0E13	2.2E13	4.6E13	1.0E14	2.2E14	4.6E14	1.0E15
1500	3.5E-23	2.9E-23	2.5E-23	2.2E-23	2.1E-23	2.0E-23	1.9E-23	1.9E-23	1.9E-23	1.9E-23
1750	2.1E-23	1.7E-23	1.4E-23	1.2E-23	1.1E-23	1.0E-23	9.7E-24	9.5E-24	9.4E-24	9.4E-24
2000	1.4E-23	1.1E-23	8.5E-24	7.1E-24	6.3E-24	5.7E-24	5.4E-24	5.3E-24	5.2E-24	5.2E-24
2250	9.9E-24	7.3E-24	5.7E-24	4.6E-24	3.9E-24	3.5E-24	3.3E-24	3.2E-24	3.1E-24	3.1E-24
2500	7.3E-24	5.3E-24	4.0E-24	3.1E-24	2.6E-24	2.3E-24	2.1E-24	2.0E-24	2.0E-24	1.9E-24
2750	5.6E-24	3.9E-24	2.9E-24	2.2E-24	1.8E-24	1.5E-24	1.4E-24	1.3E-24	1.3E-24	1.3E-24
3000	4.4E-24	3.0E-24	2.2E-24	1.6E-24	1.3E-24	1.1E-24	9.6E-25	9.1E-25	8.9E-25	8.7E-25
3250	3.6E-24	2.4E-24	1.7E-24	1.2E-24	9.3E-25	7.7E-25	6.8E-25	6.4E-25	6.2E-25	6.1E-25
3500	2.9E-24	1.9E-24	1.3E-24	9.2E-25	6.9E-25	5.6E-25	5.0E-25	4.6E-25	4.5E-25	4.4E-25
3750	2.4E-24	1.6E-24	1.0E-24	7.1E-25	5.2E-25	4.2E-25	3.7E-25	3.4E-25	3.3E-25	3.2E-25
4000	2.0E-24	1.3E-24	8.4E-25	5.6E-25	4.0E-25	3.2E-25	2.8E-25	2.5E-25	2.5E-25	2.4E-25
4250	1.7E-24	1.1E-24	6.8E-25	4.4E-25	3.1E-25	2.4E-25	2.1E-25	1.9E-25	1.9E-25	1.8E-25
4500	1.5E-24	9.0E-25	5.5E-25	3.5E-25	2.4E-25	1.9E-25	1.6E-25	1.5E-25	1.4E-25	1.4E-25

FIGURE 9: THE RECOMBINATION RATE CONSTANT β, IN CM^6/SEC, IS SHOWN FOR VARIOUS ELECTRON TEMPERAUTRES AND DENSITIES. THIS TABLE IS DISCUSSED IN SECTION IV.C.

	1.0E12	2.2E12	4.6E12	1.0E13	2.2E13	4.6E13	1.0E14	2.2E14	4.6E14	1.0E15
1500	8.3E-18	1.9E-17	4.2E-17	7.8E-17	1.2E-16	1.6E-16	1.8E-16	2.0E-16	2.1E-16	2.1E-16
1750	4.7E-16	1.0E-15	2.1E-15	3.9E-15	5.8E-15	7.6E-15	8.7E-15	9.3E-15	9.7E-15	9.8E-15
2000	9.5E-15	2.0E-14	4.0E-14	7.0E-14	1.0E-13	1.3E-13	1.5E-13	1.6E-13	1.6E-13	1.7E-13
2250	9.9E-14	2.0E-13	3.9E-13	6.5E-13	9.4E-13	1.2E-12	1.3E-12	1.4E-12	1.4E-12	1.5E-12
2500	6.5E-13	1.3E-12	2.4E-12	3.8E-12	5.4E-12	6.6E-12	7.3E-12	7.7E-12	7.9E-12	8.0E-12
2750	3.0E-12	5.7E-12	1.0E-11	1.6E-11	2.2E-11	2.6E-11	2.9E-11	3.1E-11	3.1E-11	3.2E-11
3000	1.1E-11	2.0E-11	3.4E-11	5.2E-11	7.0E-11	8.2E-11	9.0E-11	9.4E-11	9.6E-11	9.7E-11
3250	3.2E-11	5.7E-11	9.5E-11	1.4E-10	1.8E-10	2.1E-10	2.3E-10	2.4E-10	2.4E-10	2.4E-10
3500	8.0E-11	1.4E-10	2.2E-10	3.2E-10	4.1E-10	4.7E-10	5.0E-10	5.2E-10	5.3E-10	5.3E-10
3750	1.8E-10	3.0E-10	4.7E-10	6.6E-10	8.1E-10	9.1E-10	9.7E-10	1.0E-9	1.0E-9	1.0E-9
4000	3.6E-10	5.8E-10	8.9E-10	1.2E-9	1.5E-9	1.6E-9	1.7E-9	1.7E-9	1.8E-9	1.8E-9
4250	6.6E-10	1.0E-9	1.5E-9	2.0E-9	2.4E-9	2.6E-9	2.7E-9	2.8E-9	2.8E-9	2.9E-9
4500	1.1E-9	1.7E-9	2.5E-9	3.2E-9	3.7E-9	4.0E-9	4.2E-9	4.2E-9	4.3E-9	4.3E-9

FIGURE 10: THE IONIZATION RATE CONSTANT α IN CM^3/SEC IS SHOWN FOR VARIOUS ELECTRON TEMPERATURES AND DENSITIES. THIS TABLE IS DISCUSSED IN SECTION IV.C

	1.0E12	2.2E12	4.6E12	1.0E13	2.2E13	4.6E13	1.0E14	2.2E14	4.6E14	1.0E15
1500	48.54	17.12	6.79	3.25	1.94	1.41	1.19	1.08	1.04	1.02
1750	48.54	17.31	6.90	3.31	1.96	1.42	1.19	1.09	1.04	1.02
2000	48.30	17.42	6.99	3.35	1.99	1.43	1.20	1.09	1.04	1.02
2250	47.88	17.46	7.06	3.39	2.01	1.44	1.20	1.09	1.04	1.02
2500	47.34	17.46	7.10	3.42	2.02	1.45	1.20	1.09	1.04	1.02
2750	46.72	17.41	7.14	3.45	2.04	1.46	1.21	1.10	1.04	1.02
3000	46.04	17.33	7.16	3.47	2.05	1.46	1.21	1.10	1.04	1.02
3250	45.32	17.22	7.16	3.49	2.06	1.47	1.21	1.10	1.05	1.02
3500	44.57	17.10	7.16	3.50	2.07	1.47	1.22	1.10	1.05	1.02
3750	43.79	16.95	7.15	3.50	2.07	1.48	1.22	1.10	1.05	1.02
4000	43.00	16.78	7.13	3.51	2.08	1.48	1.22	1.10	1.05	1.02
4250	42.21	16.60	7.09	3.51	2.08	1.48	1.22	1.10	1.05	1.02
4500	41.41	16.41	7.06	3.50	2.08	1.48	1.22	1.10	1.05	1.02

FIGURE 11: THE QUANTITY ρ_0 WHICH INDICATES THE DEPARTURE OF STEADY-STATE ELECTRON FROM SAHA DUE TO RADIATIVE LOSS. THIS IS A NONDIMENSIONAL RATIO OF THE RECOMBINATION COEFFICIENT TO THE IONIZATION COEFFICIENT. THIS TABLE IS DISCUSSED IN SECTION IV.C.

	1.0E12	2.2E12	4.6E12	1.0E13	2.2E13	4.6E13	1.0E14	2.2E14	4.6E14	1.0E15
1500	0.018	0.041	0.088	0.165	0.256	0.336	0.390	0.421	0.437	0.444
1750	0.021	0.047	0.097	0.175	0.266	0.344	0.396	0.425	0.440	0.447
2000	0.026	0.054	0.108	0.188	0.278	0.353	0.402	0.429	0.443	0.450
2250	0.031	0.063	0.120	0.203	0.292	0.364	0.410	0.435	0.448	0.454
2500	0.037	0.073	0.134	0.219	0.307	0.376	0.419	0.442	0.454	0.459
2750	0.044	0.084	0.150	0.236	0.323	0.388	0.428	0.449	0.460	0.465
3000	0.052	0.096	0.166	0.254	0.338	0.400	0.436	0.456	0.465	0.470
3250	0.062	0.110	0.183	0.272	0.353	0.410	0.443	0.461	0.469	0.473
3500	0.072	0.124	0.201	0.289	0.366	0.418	0.448	0.464	0.471	0.475
3750	0.083	0.139	0.218	0.305	0.377	0.424	0.451	0.464	0.471	0.474
4000	0.095	0.155	0.235	0.319	0.385	0.428	0.451	0.463	0.469	0.472
4250	0.108	0.171	0.251	0.331	0.392	0.430	0.450	0.460	0.465	0.468
4500	0.122	0.187	0.266	0.341	0.397	0.430	0.448	0.456	0.461	0.463

FIGURE 12: THE NONDIMENSIONAL RATIO C_T/p_0 IS SHOWN FOR VARIOUS ELECTRON TEMPERATURES AND DENSITIES. THIS SHOWS THE EFFECT OF RADIATION OR THE IONIZATION RATE CONSTANT. THIS IS DISCUSSED IN SECTION IV.C.

	1.0E12	2.2E12	4.6E12	1.0E13	2.2E13	4.6E13	1.0E14	2.2E14	4.6E14	1.0E15
1500	1.022	1.015	1.009	1.005	1.002	1.001	1.000	1.000	1.000	1.000
1750	1.034	1.023	1.014	1.007	1.004	1.002	1.001	1.000	1.000	1.000
2000	1.048	1.033	1.019	1.010	1.005	1.002	1.000	0.999	0.999	0.999
2250	1.063	1.043	1.025	1.013	1.005	1.000	0.998	0.997	0.996	0.996
2500	1.078	1.053	1.030	1.014	1.002	0.996	0.992	0.991	0.990	0.989
2750	1.092	1.062	1.034	1.011	0.996	0.986	0.981	0.979	0.977	0.977
3000	1.105	1.069	1.034	1.005	0.983	0.970	0.963	0.960	0.958	0.957
3250	1.117	1.073	1.029	0.992	0.964	0.947	0.938	0.933	0.931	0.929
3500	1.126	1.073	1.019	0.972	0.937	0.916	0.904	0.899	0.896	0.894
3750	1.130	1.068	1.003	0.945	0.904	0.878	0.865	0.858	0.855	0.853
4000	1.131	1.057	0.980	0.913	0.865	0.836	0.821	0.813	0.809	0.808
4250	1.126	1.040	0.951	0.875	0.821	0.790	0.774	0.765	0.762	0.760
4500	1.116	1.018	0.917	0.833	0.776	0.743	0.726	0.717	0.713	0.711

FIGURE 13: THE V' COEFFICIENT IS SHOWN FOR LEVEL 6P
THIS INDICATES THE DEPENDENCE OF THIS LEVEL'S POPULATION ON THE GROUND STATE'S POPULATION. THIS TABLE IS DISCUSSED IN SECTION IV.C.

	1.0E12	2.2E12	4.6E12	1.0E13	2.2E13	4.6E13	1.0E14	2.2E14	4.6E14	1.0E15
1500	0.0001									
1750	0.0006	0.0005	0.0004	0.0003	0.0003	0.0003	0.0002	0.0002	0.0002	0.0002
2000	0.0038	0.0028	0.0022	0.0018	0.0015	0.0014	0.0013	0.0013	0.0012	0.0012
2250	0.0157	0.0113	0.0085	0.0067	0.0056	0.0050	0.0046	0.0044	0.0043	0.0043
2500	0.0487	0.0341	0.0249	0.0191	0.0155	0.0134	0.0122	0.0116	0.0114	0.0112
2750	0.1230	0.0839	0.0594	0.0441	0.0348	0.0294	0.0265	0.0251	0.0244	0.0240
3000	0.2653	0.1765	0.1214	0.0874	0.0670	0.0555	0.0494	0.0464	0.0449	0.0443
3250	0.5064	0.3290	0.2199	0.1537	0.1146	0.0930	0.0819	0.0764	0.0738	0.0725
3500	0.8780	0.5572	0.3621	0.2455	0.1784	0.1422	0.1237	0.1148	0.1105	0.1085
3750	1.4077	0.8726	0.5514	0.3631	0.2574	0.2016	0.1736	0.1601	0.1538	0.1508
4000	2.1162	1.2811	0.7870	0.5038	0.3489	0.2689	0.2294	0.2106	0.2017	0.1975
4250	3.0135	1.7813	1.0644	0.6630	0.4493	0.3413	0.2888	0.2639	0.2521	0.2467
4500	4.0982	2.3651	1.3754	0.8351	0.5549	0.4161	0.3494	0.3180	0.3032	0.2964

FIGURE 14: THE V COEFFICIENT IS SHOWN FOR LEVEL 6P
THIS INDICATES THE DEPENDENCE OF THIS LEVEL'S POPULATION ON THE FREE ELECTRON POPULATION. THIS TABLE IS DISCUSSED IN SECTION IV.C.

	1.0E12	2.2E12	4.6E12	1.0E13	2.2E13	4.6E13	1.0E14	2.2E14	4.6E14	1.0E15
1500	0.4539	0.6394	0.7907	0.8896	0.9452	0.9736	0.9875	0.9941	0.9972	0.9987
1750	0.4495	0.6337	0.7851	0.8855	0.9425	0.9720	0.9865	0.9934	0.9966	0.9982
2000	0.4459	0.6283	0.7794	0.8806	0.9389	0.9693	0.9842	0.9914	0.9947	0.9963
2250	0.4428	0.6230	0.7730	0.8745	0.9333	0.9640	0.9792	0.9864	0.9898	0.9914
2500	0.4399	0.6175	0.7655	0.8660	0.9242	0.9545	0.9694	0.9764	0.9798	0.9813
2750	0.4371	0.6113	0.7561	0.8539	0.9100	0.9388	0.9528	0.9594	0.9625	0.9639
3000	0.4339	0.6040	0.7440	0.8371	0.8893	0.9155	0.9280	0.9338	0.9365	0.9377
3250	0.4302	0.5950	0.7284	0.8148	0.8616	0.8842	0.8946	0.8994	0.9016	0.9026
3500	0.4257	0.5840	0.7089	0.7867	0.8268	0.8452	0.8533	0.8569	0.8586	0.8593
3750	0.4200	0.5706	0.6853	0.7533	0.7859	0.7999	0.8057	0.8082	0.8093	0.8098
4000	0.4130	0.5546	0.6579	0.7153	0.7406	0.7503	0.7540	0.7554	0.7561	0.7563
4250	0.4046	0.5361	0.6273	0.6741	0.6925	0.6985	0.7004	0.7010	0.7012	0.7013
4500	0.3946	0.5154	0.5943	0.6312	0.6435	0.6465	0.6469	0.6468	0.6467	0.6467

FIGURE 15: THE V' COEFFICIENT IS SHOWN FOR LEVEL 5D
THIS INDICATES THE DEPENDENCE OF THIS LEVEL'S POPULATION ON THE
GROUND STATE'S POPULATION. THIS TABLE IS DISCUSSED IN SECTION IV.C.

	1.0E12	2.2E12	4.6E12	1.0E13	2.2E13	4.6E13	1.0E14	2.2E14	4.6E14	1.0E15
1500	0.0001	0.0001	0.0001	0.0001	0.0001	0.0001	0.0001	0.0001	0.0001	0.0001
1750	0.0005	0.0006	0.0006	0.0005	0.0005	0.0005	0.0005	0.0005	0.0005	0.0005
2000	0.0027	0.0028	0.0028	0.0026	0.0025	0.0024	0.0024	0.0023	0.0023	0.0023
2250	0.0099	0.0102	0.0097	0.0088	0.0082	0.0077	0.0074	0.0073	0.0072	0.0072
2500	0.0282	0.0282	0.0260	0.0232	0.0207	0.0191	0.0182	0.0178	0.0175	0.0174
2750	0.0662	0.0647	0.0582	0.0503	0.0439	0.0396	0.0372	0.0360	0.0354	0.0351
3000	0.1347	0.1286	0.1127	0.0950	0.0807	0.0714	0.0663	0.0636	0.0623	0.0617
3250	0.2451	0.2287	0.1955	0.1603	0.1329	0.1155	0.1059	0.1010	0.0987	0.0975
3500	0.4078	0.3720	0.3100	0.2476	0.2004	0.1712	0.1553	0.1473	0.1435	0.1416
3750	0.6311	0.5626	0.4568	0.3555	0.2814	0.2365	0.2126	0.2006	0.1949	0.1922
4000	0.9198	0.8009	0.6336	0.4806	0.3725	0.3087	0.2750	0.2584	0.2505	0.2467
4250	1.2744	1.0835	0.8352	0.6181	0.4699	0.3844	0.3400	0.3182	0.3078	0.3029
4500	1.6915	1.4038	1.0547	0.7626	0.5696	0.4608	0.4049	0.3777	0.3648	0.3587

FIGURE 16: THE V COEFFICIENT IS SHOWN FOR LEVEL 5D
THIS INDICATES THE DEPENDENCE OF THIS LEVEL'S POPULATION ON THE FREE ELECTRON POPULATION. THIS TABLE IS DISCUSSED IN SECTION IV.C.

	1.0E12	2.2E12	4.6E12	1.0E13	2.2E13	4.6E13	1.0E14	2.2E14	4.6E14	1.0E15
1500	0.1604	0.3200	0.5254	0.7145	0.8466	0.9230	0.9627	0.9822	0.9914	0.9958
1750	0.1585	0.3160	0.5199	0.7092	0.8424	0.9201	0.9605	0.9804	0.9899	0.9943
2000	0.1574	0.3130	0.5150	0.7037	0.8373	0.9155	0.9564	0.9765	0.9861	0.9906
2250	0.1567	0.3104	0.5101	0.6972	0.8302	0.9081	0.9489	0.9689	0.9785	0.9830
2500	0.1563	0.3081	0.5047	0.6889	0.8197	0.8961	0.9360	0.9556	0.9650	0.9693
2750	0.1560	0.3056	0.4983	0.6778	0.8045	0.8781	0.9163	0.9349	0.9438	0.9480
3000	0.1556	0.3026	0.4901	0.6631	0.7836	0.8529	0.8886	0.9059	0.9142	0.9180
3250	0.1551	0.2988	0.4797	0.6440	0.7566	0.8204	0.8528	0.8686	0.8760	0.8795
3500	0.1543	0.2939	0.4668	0.6206	0.7237	0.7811	0.8100	0.8239	0.8305	0.8336
3750	0.1530	0.2879	0.4513	0.5931	0.6859	0.7366	0.7618	0.7739	0.7795	0.7822
4000	0.1512	0.2805	0.4333	0.5623	0.6446	0.6887	0.7104	0.7207	0.7255	0.7277
4250	0.1488	0.2719	0.4133	0.5293	0.6014	0.6393	0.6578	0.6665	0.6705	0.6724
4500	0.1459	0.2621	0.3918	0.4951	0.5578	0.5902	0.6058	0.6132	0.6166	0.6182

FIGURE 17: THE V' COEFFICIENT IS SHOWN FOR LEVEL 75
THIS INDICATES THE DEPENDENCE OF THIS LEVEL'S POPULATION ON THE GROUND STATE'S POPULATION. THIS TABLE IS DISCUSSED IN SECTION IV.C.

	1.0E12	2.2E12	4.6E12	1.0E13	2.2E13	4.6E13	1.0E14	2.2E14	4.6E14	1.0E15
1500	0.0001	0.0001	0.0002	0.0002	0.0003	0.0004	0.0004	0.0004	0.0004	0.0004
1750	0.0004	0.0006	0.0009	0.0011	0.0014	0.0016	0.0017	0.0017	0.0017	0.0018
2000	0.0015	0.0023	0.0032	0.0039	0.0045	0.0049	0.0052	0.0053	0.0054	0.0054
2250	0.0047	0.0069	0.0090	0.0107	0.0117	0.0124	0.0127	0.0129	0.0130	0.0131
2500	0.0119	0.0170	0.0215	0.0244	0.0258	0.0264	0.0266	0.0267	0.0268	0.0268
2750	0.0261	0.0363	0.0445	0.0486	0.0496	0.0493	0.0489	0.0486	0.0485	0.0484
3000	0.0508	0.0691	0.0820	0.0865	0.0854	0.0828	0.0809	0.0797	0.0791	0.0788
3250	0.0901	0.1194	0.1376	0.1403	0.1343	0.1274	0.1226	0.1200	0.1187	0.1180
3500	0.1476	0.1906	0.2131	0.2106	0.1960	0.1821	0.1732	0.1684	0.1660	0.1648
3750	0.2261	0.2846	0.3088	0.2961	0.2685	0.2450	0.2305	0.2228	0.2189	0.2171
4000	0.3276	0.4016	0.4230	0.3939	0.3488	0.3132	0.2919	0.2807	0.2752	0.2726
4250	0.4523	0.5399	0.5523	0.5003	0.4335	0.3838	0.3548	0.3398	0.3325	0.3290
4500	0.5992	0.6962	0.6921	0.6111	0.5193	0.4541	0.4169	0.3979	0.3886	0.3842

FIGURE 18: THE V COEFFICIENT IS SHOWN FOR LEVEL 75
THIS INDICATES THE DEPENDENCE OF THIS LEVEL'S POPULATION ON THE FREE ELECTRON POPULATION. THIS TABLE IS DISCUSSED IN SECTION IV.C.

	1.0E12	2.2E12	4.6E12	1.0E13	2.2E13	4.6E13	1.0E14	2.2E14	4.6E14	1.0E15
1500	0.1093	0.2216	0.3800	0.5550	0.7117	0.8267	0.8976	0.9360	0.9553	0.9646
1750	0.1062	0.2135	0.3646	0.5326	0.6841	0.7956	0.8644	0.9016	0.9203	0.9293
2000	0.1036	0.2063	0.3501	0.5095	0.6527	0.7572	0.8210	0.8554	0.8726	0.8809
2250	0.1015	0.1998	0.3359	0.4856	0.6181	0.7133	0.7707	0.8013	0.8165	0.8238
2500	0.0995	0.1935	0.3219	0.4608	0.5813	0.6659	0.7161	0.7426	0.7557	0.7619
2750	0.0977	0.1874	0.3076	0.4350	0.5426	0.6164	0.6592	0.6816	0.6926	0.6978
3000	0.0959	0.1811	0.2930	0.4083	0.5027	0.5656	0.6014	0.6199	0.6290	0.6333
3250	0.0940	0.1747	0.2777	0.3806	0.4620	0.5146	0.5440	0.5590	0.5662	0.5697
3500	0.0919	0.1679	0.2619	0.3523	0.4212	0.4644	0.4880	0.4999	0.5057	0.5084
3750	0.0897	0.1607	0.2455	0.3239	0.3812	0.4160	0.4347	0.4440	0.4485	0.4506
4000	0.0873	0.1531	0.2288	0.2957	0.3427	0.3703	0.3849	0.3921	0.3956	0.3972
4250	0.0846	0.1452	0.2120	0.2684	0.3064	0.3282	0.3394	0.3449	0.3475	0.3488
4500	0.0817	0.1370	0.1954	0.2424	0.2729	0.2899	0.2985	0.3027	0.3047	0.3056

FIGURE 19: THE V' COEFFICIENT IS SHOWN FOR LEVEL 7P
THIS INDICATES THE DEPENDENCE OF THIS LEVEL'S POPULATION ON THE GROUND STATE'S POPULATION. THIS TABLE IS DISCUSSED IN SECTION IV.C.

	1.0E12	2.2E12	4.6E12	1.0E13	2.2E13	4.6E13	1.0E14	2.2E14	4.6E14	1.0E15
1500	0.0025	0.0043	0.0074	0.0118	0.0168	0.0211	0.0240	0.0256	0.0264	0.0268
1750	0.0069	0.0115	0.0188	0.0290	0.0402	0.0496	0.0559	0.0593	0.0611	0.0620
2000	0.0149	0.0239	0.0374	0.0555	0.0748	0.0905	0.1007	0.1063	0.1092	0.1105
2250	0.0275	0.0424	0.0637	0.0910	0.1189	0.1409	0.1548	0.1624	0.1662	0.1681
2500	0.0458	0.0681	0.0983	0.1350	0.1708	0.1980	0.2148	0.2239	0.2284	0.2306
2750	0.0709	0.1022	0.1418	0.1871	0.2291	0.2599	0.2784	0.2883	0.2931	0.2955
3000	0.1046	0.1459	0.1947	0.2469	0.2927	0.3249	0.3438	0.3537	0.3586	0.3609
3250	0.1481	0.2004	0.2574	0.3137	0.3603	0.3916	0.4095	0.4187	0.4232	0.4254
3500	0.2029	0.2662	0.3292	0.3861	0.4301	0.4582	0.4739	0.4819	0.4858	0.4876
3750	0.2698	0.3433	0.4089	0.4623	0.5002	0.5232	0.5357	0.5419	0.5449	0.5463
4000	0.3489	0.4305	0.4945	0.5398	0.5687	0.5850	0.5935	0.5977	0.5996	0.6006
4250	0.4396	0.5260	0.5835	0.6164	0.6337	0.6424	0.6465	0.6484	0.6494	0.6498
4500	0.5406	0.6275	0.6730	0.6899	0.6941	0.6945	0.6942	0.6939	0.6937	0.6937

FIGURE 20: THE V COEFFICIENT IS SHOWN FOR LEVEL 7P
THIS INDICATES THE DEPENDENCE OF THIS LEVEL'S POPULATION ON THE FREE ELECTRON POPULATION. THIS TABLE IS DISCUSSED IN SECTION IV.C.

LE .5

	1.0E12	2.2E12	4.6E12	1.0E13	2.2E13	4.6E13	1.0E14	2.2E14	4.6E14	1.0E15
1500	0.0279	0.0762	0.1809	0.3505	0.5485	0.7173	0.8294	0.8925	0.9247	0.9403
1750	0.0273	0.0740	0.1744	0.3358	0.5228	0.6811	0.7857	0.8442	0.8741	0.8886
2000	0.0268	0.0720	0.1679	0.3198	0.4927	0.6368	0.7307	0.7829	0.8094	0.8223
2250	0.0264	0.0701	0.1613	0.3026	0.4598	0.5878	0.6699	0.7151	0.7379	0.7489
2500	0.0260	0.0682	0.1544	0.2847	0.4254	0.5371	0.6074	0.6456	0.6647	0.6740
2750	0.0257	0.0663	0.1473	0.2662	0.3906	0.4864	0.5456	0.5774	0.5932	0.6008
3000	0.0253	0.0642	0.1399	0.2473	0.3558	0.4370	0.4860	0.5121	0.5250	0.5312
3250	0.0249	0.0620	0.1322	0.2282	0.3217	0.3895	0.4297	0.4508	0.4612	0.4662
3500	0.0244	0.0597	0.1242	0.2091	0.2886	0.3447	0.3772	0.3941	0.4024	0.4063
3750	0.0239	0.0572	0.1160	0.1903	0.2573	0.3030	0.3292	0.3426	0.3491	0.3522
4000	0.0233	0.0546	0.1077	0.1721	0.2279	0.2651	0.2859	0.2965	0.3017	0.3041
4250	0.0226	0.0518	0.0994	0.1548	0.2010	0.2310	0.2475	0.2559	0.2600	0.2619
4500	0.0219	0.0489	0.0913	0.1386	0.1767	0.2008	0.2140	0.2206	0.2238	0.2253

FIGURE 21: THE V' COEFFICIENT IS SHOWN FOR LEVEL 6D
THIS INDICATES THE DEPENDENCE OF THIS LEVEL'S POPULATION ON THE GROUND STATE'S POPULATION. THIS TABLE IS DISCUSSED IN SECTION IV.C.

	1.0E12	2.2E12	4.6E12	1.0E13	2.2E13	4.6E13	1.0E14	2.2E14	4.6E14	1.0E15
1500	0.0018	0.0040	0.0086	0.0162	0.0255	0.0338	0.0394	0.0426	0.0442	0.0450
1750	0.0046	0.0098	0.0202	0.0369	0.0568	0.0740	0.0856	0.0921	0.0955	0.0971
2000	0.0092	0.0189	0.0377	0.0666	0.0998	0.1277	0.1461	0.1563	0.1615	0.1641
2250	0.0158	0.0315	0.0607	0.1038	0.1511	0.1897	0.2145	0.2281	0.2350	0.2384
2500	0.0246	0.0477	0.0888	0.1468	0.2079	0.2558	0.2859	0.3022	0.3104	0.3143
2750	0.0357	0.0675	0.1217	0.1946	0.2678	0.3232	0.3571	0.3752	0.3843	0.3886
3000	0.0495	0.0911	0.1592	0.2463	0.3295	0.3901	0.4263	0.4454	0.4548	0.4593
3250	0.0662	0.1189	0.2011	0.3009	0.3917	0.4552	0.4923	0.5115	0.5210	0.5255
3500	0.0861	0.1508	0.2470	0.3575	0.4530	0.5174	0.5540	0.5728	0.5820	0.5864
3750	0.1094	0.1867	0.2960	0.4147	0.5122	0.5756	0.6108	0.6287	0.6373	0.6414
4000	0.1361	0.2261	0.3470	0.4712	0.5682	0.6290	0.6621	0.6787	0.6867	0.6904
4250	0.1659	0.2684	0.3989	0.5256	0.6199	0.6771	0.7076	0.7228	0.7300	0.7335
4500	0.1985	0.3126	0.4503	0.5769	0.6669	0.7198	0.7475	0.7612	0.7677	0.7707

FIGURE 22: THE V COEFFICIENT IS SHOWN FOR LEVEL 6D
THIS INDICATES THE DEPENDENCE OF THIS LEVEL'S POPULATION ON THE FREE ELECTRON POPULATION. THIS TABLE IS DISCUSSED IN SECTION IV.C.

ILE 6

	1.0E12	2.2E12	4.6E12	1.0E13	2.2E13	4.6E13	1.0E14	2.2E14	4.6E14	1.0E15
1500	0.0774	0.1552	0.2783	0.4402	0.6101	0.7484	0.8384	0.8885	0.9141	0.9265
1750	0.0754	0.1500	0.2669	0.4195	0.5781	0.7059	0.7885	0.8344	0.8576	0.8689
2000	0.0737	0.1452	0.2557	0.3977	0.5425	0.6570	0.7300	0.7702	0.7905	0.8003
2250	0.0722	0.1405	0.2444	0.3752	0.5051	0.6054	0.6682	0.7023	0.7195	0.7278
2500	0.0708	0.1359	0.2332	0.3525	0.4674	0.5536	0.6065	0.6349	0.6491	0.6559
2750	0.0693	0.1314	0.2219	0.3296	0.4299	0.5029	0.5467	0.5700	0.5815	0.5870
3000	0.0679	0.1268	0.2105	0.3067	0.3930	0.4539	0.4897	0.5084	0.5177	0.5221
3250	0.0665	0.1221	0.1988	0.2837	0.3570	0.4070	0.4358	0.4507	0.4580	0.4615
3500	0.0649	0.1172	0.1868	0.2608	0.3222	0.3627	0.3856	0.3973	0.4029	0.4057
3750	0.0632	0.1120	0.1746	0.2384	0.2890	0.3214	0.3393	0.3484	0.3528	0.3549
4000	0.0614	0.1066	0.1623	0.2165	0.2578	0.2835	0.2974	0.3044	0.3077	0.3093
4250	0.0594	0.1010	0.1501	0.1957	0.2290	0.2492	0.2599	0.2652	0.2678	0.2690
4500	0.0573	0.0953	0.1381	0.1761	0.2028	0.2186	0.2268	0.2309	0.2329	0.2338

FIGURE 23: THE V' COEFFICIENT IS SHOWN FOR LEVEL 8S
THIS INDICATES THE DEPENDENCE OF THIS LEVEL'S POPULATION ON THE
GROUND STATE'S POPULATION. THIS TABLE IS DISCUSSED IN SECTION IV.C.

	1.0E12	2.2E12	4.6E12	1.0E13	2.2E13	4.6E13	1.0E14	2.2E14	4.6E14	1.0E15
1500	0.0089	0.0145	0.0225	0.0326	0.0429	0.0512	0.0566	0.0596	0.0611	0.0619
1750	0.0183	0.0292	0.0447	0.0640	0.0838	0.0996	0.1099	0.1155	0.1184	0.1198
2000	0.0314	0.0492	0.0739	0.1043	0.1349	0.1591	0.1744	0.1829	0.1871	0.1892
2250	0.0480	0.0738	0.1089	0.1511	0.1923	0.2240	0.2438	0.2546	0.2600	0.2626
2500	0.0683	0.1031	0.1491	0.2026	0.2532	0.2909	0.3139	0.3263	0.3325	0.3354
2750	0.0927	0.1373	0.1942	0.2579	0.3158	0.3575	0.3824	0.3956	0.4022	0.4053
3000	0.1221	0.1770	0.2444	0.3165	0.3792	0.4229	0.4483	0.4616	0.4682	0.4713
3250	0.1575	0.2229	0.2997	0.3779	0.4427	0.4861	0.5109	0.5236	0.5299	0.5328
3500	0.1997	0.2755	0.3599	0.4412	0.5052	0.5465	0.5695	0.5812	0.5869	0.5896
3750	0.2493	0.3348	0.4243	0.5053	0.5658	0.6033	0.6237	0.6340	0.6389	0.6413
4000	0.3066	0.4000	0.4915	0.5687	0.6232	0.6557	0.6730	0.6816	0.6857	0.6876
4250	0.3712	0.4702	0.5598	0.6300	0.6766	0.7032	0.7171	0.7239	0.7271	0.7286
4500	0.4423	0.5437	0.6277	0.6879	0.7252	0.7457	0.7560	0.7610	0.7633	0.7645

FIGURE 24: THE V COEFFICIENT IS SHOWN FOR LEVEL 85
THIS INDICATES THE DEPENDENCE OF THIS LEVEL'S POPULATION ON THE FREE ELECTRON POPULATION. THIS TABLE IS DISCUSSED IN SECTION IV.C.

	1.0E12	2.2E12	4.6E12	1.0E13	2.2E13	4.6E13	1.0E14	2.2E14	4.6E14	1.0E15
1500	0.0161	0.0479	0.1254	0.2669	0.4488	0.6141	0.7277	0.7927	0.8262	0.8426
1750	0.0158	0.0461	0.1181	0.2461	0.4065	0.5493	0.6462	0.7013	0.7295	0.7433
2000	0.0155	0.0442	0.1105	0.2244	0.3623	0.4819	0.5615	0.6062	0.6291	0.6402
2250	0.0152	0.0423	0.1029	0.2030	0.3197	0.4178	0.4816	0.5170	0.5350	0.5437
2500	0.0148	0.0404	0.0954	0.1826	0.2803	0.3596	0.4101	0.4377	0.4516	0.4583
2750	0.0145	0.0384	0.0881	0.1636	0.2447	0.3081	0.3476	0.3689	0.3796	0.3847
3000	0.0141	0.0365	0.0812	0.1460	0.2127	0.2630	0.2937	0.3100	0.3181	0.3219
3250	0.0137	0.0346	0.0745	0.1298	0.1841	0.2238	0.2473	0.2597	0.2658	0.2688
3500	0.0133	0.0326	0.0680	0.1149	0.1588	0.1898	0.2078	0.2171	0.2217	0.2239
3750	0.0129	0.0307	0.0619	0.1012	0.1364	0.1605	0.1742	0.1812	0.1847	0.1863
4000	0.0124	0.0287	0.0561	0.0888	0.1169	0.1355	0.1458	0.1511	0.1537	0.1549
4250	0.0119	0.0268	0.0505	0.0776	0.0999	0.1142	0.1221	0.1261	0.1280	0.1289
4500	0.0114	0.0249	0.0454	0.0677	0.0854	0.0964	0.1024	0.1054	0.1068	0.1075

FIGURE 25: THE V' COEFFICIENT IS SHOWN FOR LEVEL 4F
THIS INDICATES THE DEPENDENCE OF THIS LEVEL'S POPULATION ON THE
GROUND STATE'S POPULATION. THIS TABLE IS DISCUSSED IN SECTION IV.C.

	1.0E12	2.2E12	4.6E12	1.0E13	2.2E13	4.6E13	1.0E14	2.2E14	4.6E14	1.0E15
1500	0.0161	0.0282	0.0477	0.0731	0.0983	0.1177	0.1298	0.1365	0.1398	0.1414
1750	0.0311	0.0526	0.0865	0.1293	0.1713	0.2033	0.2232	0.2340	0.2395	0.2421
2000	0.0504	0.0828	0.1322	0.1930	0.2512	0.2948	0.3216	0.3361	0.3434	0.3469
2250	0.0729	0.1167	0.1814	0.2588	0.3308	0.3835	0.4154	0.4324	0.4409	0.4450
2500	0.0976	0.1528	0.2320	0.3236	0.4061	0.4650	0.4999	0.5184	0.5275	0.5319
2750	0.1239	0.1902	0.2825	0.3857	0.4757	0.5379	0.5742	0.5931	0.6024	0.6069
3000	0.1513	0.2282	0.3323	0.4446	0.5390	0.6024	0.6386	0.6573	0.6665	0.6708
3250	0.1796	0.2668	0.3811	0.5001	0.5964	0.6591	0.6943	0.7122	0.7209	0.7250
3500	0.2088	0.3057	0.4287	0.5519	0.6479	0.7086	0.7420	0.7588	0.7669	0.7708
3750	0.2388	0.3446	0.4747	0.5999	0.6938	0.7516	0.7826	0.7982	0.8057	0.8092
4000	0.2693	0.3834	0.5188	0.6440	0.7344	0.7884	0.8171	0.8312	0.8380	0.8412
4250	0.3004	0.4218	0.5607	0.6839	0.7698	0.8199	0.8460	0.8588	0.8649	0.8678
4500	0.3318	0.4593	0.5998	0.7197	0.8005	0.8464	0.8701	0.8816	0.8871	0.8897

FIGURE 26: THE V COEFFICIENT IS SHOWN FOR LEVEL 4F
THIS INDICATES THE DEPENDENCE OF THIS LEVEL'S POPULATION ON THE FREE ELECTRON POPULATION. THIS TABLE IS DISCUSSED IN SECTION IV.C.

E 8

	1.0E12	2.2E12	4.6E12	1.0E13	2.2E13	4.6E13	1.0E14	2.2E14	4.6E14	1.0E15
1500	0.0456	0.0923	0.1783	0.3102	0.4643	0.5977	0.6874	0.7382	0.7643	0.7769
1750	0.0430	0.0856	0.1622	0.2769	0.4079	0.5194	0.5934	0.6351	0.6563	0.6666
2000	0.0407	0.0793	0.1471	0.2455	0.3546	0.4450	0.5040	0.5368	0.5534	0.5615
2250	0.0386	0.0736	0.1332	0.2170	0.3066	0.3786	0.4246	0.4499	0.4627	0.4688
2500	0.0366	0.0683	0.1207	0.1916	0.2645	0.3213	0.3567	0.3759	0.3856	0.3902
2750	0.0348	0.0634	0.1093	0.1690	0.2279	0.2723	0.2993	0.3138	0.3210	0.3245
3000	0.0330	0.0589	0.0989	0.1488	0.1961	0.2305	0.2510	0.2618	0.2672	0.2697
3250	0.0314	0.0547	0.0894	0.1309	0.1685	0.1949	0.2103	0.2183	0.2222	0.2241
3500	0.0298	0.0507	0.0807	0.1148	0.1444	0.1645	0.1760	0.1819	0.1848	0.1861
3750	0.0283	0.0469	0.0725	0.1004	0.1235	0.1386	0.1471	0.1515	0.1536	0.1546
4000	0.0267	0.0433	0.0650	0.0875	0.1054	0.1168	0.1230	0.1262	0.1277	0.1284
4250	0.0253	0.0399	0.0581	0.0761	0.0898	0.0983	0.1029	0.1052	0.1063	0.1068
4500	0.0238	0.0365	0.0518	0.0661	0.0766	0.0829	0.0863	0.0879	0.0887	0.0891

FIGURE 27: THE V' COEFFICIENT IS SHOWN FOR LEVEL 8P
THIS INDICATES THE DEPENDENCE OF THIS LEVEL'S POPULATION ON THE GROUND STATE'S POPULATION. THIS TABLE IS DISCUSSED IN SECTION IV.C.

	1.0E12	2.2E12	4.6E12	1.0E13	2.2E13	4.6E13	1.0E14	2.2E14	4.6E14	1.0E15
1500	0.0677	0.0948	0.1244	0.1525	0.1757	0.1919	0.2016	0.2068	0.2094	0.2106
1750	0.1108	0.1507	0.1936	0.2348	0.2694	0.2939	0.3087	0.3166	0.3206	0.3225
2000	0.1587	0.2102	0.2649	0.3175	0.3617	0.3929	0.4117	0.4217	0.4268	0.4292
2250	0.2083	0.2698	0.3342	0.3956	0.4468	0.4825	0.5038	0.5150	0.5206	0.5233
2500	0.2581	0.3277	0.3996	0.4674	0.5228	0.5608	0.5831	0.5947	0.6005	0.6033
2750	0.3073	0.3834	0.4608	0.5326	0.5899	0.6283	0.6503	0.6618	0.6674	0.6701
3000	0.3558	0.4370	0.5182	0.5917	0.6489	0.6862	0.7072	0.7180	0.7233	0.7258
3250	0.4039	0.4888	0.5720	0.6455	0.7008	0.7359	0.7553	0.7652	0.7700	0.7722
3500	0.4517	0.5390	0.6227	0.6943	0.7464	0.7785	0.7959	0.8047	0.8089	0.8109
3750	0.4996	0.5880	0.6704	0.7386	0.7864	0.8149	0.8301	0.8377	0.8414	0.8431
4000	0.5476	0.6355	0.7150	0.7783	0.8210	0.8459	0.8588	0.8652	0.8683	0.8697
4250	0.5957	0.6814	0.7564	0.8137	0.8509	0.8719	0.8827	0.8880	0.8905	0.8917
4500	0.6434	0.7254	0.7943	0.8448	0.8764	0.8938	0.9025	0.9068	0.9088	0.9098

FIGURE 28: THE V COEFFICIENT IS SHOWN FOR LEVEL 8P
THIS INDICATES THE DEPENDENCE OF THIS LEVEL'S POPULATION ON THE FREE ELECTRON POPULATION. THIS TABLE IS DISCUSSED IN SECTION IV.C.

	1.0E12	2.2E12	4.6E12	1.0E13	2.2E13	4.6E13	1.0E14	2.2E14	4.6E14	1.0E15
1500	0.0199	0.0541	0.1280	0.2502	0.3982	0.5283	0.6164	0.6665	0.6922	0.7047
1750	0.0188	0.0497	0.1140	0.2172	0.3387	0.4434	0.5134	0.5528	0.5730	0.5828
2000	0.0177	0.0456	0.1013	0.1874	0.2855	0.3677	0.4216	0.4517	0.4670	0.4744
2250	0.0168	0.0418	0.0900	0.1616	0.2400	0.3037	0.3445	0.3670	0.3784	0.3839
2500	0.0159	0.0384	0.0801	0.1394	0.2018	0.2508	0.2815	0.2982	0.3065	0.3106
2750	0.0151	0.0354	0.0714	0.1205	0.1699	0.2074	0.2303	0.2426	0.2488	0.2517
3000	0.0143	0.0326	0.0637	0.1041	0.1431	0.1717	0.1888	0.1978	0.2023	0.2044
3250	0.0136	0.0300	0.0568	0.0900	0.1206	0.1422	0.1549	0.1615	0.1648	0.1663
3500	0.0129	0.0276	0.0505	0.0777	0.1016	0.1179	0.1272	0.1320	0.1344	0.1355
3750	0.0122	0.0254	0.0449	0.0669	0.0854	0.0977	0.1045	0.1080	0.1097	0.1105
4000	0.0115	0.0233	0.0399	0.0576	0.0719	0.0810	0.0860	0.0886	0.0898	0.0904
4250	0.0109	0.0213	0.0353	0.0495	0.0604	0.0672	0.0709	0.0728	0.0736	0.0741
4500	0.0103	0.0194	0.0311	0.0425	0.0509	0.0559	0.0586	0.0600	0.0606	0.0609

FIGURE 29: THE V' COEFFICIENT IS SHOWN FOR LEVEL 7D
THIS INDICATES THE DEPENDENCE OF THIS LEVEL'S POPULATION ON THE
GROUND STATE'S POPULATION. THIS TABLE IS DISCUSSED IN SECTION IV.C.

	1.0E12	2.2E12	4.6E12	1.0E13	2.2E13	4.6E13	1.0E14	2.2E14	4.6E14	1.0E15
1500	0.0570	0.1016	0.1530	0.1996	0.2348	0.2578	0.2709	0.2777	0.2811	0.2827
1750	0.0896	0.1541	0.2259	0.2902	0.3390	0.3711	0.3896	0.3993	0.4041	0.4064
2000	0.1247	0.2076	0.2969	0.3756	0.4350	0.4739	0.4963	0.5080	0.5138	0.5166
2250	0.1602	0.2593	0.3629	0.4523	0.5189	0.5620	0.5866	0.5994	0.6056	0.6086
2500	0.1952	0.3082	0.4229	0.5197	0.5905	0.6355	0.6608	0.6738	0.6802	0.6832
2750	0.2293	0.3540	0.4772	0.5787	0.6512	0.6963	0.7213	0.7340	0.7402	0.7431
3000	0.2623	0.3970	0.5264	0.6304	0.7028	0.7467	0.7706	0.7827	0.7885	0.7913
3250	0.2944	0.4374	0.5712	0.6759	0.7467	0.7886	0.8110	0.8222	0.8276	0.8301
3500	0.3257	0.4757	0.6123	0.7161	0.7842	0.8235	0.8441	0.8543	0.8592	0.8615
3750	0.3564	0.5121	0.6500	0.7516	0.8162	0.8526	0.8713	0.8805	0.8849	0.8870
4000	0.3866	0.5467	0.6845	0.7829	0.8435	0.8767	0.8936	0.9018	0.9057	0.9075
4250	0.4162	0.5795	0.7159	0.8102	0.8665	0.8967	0.9118	0.9191	0.9226	0.9242
4500	0.4453	0.6105	0.7443	0.8339	0.8859	0.9132	0.9266	0.9331	0.9362	0.9376

FIGURE 30: THE V COEFFICIENT IS SHOWN FOR LEVEL 7D
THIS INDICATES THE DEPENDENCE OF THIS LEVEL'S POPULATION ON THE FREE ELECTRON POPULATION. THIS TABLE IS DISCUSSED IN SECTION IV.C.

	1.0E12	2.2E12	4.6E12	1.0E13	2.2E13	4.6E13	1.0E14	2.2E14	4.6E14	1.0E15
1500	0.0360	0.0764	0.1537	0.2746	0.4173	0.5414	0.6249	0.6723	0.6966	0.7084
1750	0.0341	0.0706	0.1385	0.2418	0.3607	0.4622	0.5297	0.5677	0.5871	0.5965
2000	0.0323	0.0653	0.1249	0.2125	0.3101	0.3912	0.4442	0.4737	0.4887	0.4960
2250	0.0307	0.0606	0.1127	0.1867	0.2662	0.3303	0.3713	0.3938	0.4051	0.4106
2500	0.0292	0.0563	0.1020	0.1644	0.2288	0.2790	0.3104	0.3274	0.3359	0.3400
2750	0.0278	0.0524	0.0924	0.1448	0.1968	0.2359	0.2598	0.2726	0.2790	0.2820
3000	0.0266	0.0489	0.0838	0.1276	0.1693	0.1996	0.2177	0.2273	0.2320	0.2343
3250	0.0254	0.0455	0.0759	0.1124	0.1456	0.1689	0.1825	0.1896	0.1931	0.1948
3500	0.0242	0.0424	0.0687	0.0988	0.1250	0.1428	0.1530	0.1582	0.1608	0.1620
3750	0.0231	0.0394	0.0620	0.0866	0.1072	0.1207	0.1282	0.1320	0.1339	0.1348
4000	0.0219	0.0365	0.0558	0.0758	0.0917	0.1019	0.1075	0.1103	0.1116	0.1123
4250	0.0208	0.0337	0.0500	0.0661	0.0785	0.0861	0.0902	0.0922	0.0932	0.0937
4500	0.0197	0.0311	0.0448	0.0577	0.0671	0.0728	0.0758	0.0773	0.0781	0.0784

FIGURE 31: THE V' COEFFICIENT IS SHOWN FOR LEVEL 95
THIS INDICATES THE DEPENDENCE OF THIS LEVEL'S POPULATION ON THE GROUND STATE'S POPULATION. THIS TABLE IS DISCUSSED IN SECTION IV.C.

	1.0E12	2.2E12	4.6E12	1.0E13	2.2E13	4.6E13	1.0E14	2.2E14	4.6E14	1.0E15
1500	0.0985	0.1385	0.1790	0.2144	0.2416	0.2597	0.2702	0.2758	0.2786	0.2799
1750	0.1443	0.1985	0.2529	0.3010	0.3387	0.3643	0.3795	0.3875	0.3915	0.3934
2000	0.1908	0.2575	0.3235	0.3821	0.4283	0.4598	0.4784	0.4883	0.4931	0.4955
2250	0.2364	0.3135	0.3888	0.4553	0.5075	0.5428	0.5634	0.5743	0.5797	0.5822
2500	0.2802	0.3659	0.4484	0.5204	0.5763	0.6134	0.6348	0.6459	0.6514	0.6540
2750	0.3222	0.4150	0.5028	0.5784	0.6357	0.6731	0.6942	0.7052	0.7105	0.7130
3000	0.3628	0.4614	0.5530	0.6302	0.6874	0.7237	0.7439	0.7542	0.7593	0.7617
3250	0.4025	0.5057	0.5996	0.6769	0.7325	0.7668	0.7856	0.7951	0.7997	0.8019
3500	0.4418	0.5483	0.6432	0.7191	0.7719	0.8037	0.8207	0.8292	0.8333	0.8353
3750	0.4810	0.5898	0.6842	0.7573	0.8064	0.8351	0.8502	0.8577	0.8613	0.8630
4000	0.5203	0.6301	0.7226	0.7916	0.8364	0.8618	0.8749	0.8814	0.8845	0.8859
4250	0.5597	0.6691	0.7582	0.8223	0.8622	0.8843	0.8956	0.9010	0.9036	0.9048
4500	0.5992	0.7066	0.7910	0.8493	0.8844	0.9032	0.9127	0.9173	0.9194	0.9204

FIGURE 32: THE V COEFFICIENT IS SHOWN FOR LEVEL 9S
THIS INDICATES THE DEPENDENCE OF THIS LEVEL'S POPULATION ON THE FREE ELECTRON POPULATION. THIS TABLE IS DISCUSSED IN SECTION IV.C.

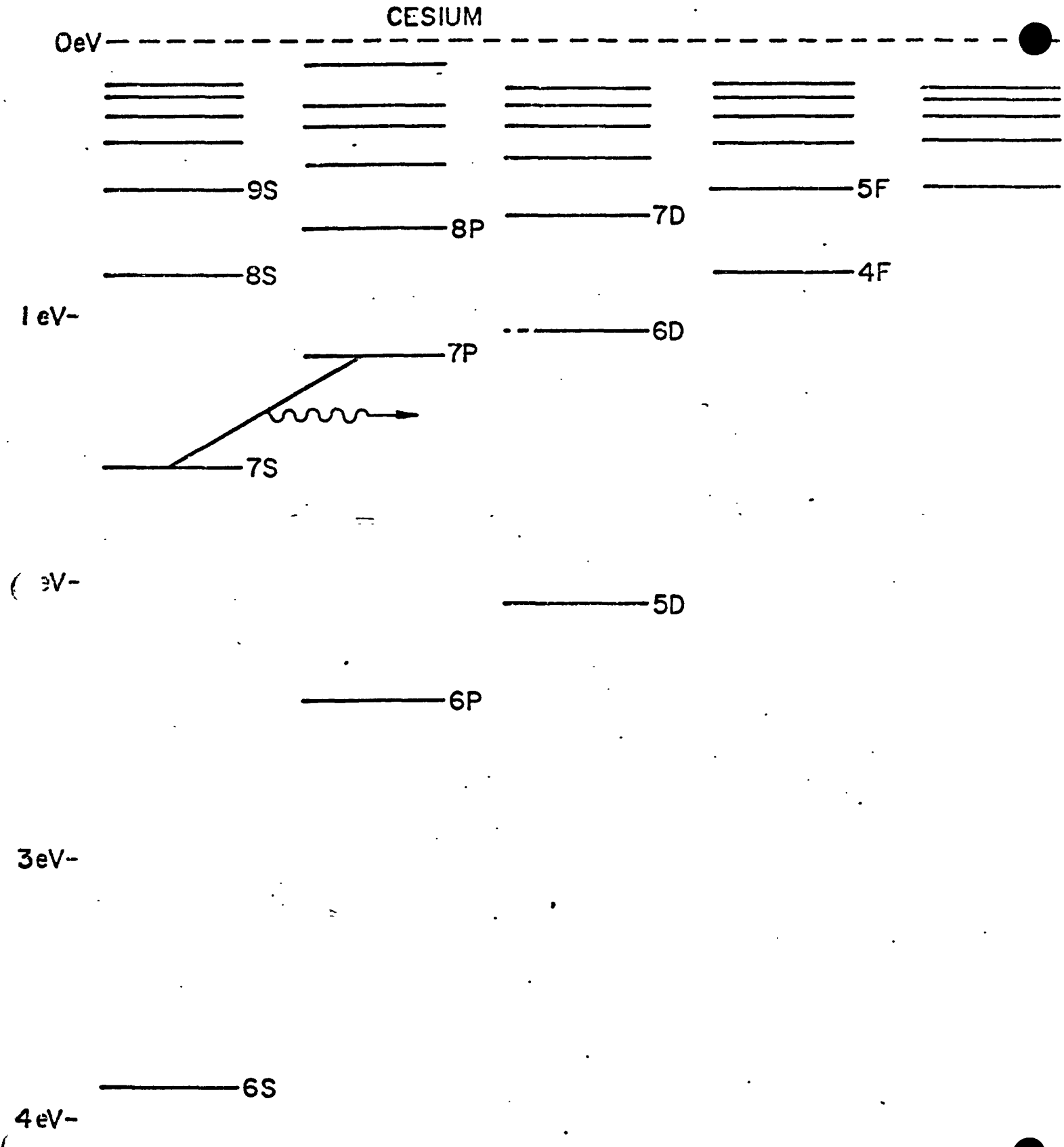

Figure 33: A Grotrian diagram of the Cesium levels used in the ionization-recombination calculations discussed in chapters IV and V.

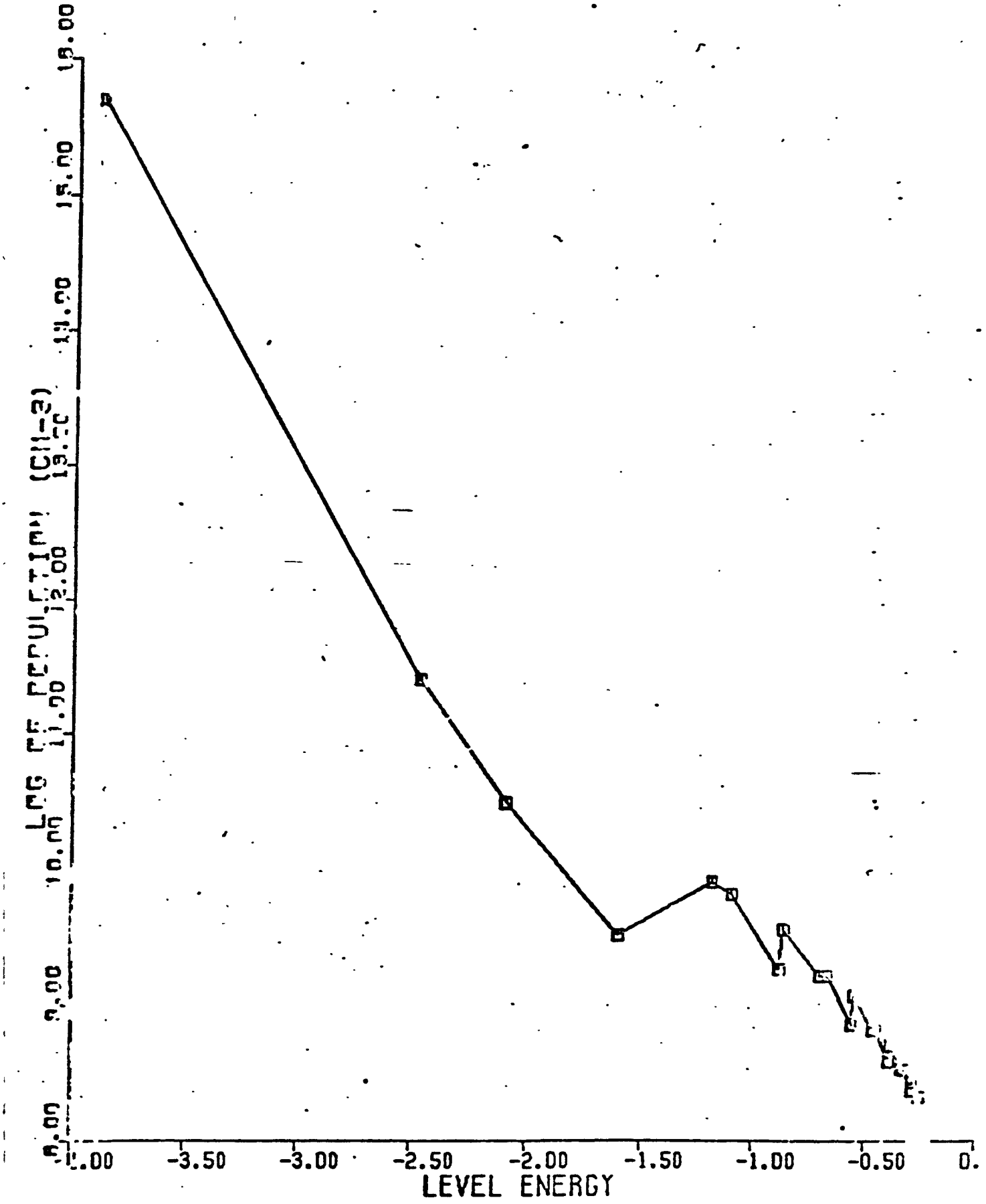

Figure 34: The population distribution of atomic Cesium levels in cm-3 is shown against the level energy in eV for an electron temperature of 1500K and an electron density of 1(14) cm-3. Mansbach and Keck rates were used. This shows the 7p-7s population inversion.

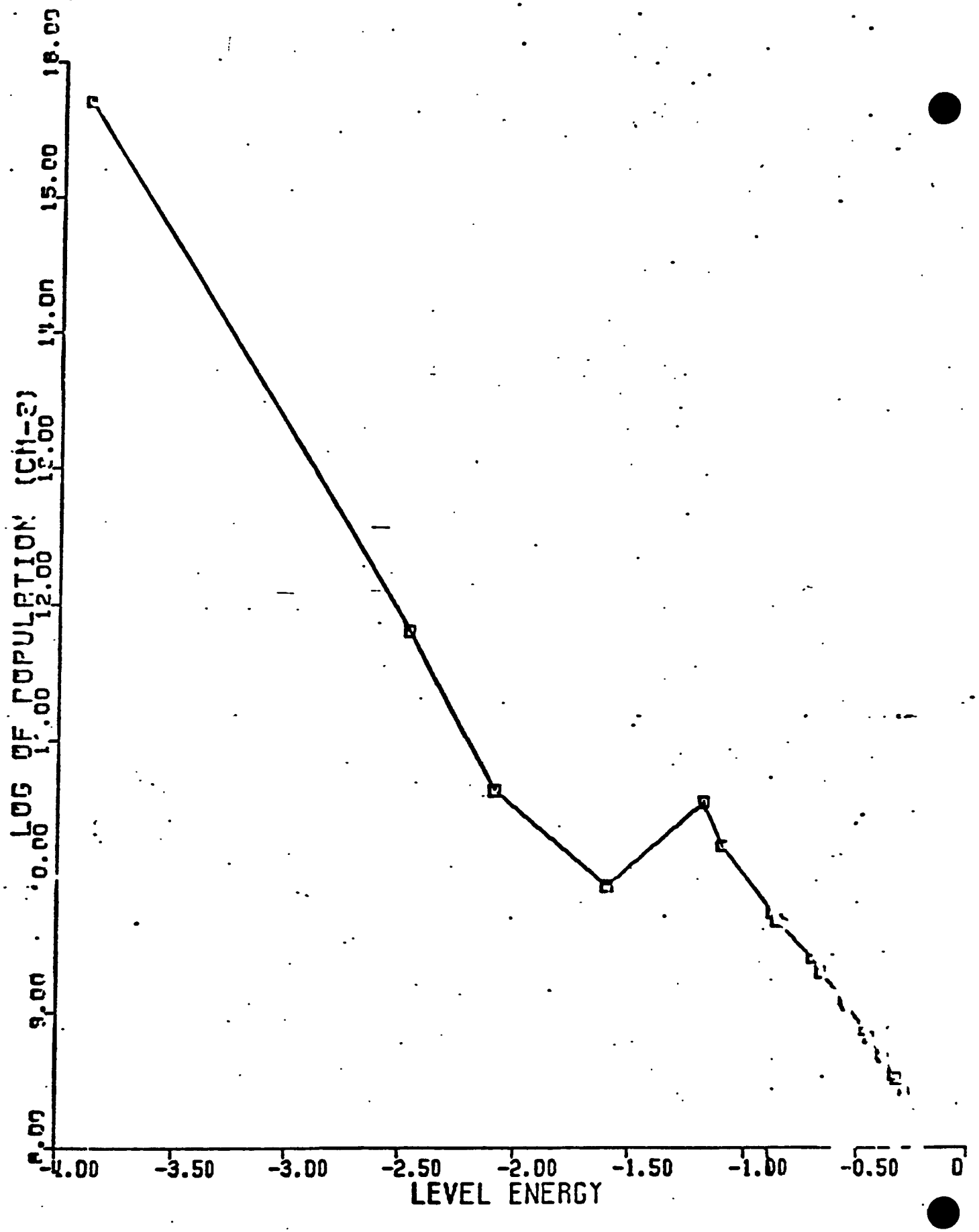

Figure 35: The population distribution of atomic Cesium levels in cm-3 is shown against the level energy in eV for an electron temperature of 1500K and an electron density of 1(14) cm-3. Stabler rates were used.

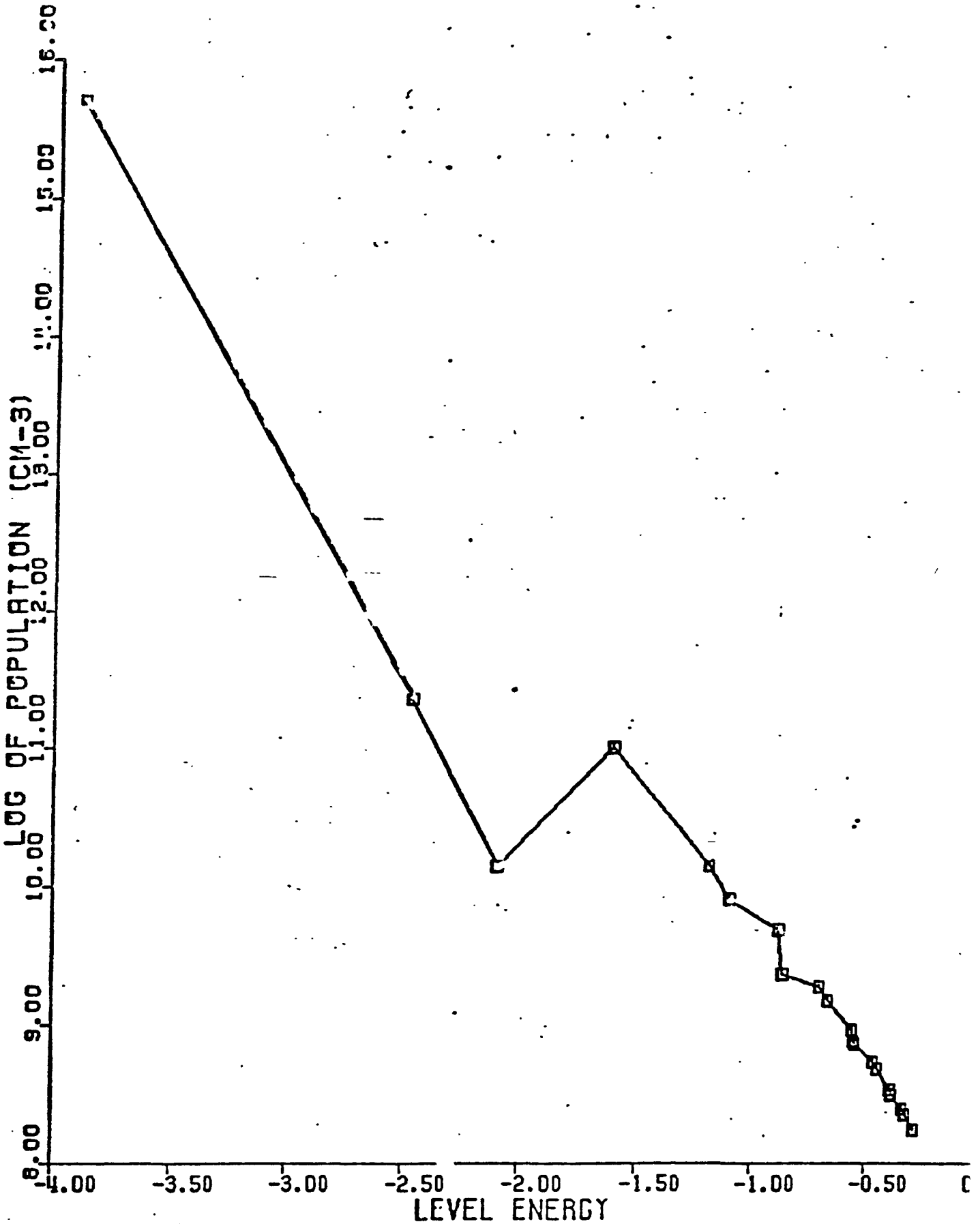

Figure 36: The population distribution of atomic Cesiu levels in cm-3 is shown against the level energy in eV fo an electron temperature of 1500K and an electron density o 1(14) cm-3. Bethe-Born rates were used.

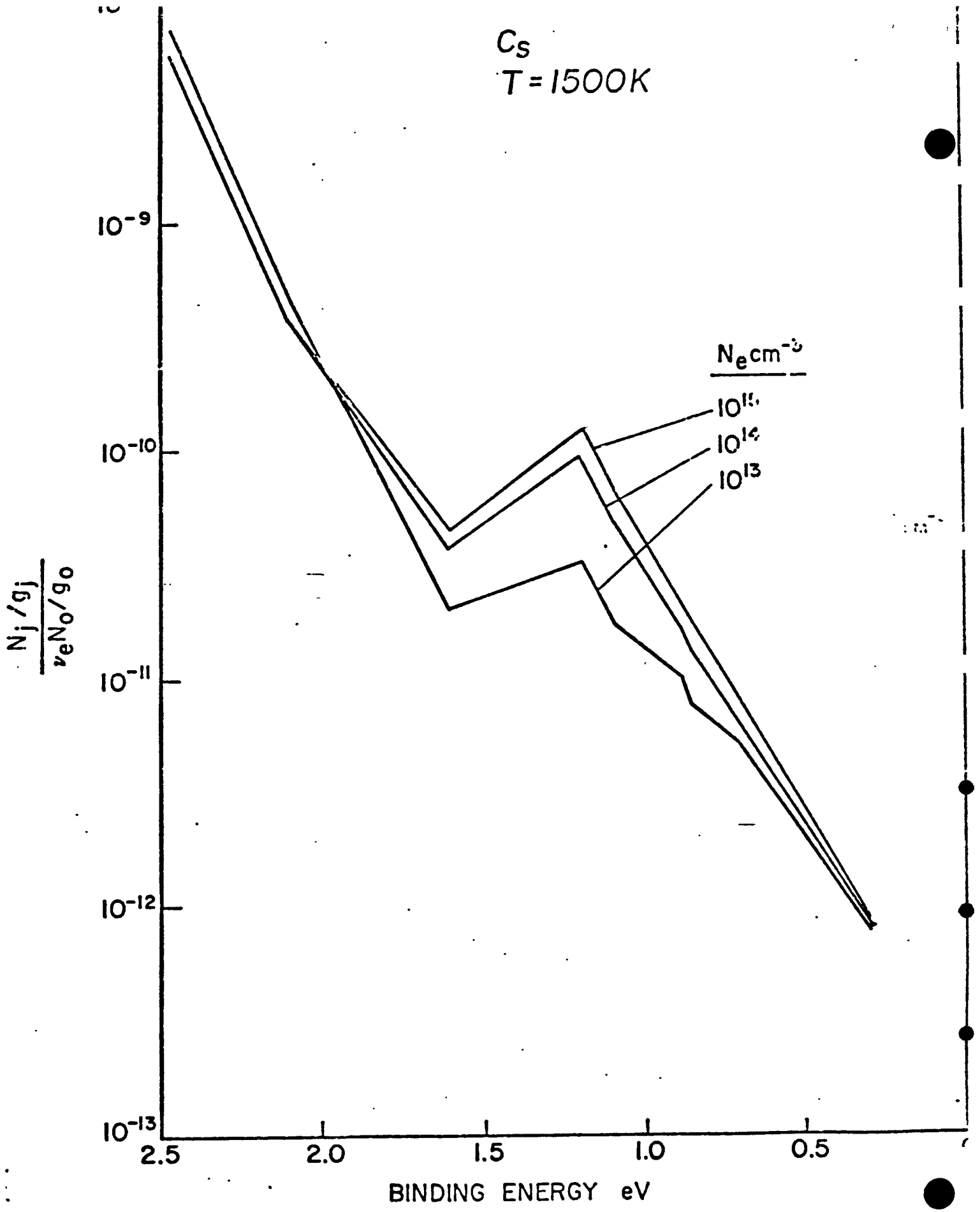

Figure 37: The population distribution of excited Cesium levels in cm-3 is shown against the binding energy in eV for an electron temperature of 1500K and for various electron densities. Gryzinski rates were used. Small ground state densities are assumed.

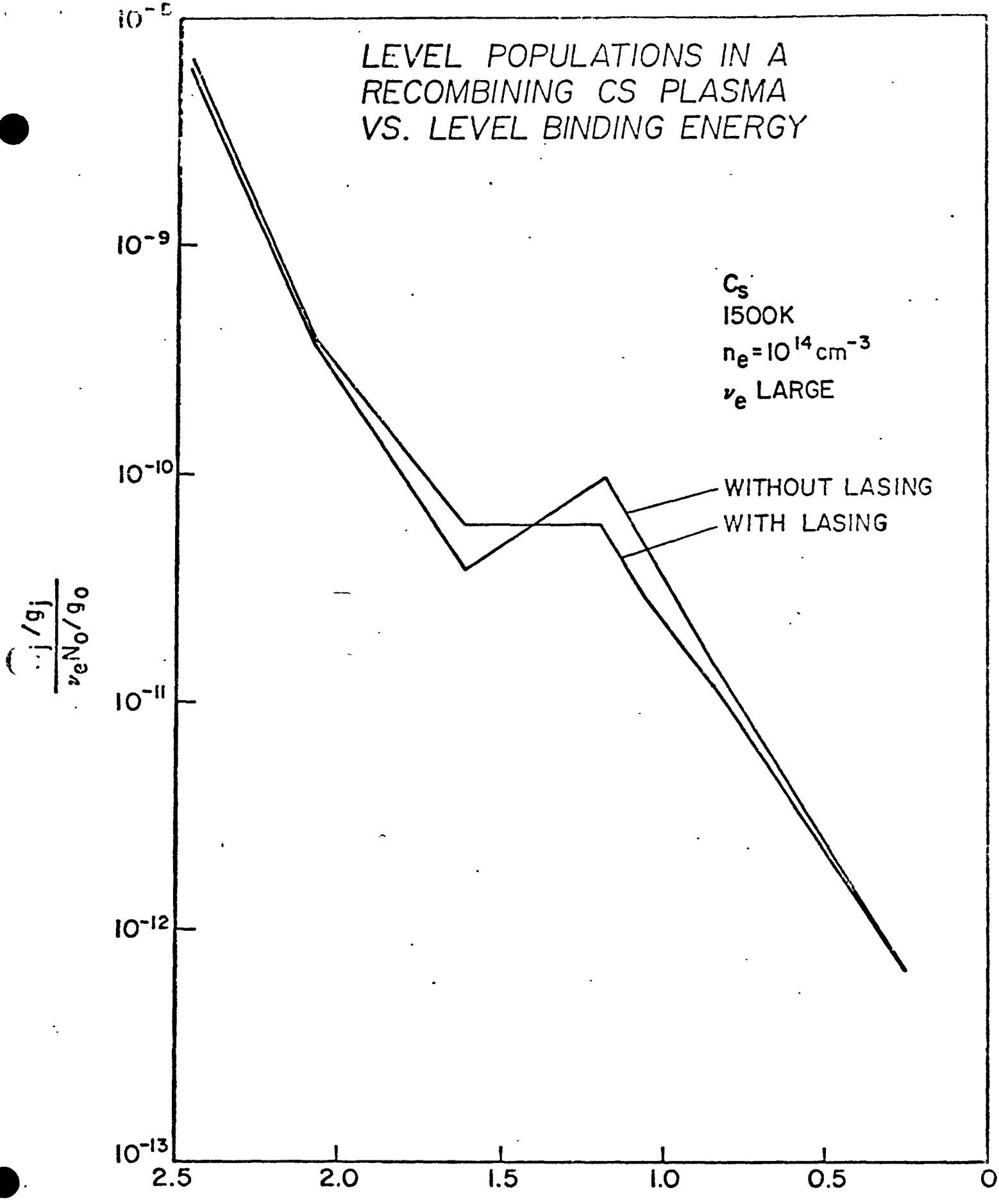

Figure 38: The population distribution of excited Cesium levels in cm-3 is shown against the binding energy in eV for an electron temperature of 1500K and an electron density of 1(14) cm-3. Gryzinski rates were used. Small ground state densities are assumed. The distribution is shown for cases both with and without recombination lasing.

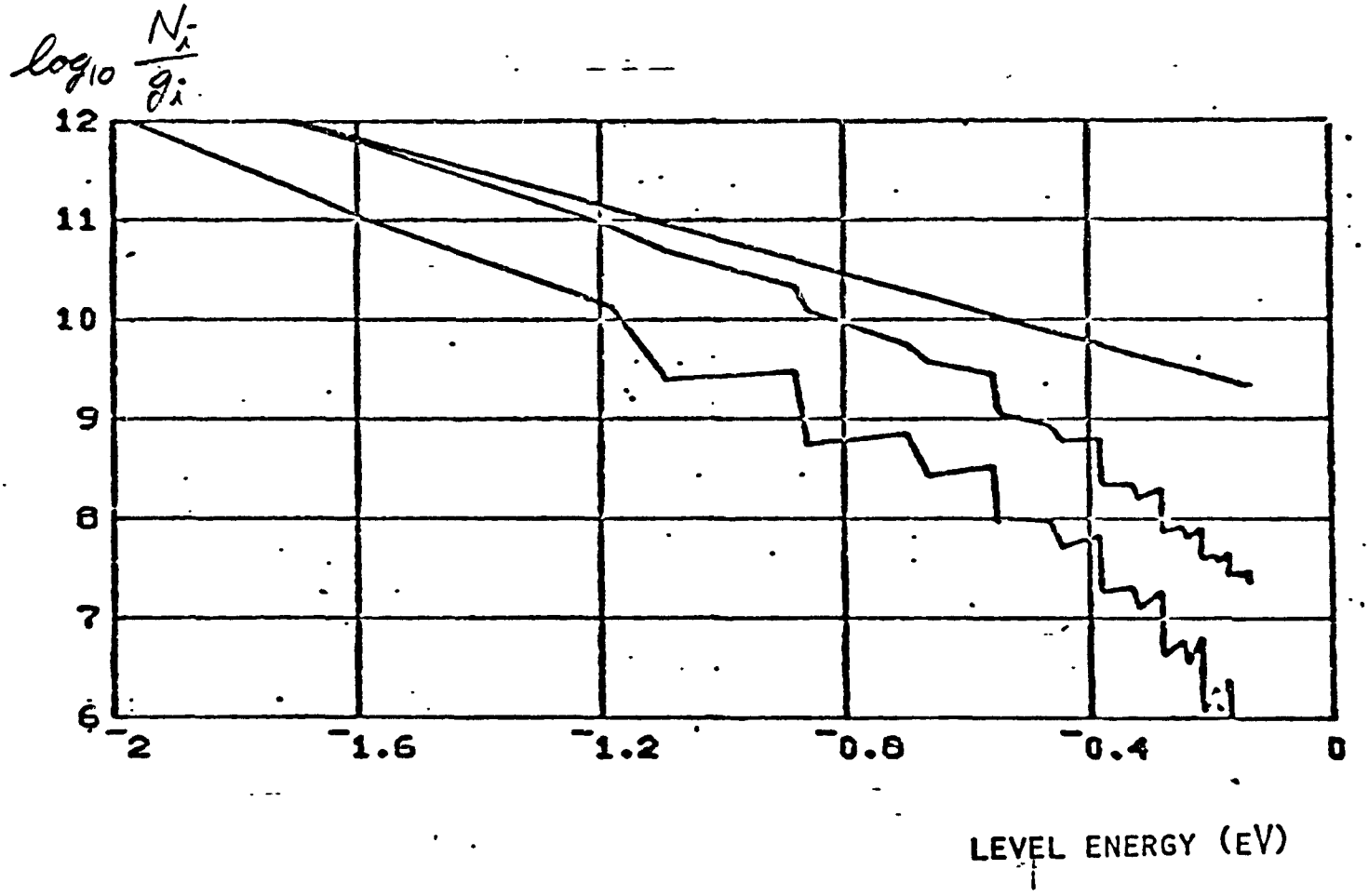

Figure 39: The population distribution of high excited levels in Cesium is shown against level energy for three electron densities. A ground state density of 1(16) cm-3 is assumed. This illustrates the difficulty in measuring electron temperature from population distributions when the lectron density is much below Saha.

IONIZATION AND RECOMBINATION RATES IN CS VS. 7P-7S RADIATION INTENSITY

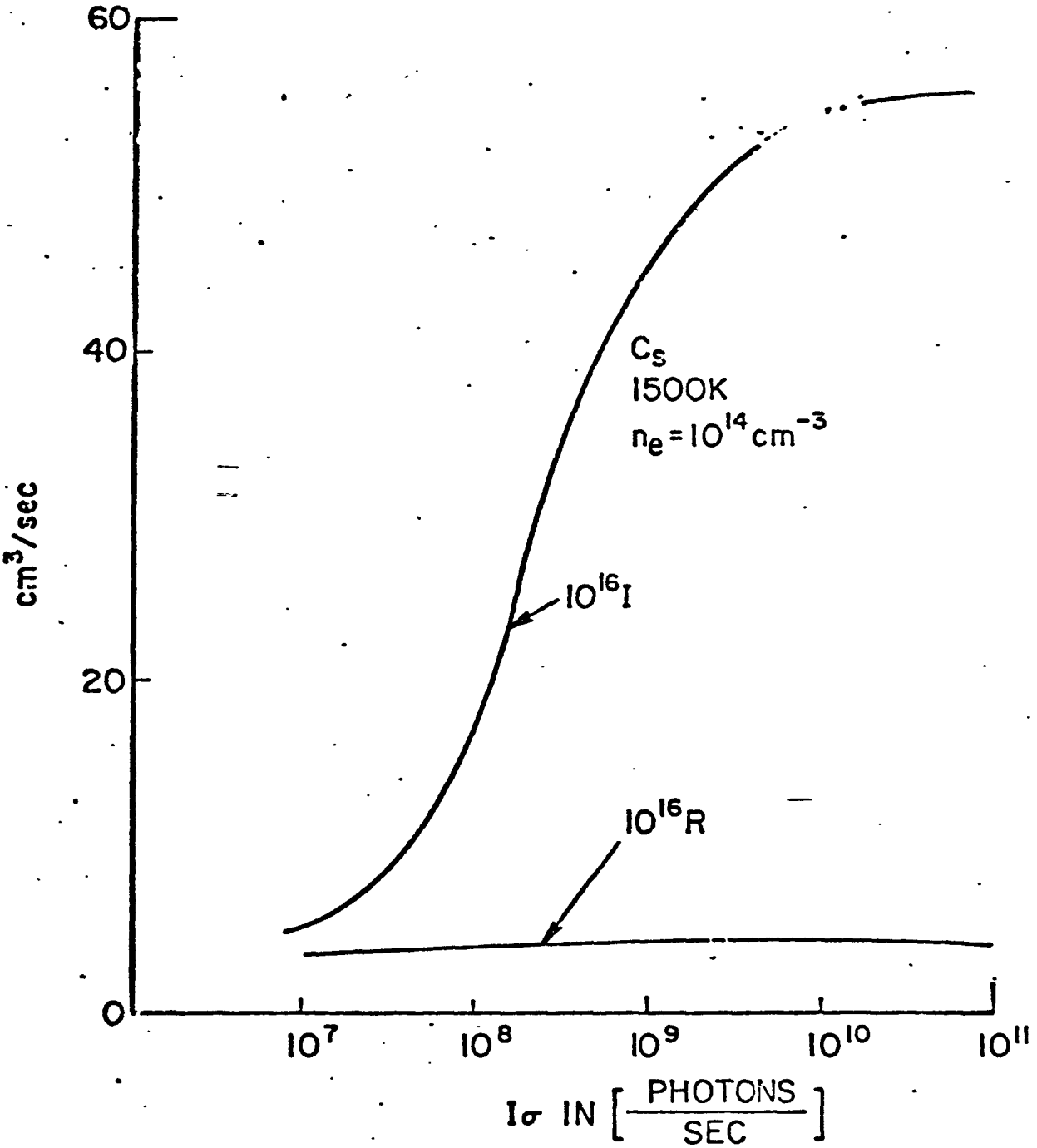

σ = absorption cross-section
I = radiation intensity
$I\sigma = 10^{10}$ photons/sec corresponds to $I \sim 1$ watt/cm^2

Figure 40.

	ϵ_j	k_j	k_{je}	
0	6.754E-11	0.000E+00	2.530E+24	6S
1	4.771E+03	4.170E+04	2.530E+24	6P
2	1.206E+07	2.647E+07	2.530E+24	5D
3	1.546E+12	3.982E+11	2.530E+24	7S
4	1.943E+16	2.288E+16	2.530E+24	7P
5	8.793E+16	8.753E+16	2.530E+24	6D
6	1.424E+19	2.431E+18	2.530E+24	8S
7	1.201E+19	1.101E+19	2.530E+24	4F
8	4.973E+20	1.737E+20	2.529E+24	8P
9	9.174E+20	3.286E+20	2.529E+24	7D
10	1.248E+22	9.432E+20	2.528E+24	9S
11	7.496E+21	3.795E+21	2.524E+24	5F
12	7.578E+21	9.917E+20	2.523E+24	5G
13	5.410E+22	6.388E+21	2.517E+24	9P
14	7.131E+22	1.094E+22	2.506E+24	8D
15	3.565E+23	5.912E+21	2.500E+24	10S
16	1.946E+23	5.686E+22	2.443E+24	6F
17	8.587E+22	1.503E+22	2.427E+24	6G,6H
18	6.203E+23	1.881E+22	2.409E+24	10P
19	6.912E+23	5.324E+22	2.355E+24	9D
20	2.160E+24	-1.516E+22	2.370E+24	11S
21	1.149E+24	2.059E+23	2.165E+24	7F
22	3.060E+23	6.346E+22	2.101E+24	7G,7H,7I
23	2.408E+24	-8.936E+21	2.110E+24	11P
24	2.430E+24	1.052E+23	2.005E+24	10D
25	6.012E+24	-7.911E+22	2.084E+24	12S
26	3.113E+24	3.598E+23	1.724E+24	8F
27	5.709E+23	1.201E+23	1.604E+24	8G,8H,8I,8J
28	5.220E+24	-7.624E+22	1.680E+24	12P
29	4.926E+24	1.301E+23	1.550E+24	11D
30	1.079E+25	-1.388E+23	1.689E+24	13S
31	5.372E+24	4.161E+23	1.273E+24	9F
32	7.267E+23	1.455E+23	1.127E+24	9G,9H,9I,9J,9K
33	8.022E+24	-1.284E+23	1.256E+24	13P
34	7.183E+24	1.222E+23	1.134E+24	12D
35	1.484E+25	-1.597E+23	1.293E+24	14S
36	7.005E+24	3.753E+23	9.180E+23	10F
37	7.275E+23	1.325E+23	7.855E+23	10G,10H,10I,10J,10K

Figure 41: The resistances of equivalent circuit theory for the levels of Cesium at 500K is shown.

	$\Omega_{\tilde{\lambda}}$	$R_{\tilde{\lambda}}$	$R_{\tilde{\lambda}e}$	
0	7.22?E-11	0.000E+00	7.064E+11	6S
1	7.83?E-02	6.848E-01	7.064E+11	6P
2	1.103E+01	2.415E+01	7.064E+11	5D
3	3.110E+04	8.002E+03	7.064E+11	7S
4	1.404E+07	1.742E+07	7.064E+11	7P
5	3.462E+07	3.071E+07	7.064E+11	6D
6	1.093E+09	1.718E+08	7.062E+11	8S
7	7.811E+08	6.912E+08	7.055E+11	4F
8	9.103E+09	2.887E+09	7.026E+11	8P
9	1.244E+10	3.831E+09	6.988E+11	7D
10	7.855E+10	3.708E+09	6.951E+11	9S
11	4.181E+10	2.035E+10	6.747E+11	5F
12	4.002E+10	4.354E+09	6.704E+11	5G
13	1.571E+11	1.236E+10	6.580E+11	9P
14	1.716E+11	2.249E+10	6.355E+11	8D
15	5.856E+11	-1.577E+09	6.371E+11	10S
16	2.830E+11	7.902E+10	5.581E+11	6F
17	1.191E+11	1.839E+10	5.397E+11	6G,6H
18	6.311E+11	4.796E+09	5.349E+11	10P
19	6.141E+11	4.051E+10	4.944E+11	9D
20	1.592E+12	-2.533E+10	5.197E+11	11S
21	7.367E+11	1.251E+11	3.946E+11	7F
22	1.868E+11	3.187E+10	3.627E+11	7G,7H,7I
23	1.271E+12	-1.701E+10	3.797E+11	11P
24	1.152E+12	4.280E+10	3.369E+11	10D
25	2.616E+12	-4.287E+10	3.798E+11	12S
26	1.169E+12	1.271E+11	2.527E+11	8F
27	2.035E+11	3.468E+10	2.180E+11	8G,8H,8I,8J
28	1.778E+12	-3.039E+10	2.494E+11	12P
29	1.533E+12	3.477E+10	2.136E+11	11D
30	3.279E+12	-4.442E+10	2.581E+11	13S
31	1.405E+12	1.018E+11	1.562E+11	9F
32	1.902E+11	2.906E+10	1.272E+11	9G,9H,9I,9J,9K
33	2.018E+12	-3.106E+10	1.582E+11	13P
34	1.675E+12	2.456E+10	1.336E+11	12D
35	3.503E+12	-3.678E+10	1.704E+11	14S
36	1.435E+12	7.192E+10	9.851E+10	10F
37	1.420E+11	2.099E+10	7.752E+10	10G,10H,10I,10J,10K,1

Figure 42: The resistances of equivalent circuit theory for the levels of Cesium at 750K is shown.

0	8.774E-11	0.000E+00	4.626E-01	6S
1	1.308E-06	1.143E-05	4.625E-01	6P
2	1.050E-05	2.187E-05	4.625E-01	5D
3	6.522E-04	1.607E-04	4.624E-01	7S
4	1.025E-02	1.260E-02	4.498E-01	7P
5	1.297E-02	8.743E-03	4.410E-01	6D
6	8.462E-02	7.889E-03	4.331E-01	8S
7	4.606E-02	3.777E-02	3.954E-01	4F
8	1.560E-01	3.242E-02	3.629E-01	8P
9	1.503E-01	3.403E-02	3.289E-01	7D
10	4.870E-01	-1.469E-03	3.304E-01	9S
11	2.027E-01	8.901E-02	2.414E-01	5F
12	1.790E-01	1.323E-02	2.281E-01	5G
13	4.192E-01	8.190E-03	2.200E-01	9P
14	3.611E-01	3.469E-02	1.853E-01	8D
15	9.312E-01	-2.079E-02	2.061E-01	10S
16	3.495E-01	8.576E-02	1.203E-01	6F
17	1.363E-01	1.408E-02	1.062E-01	6G,6H
18	5.824E-01	-7.485E-03	1.137E-01	10P
19	4.716E-01	2.280E-02	9.090E-02	9D
20	1.118E+00	-2.314E-02	1.140E-01	11S
21	3.945E-01	5.794E-02	5.610E-02	7F
22	9.295E-02	1.037E-02	4.573E-02	7G,7H,7I
23	6.029E-01	-1.017E-02	5.591E-02	11P
24	4.690E-01	1.274E-02	4.317E-02	10D
25	1.082E+00	-1.706E-02	6.023E-02	12S
26	3.654E-01	3.386E-02	2.637E-02	8F
27	5.904E-02	6.470E-03	1.990E-02	8G,8H,8I,8J
29	5.411E-01	-7.841E-03	2.774E-02	12P
29	4.088E-01	6.761E-03	2.098E-02	11D
30	9.427E-01	-1.079E-02	3.176E-02	13S
31	3.062E-01	1.873E-02	1.303E-02	9F
32	3.649E-02	3.761E-03	9.270E-03	9G,9H,9I,9J,9K
33	4.517E-01	-5.107E-03	1.438E-02	13P
34	3.338E-01	3.571E-03	1.081E-02	12D
35	7.786E-01	-6.450E-03	1.726E-02	14S
36	2.442E-01	1.027E-02	6.997E-03	10F
37	2.249E-02	2.128E-03	4.850E-03	10G,10H,...

Fisure 43: The resistances of equivalent circuit theory for the levels of Cesium at 1500K is shown.

0	8.513E-11	0.000F+00	5.823E-04	6S
1	8.270E-08	7.227E-07	5.816E-04	6P
2	3.299E-07	6.498E-07	5.810E-04	5D
3	7.929E-06	1.815E-06	5.791E-04	7S
4	5.179E-05	6.267E-05	5.165E-04	7P
5	5.471E-05	3.213E-05	4.843E-04	6D
6	2.492E-04	1.455E-05	4.698E-04	8S
7	1.195E-04	9.358E-05	3.762E-04	4F
8	3.045E-04	4.781E-05	3.284E-04	8P
9	2.637E-04	5.152E-05	2.769E-04	7D
10	7.542E-04	-1.261E-05	2.895E-04	9S
11	2.793E-04	1.151E-04	1.744E-04	5F
12	2.397E-04	1.462E-05	1.598E-04	5G
13	5.104E-04	2.479E-06	1.573E-04	9P
14	4.068E-04	3.366E-05	1.237E-04	8D
15	1.019E-03	-2.519E-05	1.489E-04	10S
16	3.393E-04	7.733E-05	7.152E-05	6F
17	1.293E-04	1.095E-05	6.056E-05	6G,6H
18	5.413E-04	-8.162E-06	6.873E-05	10P
19	4.116E-04	1.710E-05	5.163E-05	9D
20	9.927E-04	-1.960E-05	7.123E-05	11S
21	3.115E-04	4.198E-05	2.925E-05	7F
22	7.159E-05	6.500E-06	2.275E-05	7G,7H,7I
23	4.730E-04	-7.334E-06	3.009E-05	11P
24	3.487E-04	8.116E-06	2.197E-05	10D
25	8.390E-04	-1.190E-05	3.387E-05	12S
26	2.521E-04	2.130E-05	1.257E-05	8F
27	3.976E-05	3.531E-06	9.039E-06	8G,8H,8I,8J
28	3.790E-04	-4.710E-06	1.375E-05	12P
29	2.731E-04	3.860E-06	9.889E-06	11D
30	6.660E-04	-6.646E-06	1.653E-05	13S
31	1.929E-04	1.070E-05	5.832E-06	9F
32	2.245E-05	1.871E-06	3.961E-06	9G,9H,9I,9J,9K
33	2.922E-04	-2.746E-06	6.707E-06	13P
34	2.069E-04	1.888E-06	4.820E-06	12D
35	5.145E-04	-3.653E-06	8.472E-06	14S
36	1.443E-04	5.484E-06	2.989E-06	10F
37	1.299E-05	9.975E-07	1.991E-06	10G,10H,10I,10J,10K,

Figure 44: The resistances of equivalent circuit theory for the levels of Cesium at 2000K is shown.

0	8.832E-11	0.000E+00	1.218E-05	6S
1	1.562E-08	1.365E-07	1.205E-05	6P
2	4.122E-08	7.644E-08	1.197E-05	5D
3	5.629E-07	1.166E-07	1.186E-05	7S
4	2.129E-06	2.526E-06	9.327E-06	7P
5	2.004E-06	1.048E-06	8.279E-06	6D
6	7.490E-06	2.481E-07	8.031E-06	8S
7	3.237E-06	2.425E-06	5.606E-06	4F
8	7.034E-06	8.562E-07	4.750E-06	8P
9	5.672E-06	9.796E-07	3.770E-06	7D
10	1.533E-05	-3.608E-07	4.131E-06	9S
11	5.170E-06	2.006E-06	2.125E-06	5F
12	4.352E-06	2.258E-07	1.900E-06	5G
13	8.862E-06	-2.210E-08	1.922E-06	9P
14	6.697E-06	4.886E-07	1.433E-06	8D
15	1.676E-05	-4.155E-07	1.849E-06	10S
16	5.097E-06	1.082E-06	7.668E-07	6F
17	1.909E-06	1.370E-07	6.298E-07	6G,6H
18	7.980E-06	-1.215E-07	7.513E-07	10P
19	5.809E-06	2.122E-07	5.390E-07	9D
20	1.438E-05	-2.635E-07	8.025E-07	11S
21	4.125E-06	5.138E-07	2.887E-07	7F
22	9.326E-07	7.146E-08	2.172E-07	7G,7H,7I
23	6.292E-06	-8.800E-08	3.052E-07	11P
24	4.467E-06	9.122E-08	2.140E-07	10D
25	1.119E-05	-1.424E-07	3.564E-07	12S
26	3.078E-06	2.391E-07	1.173E-07	8F
27	4.778E-07	3.570E-08	8.160E-08	8G,8H,8I,8J
28	4.704E-06	-5.076E-08	1.324E-07	12P
29	3.278E-06	4.055E-08	9.181E-08	11D
30	8.386E-06	-7.375E-08	1.656E-07	13S
31	2.229E-06	1.132E-07	5.233E-08	9F
32	2.554E-07	1.788E-08	3.445E-08	9G,9H,9I,9J,9K
33	3.455E-06	-2.767E-08	6.212E-08	13P
34	2.373E-06	1.890E-08	4.322E-08	12D
35	6.216E-06	-3.846E-09	8.168E-08	14S
36	1.604E-06	5.561E-08	2.607E-08	10F
37	1.421E-07	9.163E-09	1.691E-08	10G,10H,10I,10J,10K,1

Figure 45: The resistances of equivalent circuit theory for the levels of Cesium at 2500K is shown.

0	9.093E-11	0.000E+00	1.015E-06	6S
1	5.105E-09	4.453E-08	9.705E-07	6P
2	1.025E-08	1.791E-08	9.526E-07	5D
3	9.640E-08	1.779E-08	9.348E-07	7S
4	2.499E-07	2.905E-07	6.443E-07	7P
5	2.167E-07	1.025E-07	5.418E-07	6D
6	7.186E-07	1.093E-08	5.309E-07	8S
7	2.846E-07	2.043E-07	3.265E-07	4F
8	5.603E-07	5.423E-08	2.723E-07	8P
9	4.289E-07	6.655E-08	2.058E-07	7D
10	1.129E-06	-3.033E-08	2.361E-07	9S
11	3.527E-07	1.292E-07	1.069E-07	5F
12	2.927E-07	1.322E-08	9.365E-08	5G
13	5.827E-07	-3.702E-09	9.735E-08	9P
14	4.234E-07	2.768E-08	6.967E-08	8D
15	1.070E-06	-2.567E-08	9.533E-08	10S
16	3.024E-07	6.007E-08	3.526E-08	6F
17	1.119E-07	6.970E-09	2.829E-08	6G,6H
18	4.701E-07	-6.397E-09	3.519E-08	10P
19	3.312E-07	1.082E-08	2.437E-08	9D
20	8.420E-07	-1.424E-08	3.861E-08	11S
21	2.250E-07	2.607E-08	1.254E-08	7F
22	5.028E-08	3.334E-09	9.210E-09	7G,7H,7I
23	3.458E-07	-4.365E-09	1.358E-08	11P
24	2.386E-07	4.347E-09	9.228E-09	10D
25	6.104E-07	-7.113E-09	1.634E-08	12S
26	1.591E-07	1.144E-08	4.906E-09	8F
27	2.441E-08	1.575E-09	3.330E-09	8G,8H,8I,8J
28	2.467E-07	-2.345E-09	5.675E-09	12P
29	1.677E-07	1.845E-09	3.830E-09	11D
30	4.465E-07	-3.500E-09	7.330E-09	13S
31	1.110E-07	5.200E-09	2.130E-09	9F
32	1.257E-08	7.594E-10	1.371E-09	9G,9H,9I,9J,9K
33	1.753E-07	-1.221E-09	2.592E-09	13P
34	1.177E-07	8.320E-10	1.760E-09	12D
35	3.217E-07	-1.761E-09	3.521E-09	14S
36	7.781E-08	2.480E-09	1.041E-09	10F
37	6.819E-09	3.787E-10	6.625E-10	10G,10H,10I,10J,10K,1

Figure 46: The resistances of equivalent circuit theory for the levels of Cesium at 3000K is shown.

0	9.727E-11	0.000E+00	1.179E-08	6S
1	5.232E-10	4.476E-09	7.317E-09	6P
2	6.068E-10	8.622E-10	6.455E-09	5D
3	2.781E-09	2.994E-10	6.155E-09	7S
4	3.184E-09	3.383E-09	2.773E-09	7P
5	2.302E-09	7.953E-10	1.978E-09	6D
6	6.317E-09	-1.129E-10	2.091E-09	8S
7	1.959E-09	1.204E-09	8.870E-10	4F
8	3.249E-09	1.534E-10	7.339E-10	8P
9	2.208E-09	2.458E-10	4.881E-10	7D
10	5.756E-09	-1.617E-10	6.499E-10	9S
11	1.463E-09	4.388E-10	2.111E-10	5F
12	1.176E-09	3.499E-11	1.761E-10	5G
13	2.291E-09	-2.348E-11	1.996E-10	9P
14	1.518E-09	7.070E-11	1.289E-10	8D
15	4.060E-09	-7.913E-11	2.080E-10	10S
16	9.496E-10	1.502E-10	5.787E-11	6F
17	3.417E-10	1.395E-11	4.392E-11	6G,6H
18	1.478E-09	-1.713E-11	6.104E-11	10P
19	9.647E-10	2.227E-11	3.877E-11	9D
20	2.675E-09	-3.360E-11	7.237E-11	11S
21	5.969E-10	5.405E-11	1.831E-11	7F
22	1.299E-10	5.614E-12	1.270E-11	7G,7H,7I
23	9.435E-10	-8.391E-12	2.109E-11	11P
24	6.094E-10	7.788E-12	1.330E-11	10D
25	1.752E-09	-1.429E-11	2.759E-11	12S
26	3.782E-10	2.098E-11	6.618E-12	8F
27	5.659E-11	2.368E-12	4.250E-12	8G,8H,8I,8J
28	6.114E-10	-3.906E-12	8.156E-12	12P
29	2.918E-10	3.003E-12	5.154E-12	11D
30	1.164E-09	-6.318E-12	1.147E-11	13S
31	2.449E-10	8.754E-12	2.719E-12	9F
32	2.706E-11	1.056E-12	1.663E-12	9G,9H,9I,9J,9K
33	4.056E-10	-1.853E-12	3.516E-12	13P
34	2.582E-10	1.262E-12	2.254E-12	12D
35	7.901E-10	-2.944E-12	5.198E-12	14S
36	1.627E-10	3.920E-12	1.278E-12	10F
37	1.392E-11	4.976E-13	7.803E-13	10G,10H,10I,10J,10K,1

Figure 47: The resistances of equivalent circuit theory for the levels of Cesium at 5000K is shown.

i	Ω_1	R_1	R_{1e}	
0	9.746E-11	0.000E+00	8.198E-10	6S
1	8.405E-11	6.372E-10	1.817E-10	6P
2	6.260E-11	6.196E-11	1.197E-10	5D
3	1.806E-10	3.508E-12	1.162E-10	7S
4	9.864E-11	8.547E-11	3.075E-11	7P
5	6.058E-11	1.271E-11	1.804E-11	6D
6	1.575E-10	-4.501E-12	2.254E-11	8S
7	3.637E-11	1.639E-11	6.155E-12	4F
8	5.488E-11	8.786E-13	5.276E-12	8P
9	3.343E-11	2.209E-12	3.068E-12	7D
10	9.247E-11	-1.916E-12	4.934E-12	9S
11	1.864E-11	3.845E-12	1.139E-12	5F
12	1.459E-11	2.344E-13	9.051E-13	5G
13	2.871E-11	-2.374E-13	1.142E-12	9P
14	1.747E-11	4.777E-13	6.648E-13	8D
15	5.146E-11	-6.349E-13	1.300E-12	10S
16	9.811E-12	1.029E-12	2.706E-13	6F
17	3.447E-12	7.582E-14	1.948E-13	6G,6H
18	1.559E-11	-1.100E-13	3.048E-13	10P
19	9.470E-12	1.271E-13	1.777E-13	9D
20	2.939E-11	-2.191E-13	3.968E-13	11S
21	5.429E-12	3.186E-13	7.821E-14	7F
22	1.156E-12	2.676E-14	5.145E-14	7G,7H,7I
23	8.909E-12	-4.477E-14	9.622E-14	11P
24	5.409E-12	3.978E-14	5.645E-14	10D
25	1.752E-11	-8.199E-14	1.384E-13	12S
26	3.165E-12	1.119E-13	2.658E-14	8F
27	4.636E-13	1.034E-14	1.624E-14	8G,8H,8I,8J
28	5.352E-12	-1.967E-14	3.491E-14	12P
29	3.246E-12	1.419E-14	2.072E-14	11D
30	1.088E-11	-3.320E-14	5.392E-14	13S
31	1.934E-12	4.307E-14	1.046E-14	9F
32	2.095E-13	4.337E-15	6.123E-15	9G,9H,9I,9J,9K
33	3.362E-12	-8.226E-15	1.435E-14	13P
34	2.037E-12	5.634E-15	8.715E-15	12D
35	7.033E-12	-1.452E-14	2.323E-14	14S
36	1.233E-12	1.846E-14	4.774E-15	10F
37	1.034E-13	1.956E-15	2.818E-15	10G,10H,10I,10J,10K,

Figure 48: The resistances of equivalent circuit theory for the levels of Cesium at 10,000K is shown.

0	8.359E-11	0.000E+00	1.783E-10	6S
1	2.772E-11	1.587E-10	1.961E-11	6P
2	1.589E-11	1.000E-11	9.605E-12	5D
3	3.971E-11	-6.306E-13	1.030E-11	7S
4	1.338E-11	8.484E-12	1.811E-12	7P
5	7.465E-12	8.939E-13	9.276E-13	6D
6	2.006E-11	-4.397E-13	1.367E-12	8S
7	3.724E-12	1.094E-12	2.729E-13	4F
8	5.451E-12	2.904E-14	2.438E-13	8P
9	3.111E-12	1.141E-13	1.298E-13	7D
10	9.227E-12	-1.160E-13	2.457E-13	9S
11	1.583E-12	2.012E-13	4.454E-14	5F
12	1.220E-12	1.023E-14	3.431E-14	5G
13	2.446E-12	-1.241E-14	4.671E-14	9P
14	1.414E-12	2.127E-14	2.544E-14	8D
15	4.509E-12	-3.147E-14	5.690E-14	10S
16	7.499E-13	4.707E-14	9.837E-15	6F
17	2.601E-13	2.979E-15	6.857E-15	6G,6H
18	1.214E-12	-4.726E-15	1.158E-14	10P
19	7.071E-13	5.178E-15	6.405E-15	9D
20	2.382E-12	-9.725E-15	1.613E-14	11S
21	3.890E-13	1.341E-14	2.715E-15	7F
22	8.186E-14	9.834E-16	1.732E-15	7G,7H,7I
23	6.553E-13	-1.753E-15	3.484E-15	11P
24	3.835E-13	1.529E-15	1.956E-15	10D
25	1.348E-12	-3.394E-15	5.350E-15	12S
26	2.174E-13	4.456E-15	8.944E-16	8F
27	3.143E-14	3.634E-16	5.311E-16	8G,8H,8I,8J
28	3.783E-13	-6.904E-16	1.222E-15	12P
29	2.222E-13	5.230E-16	6.985E-16	11D
30	8.074E-13	-1.310E-15	2.008E-15	13S
31	1.290E-13	1.664E-15	3.443E-16	9F
32	1.382E-14	1.477E-16	1.957E-16	9G,9H,9I,9J,9K
33	2.309E-13	-2.927E-16	4.893E-16	13P
34	1.359E-13	2.014E-16	2.879E-16	12D
35	5.076E-13	-5.531E-16	8.411E-16	14S
36	8.054E-14	6.662E-16	1.549E-16	10F
37	6.680E-15	6.509E-17	8.980E-17	10G,10H,10I,10J,10K,1

Figure 49: The resistances of equivalent circuit theory for the levels of Cesium at 20,000K is shown.

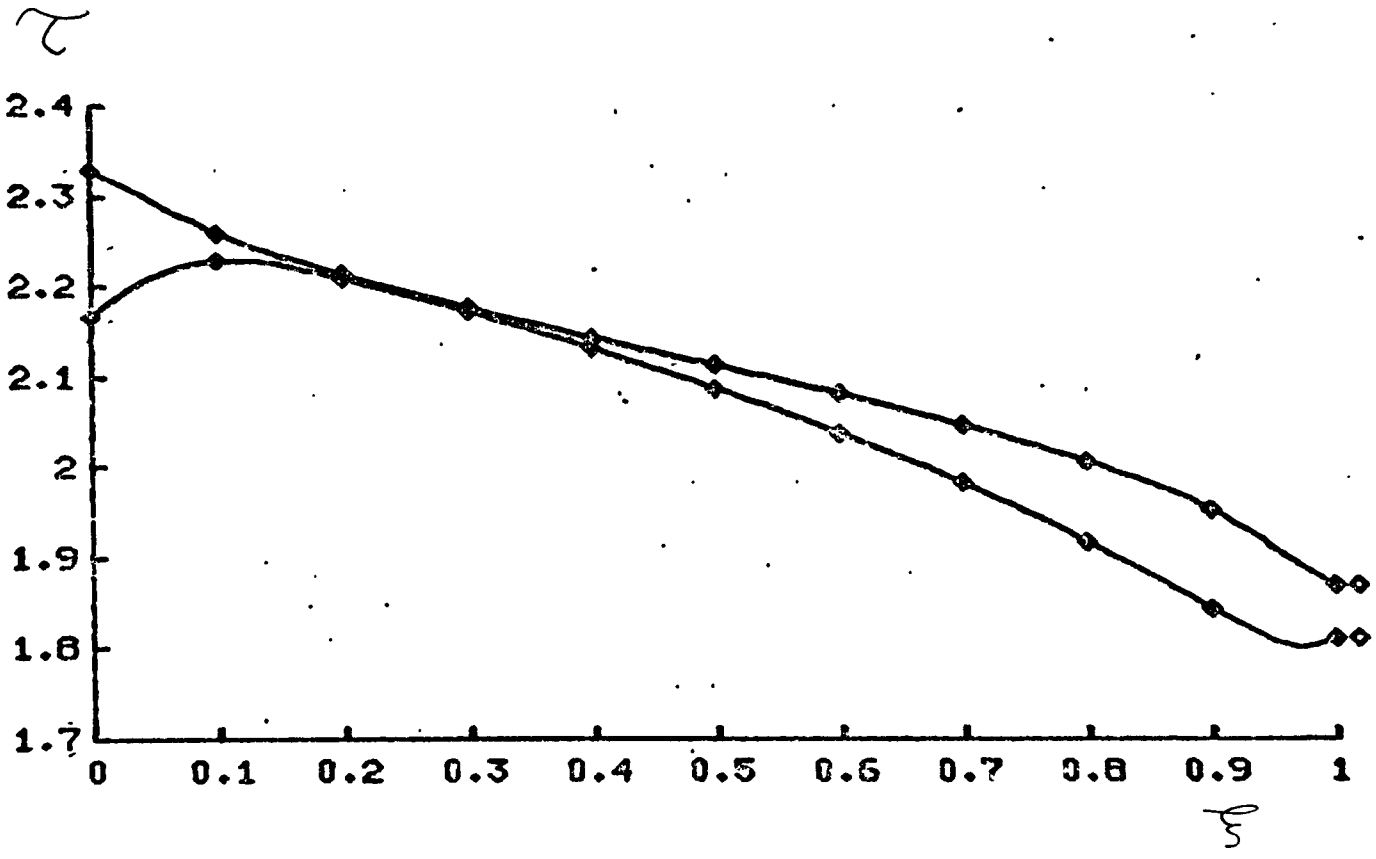

Figure 50: The electron temperature, τ, in a thermionic converter is plotted against position, ξ. Shown are two cases, I=0.5 and I=0.7, computed assuming collisional kinetics.

T_E= 1500K
P_{CS}=1 TORR
D= 10 MIL
J_R= 20 A/CM^2

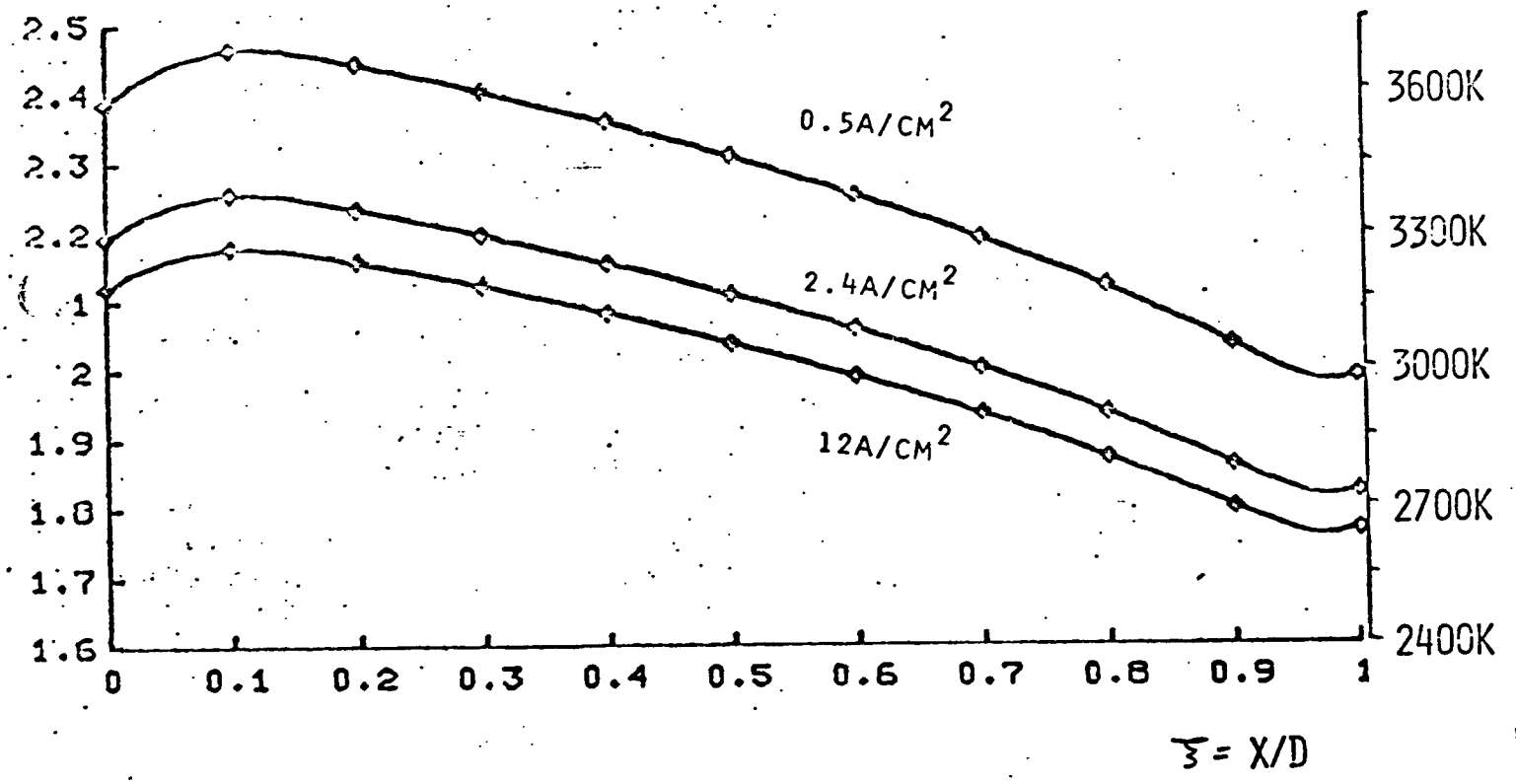

Fisure 51: The electron temperature, τ, in a thermionic converter is plotted against position, ξ. Shown are three cases, I=0.02 (0.5A/cm2), I=0.1 (2.4A/cm2), and I=0.5 (12A/cm2). These were computed using collisional-radiative ionization and recombination kinetics. The rise in temperature at low currents causes a faster than Boltzmann rise of the current voltage characteristic.

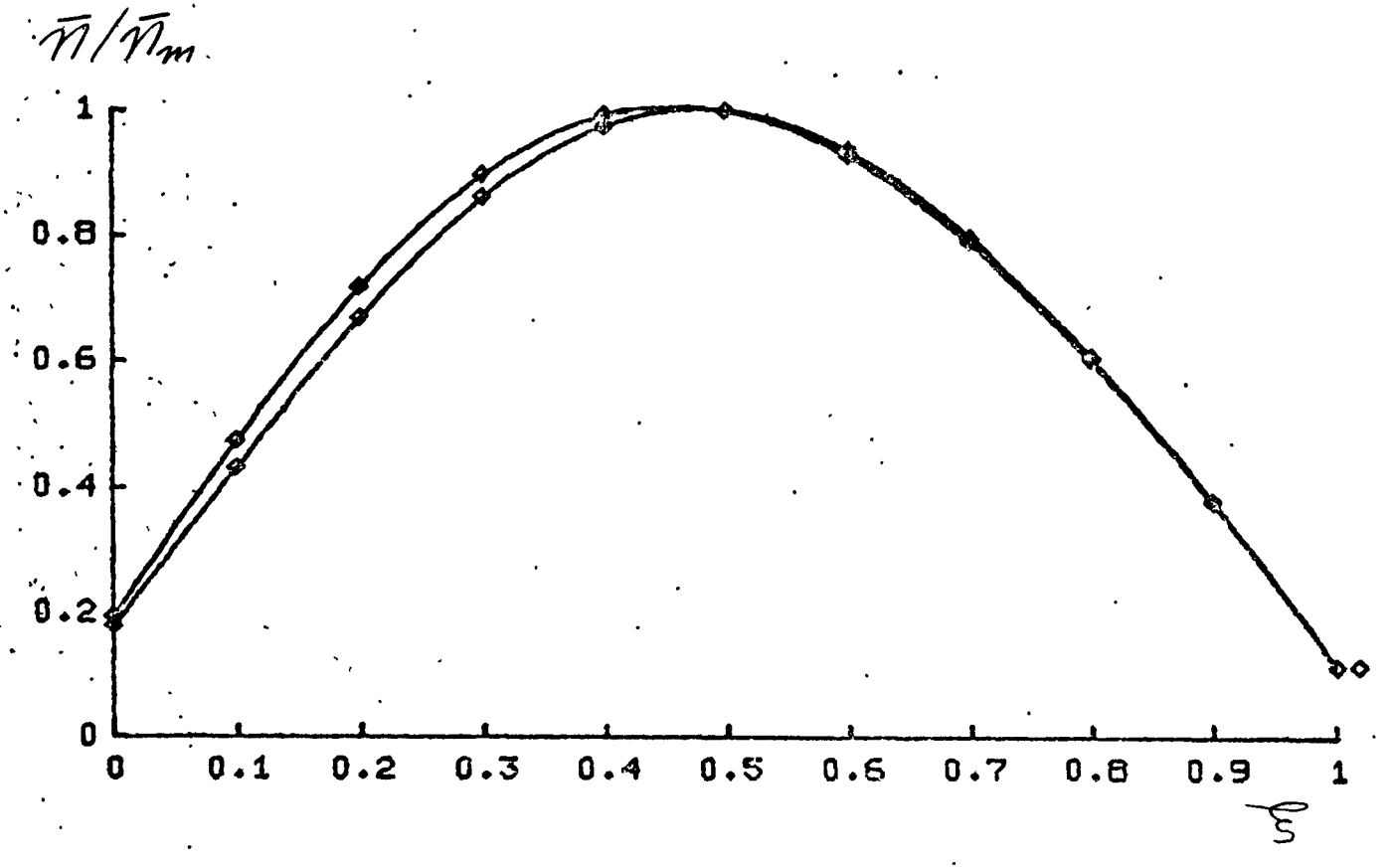

Figure 52: Electron densities, each divided by their maximum, are plotted against position, ξ, during steady thermionic converter operation. Shown are two cases, I=0.5 and I=0.02. This shows that the shape of the distribution changes little even for large changes in current.

T_E= 1500K
P_{CS}=1 TORR
D= 10 MIL
J_R= 20 A/CM^2
J = 11.8 A/CM^2

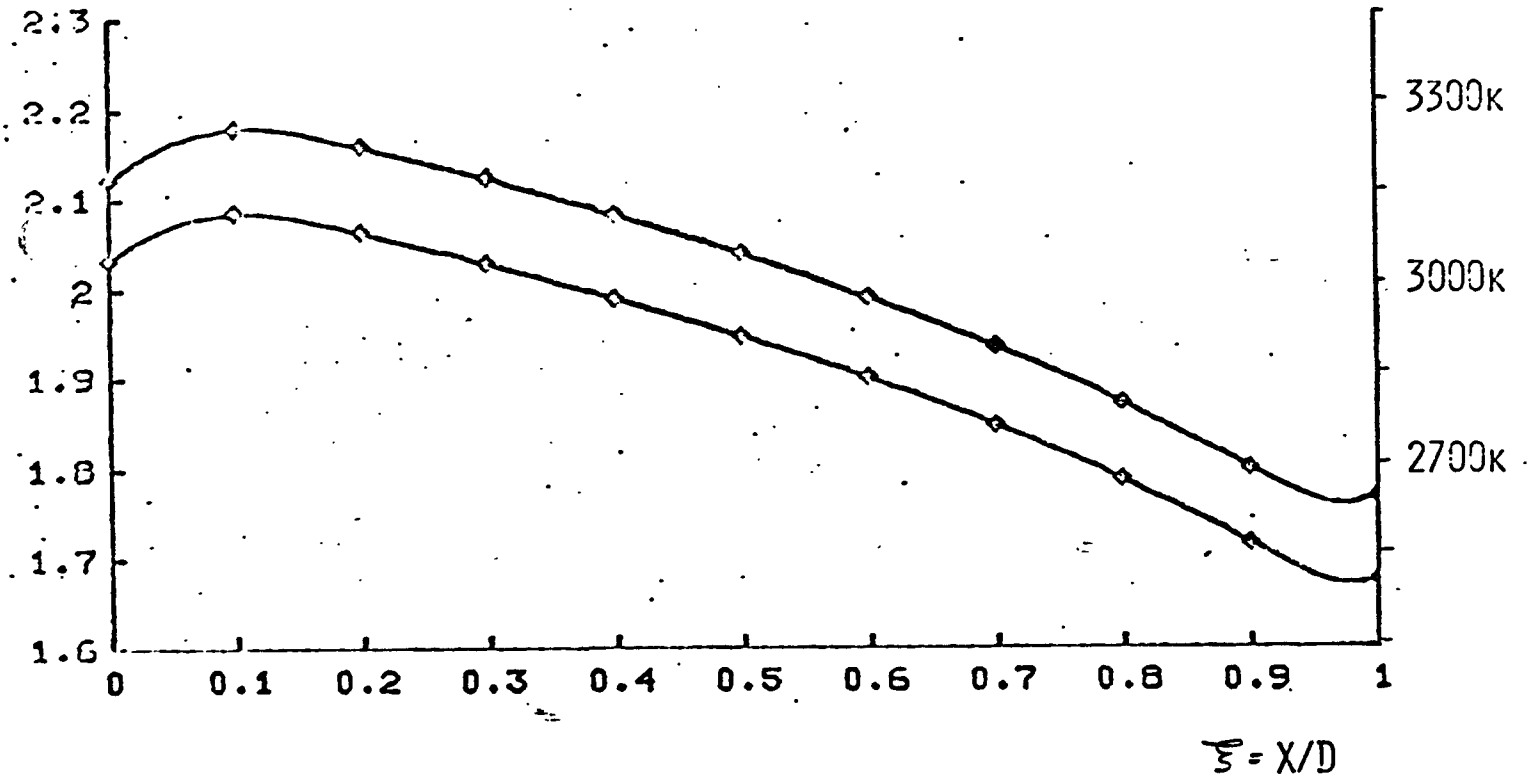

TEMPERATURE ACROSS THE GAP WITH AND WITHOUT 7S-7P LASER ENHANCEMENT

Figure 53:

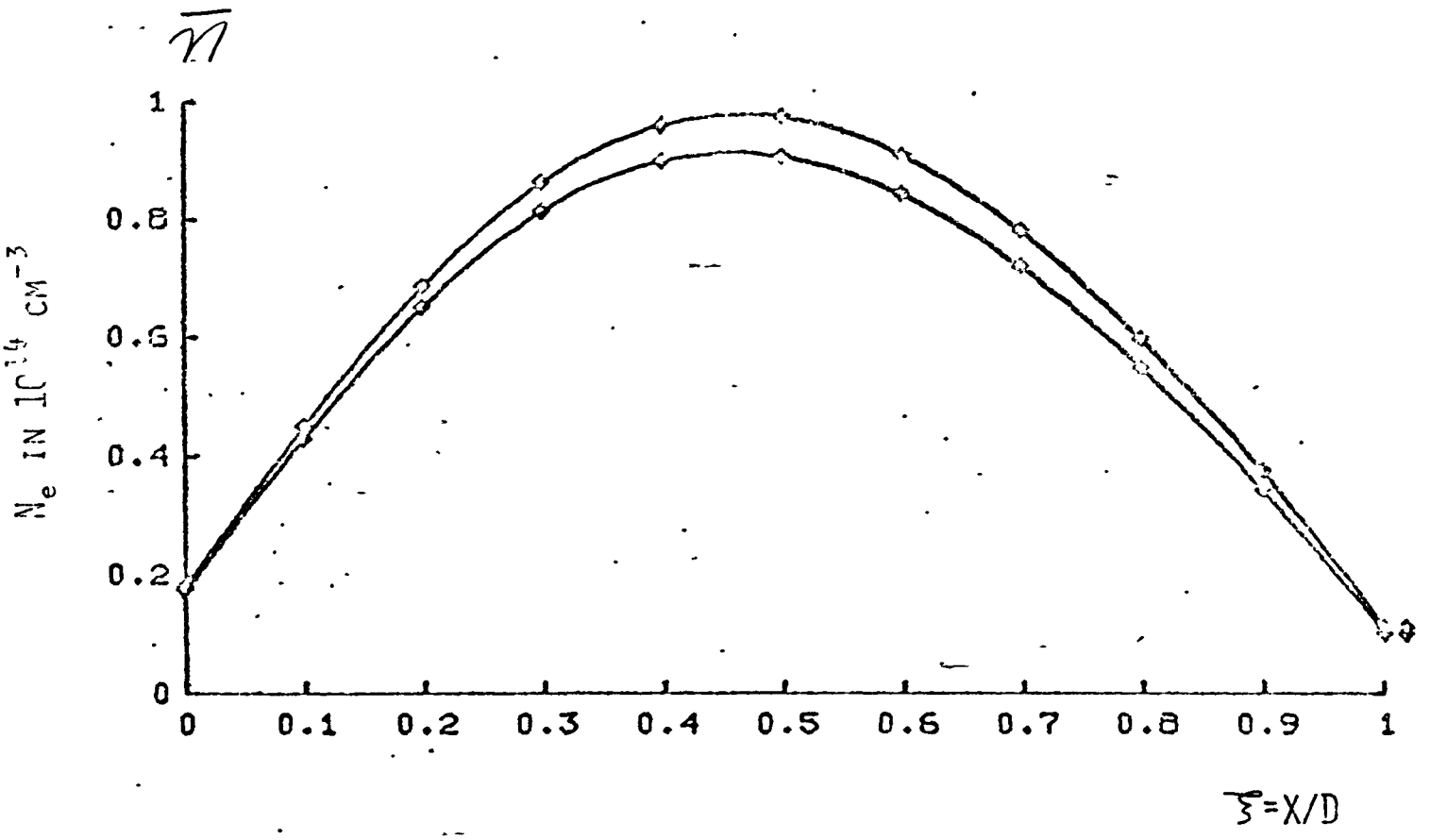

ELECTRON DENSITY ACROSS THE GAP WITH AND WITHOUT 7S-7P LASER ENHANCEMENT

Figure 54:

T_E= 1500K
P_{CS}=1 TORR
D= 10 MIL
J_R= 20 A/CM^2

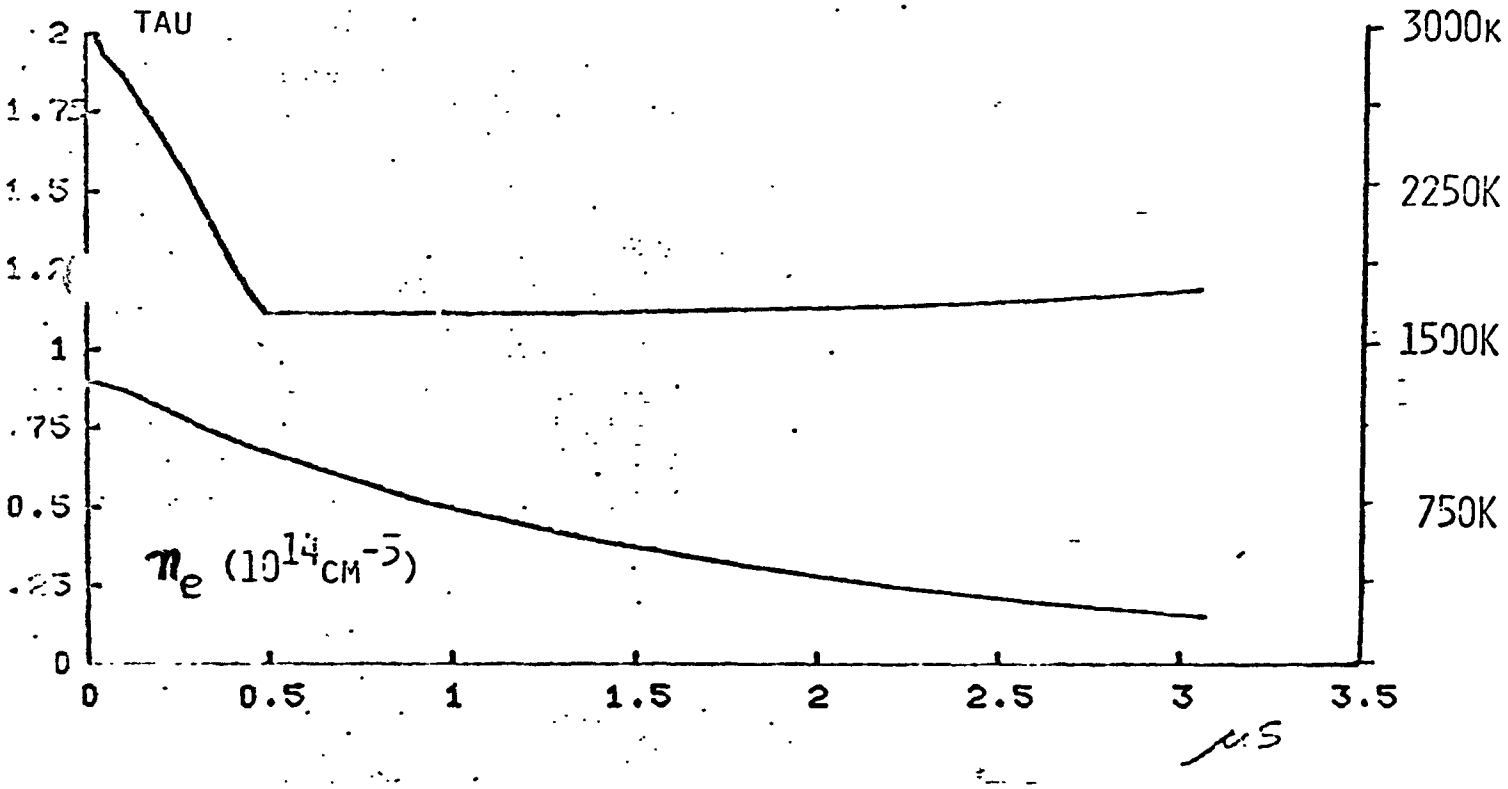

CENTERLINE ELECTRON TEMPERATURE AND DENSITY VS TIME AFTER SUDDENLY DROPPING THE CURRENT FROM 12 TO 2.4A/CM^2

Figure 55:

T_E= 1500K
P_{CS}=1 TORR
D=. 10 MIL
J_R= 20 A/CM^2
J = 11.8 A/CM^2

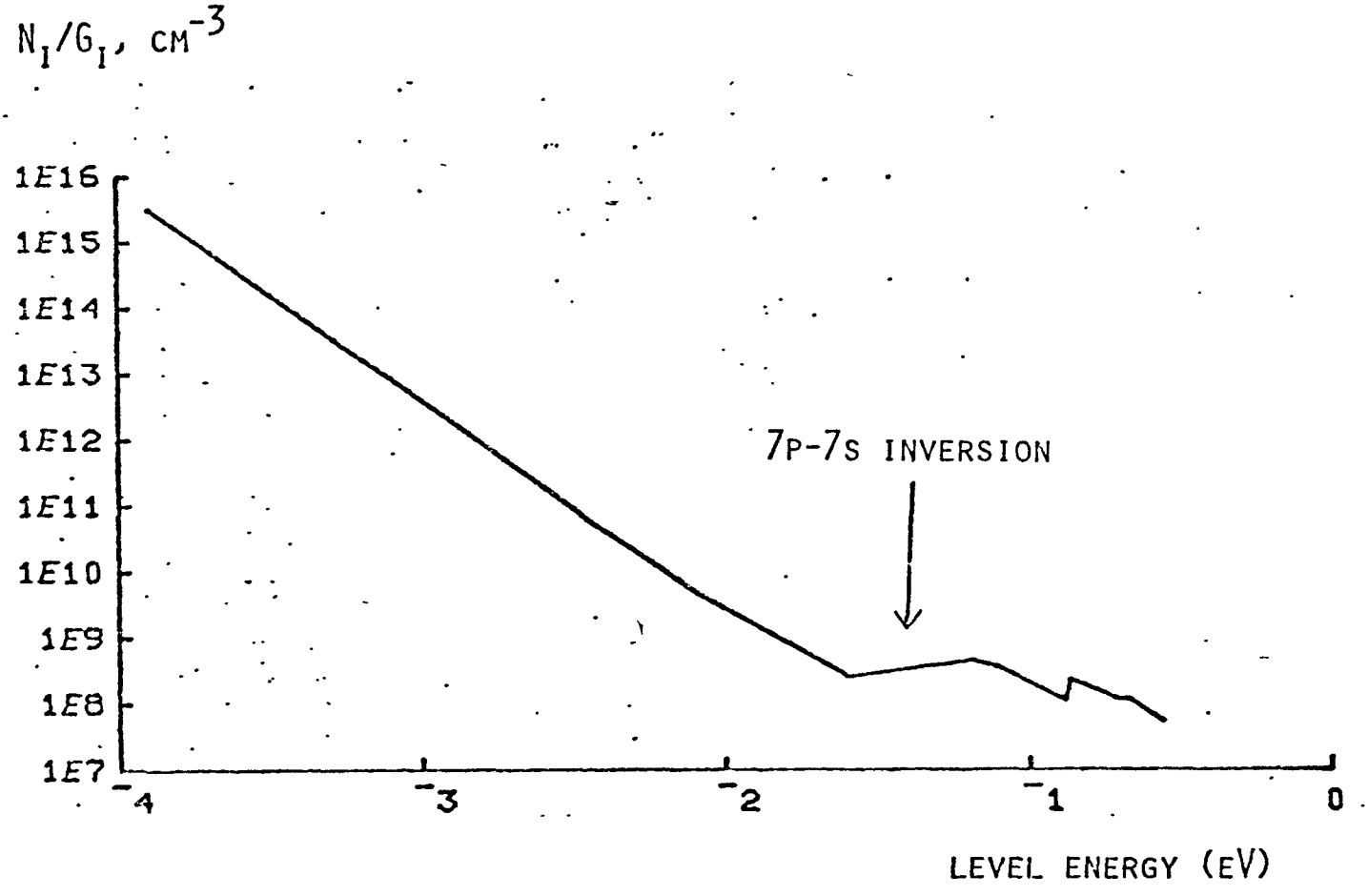

POPULATION DISTRIBUTION AMONG ATOMIC CESIUM LEVELS AT ½ MICROSECONDS AFTER CHANGING THE CURRENT AND AT $\xi = X/D = 0.9$

Figure 56:

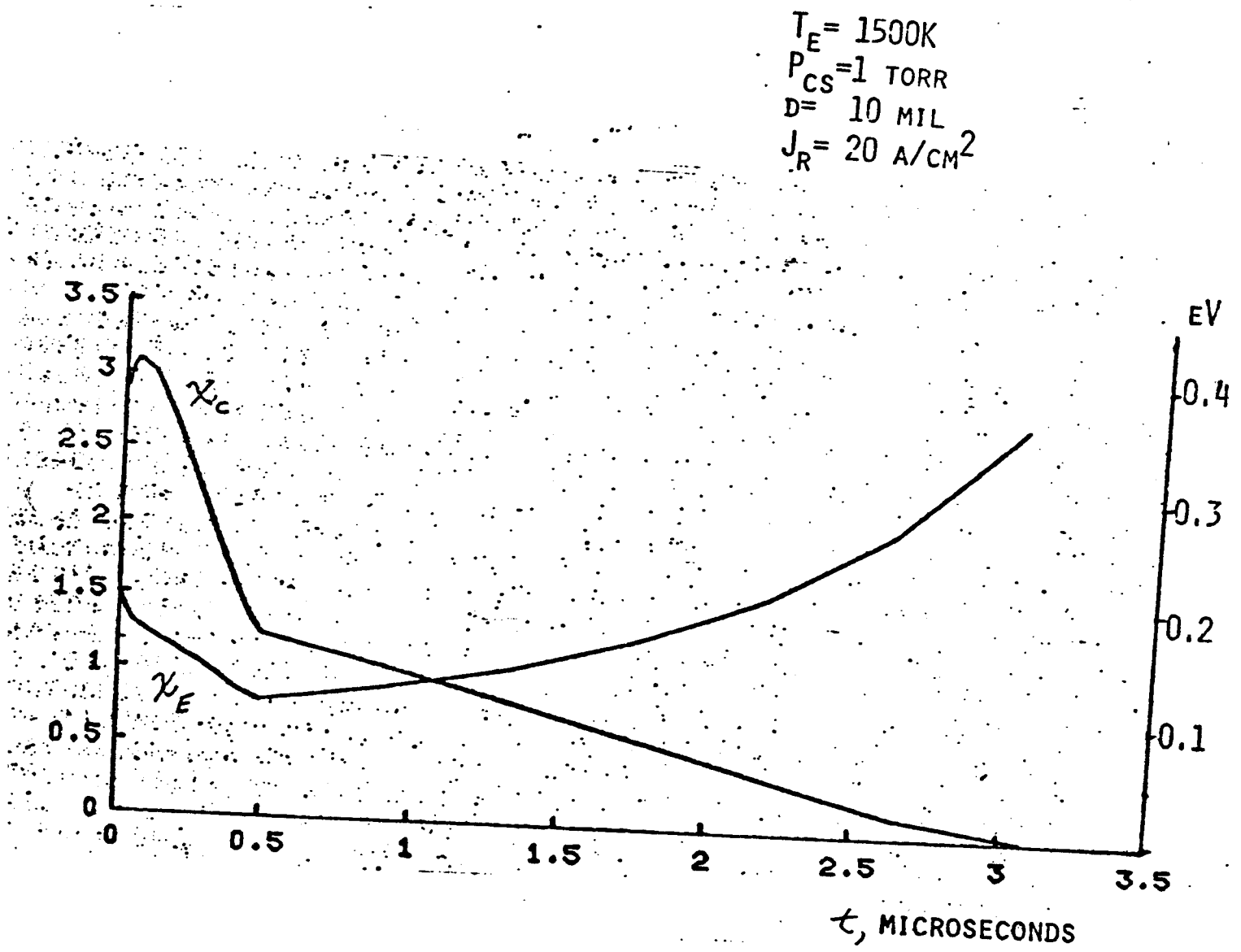

EMITTER AND COLLECTOR SHEATH HEIGHTS VS TIME
AFTER SUDDENLY DROPPING THE CURRENT FROM 12 TO 2.4A/CM^2

Figure 57:

APPENDIX A

The finite difference computer program for solving unsteady and steady thermionic converter plasmadynamics is shown on the following pages. This program is written in the PL/I programming language and was run under the optimizing compiler on Princeton's IBM 3033 computer. The numerical method used is the predictor-corrector technique with adjustable coefficients as described in[60]. Convergence to a steady state solution is typically obtained in one minute or less of CPU time.

This program is structured as an external procedure. This procedure, called PREDCOR, has the function of integrating the thermionic converter conservation equations forward in time. It does this in a specified number of time steps and then computes the voltage drop and returns to the calling program. For each of the steps forward in time, the time derivative of the density and electron temperature must be computed twice, once for the predictor and once for the corrector steps. This is done by an internal procedure called DOT. DOT performs this for all points in the field as well as set the image points to indicate proper boundary conditions.

The meaning of most of the variable names are explained in comments within the program. The most important ones will be reviewed here. PREDCOR integrates the unsteady thermionic conservation equations from a time T1 to a time T2 using a total number of time steps equal to NSTEPS. The length of each time step is DT. These times, as all other variables, are of course nondimensionalized according to the scheme presented in Chapter II. For each of these time steps new electron temperatures, TAU, and electron densities, NEB, need to be computed. This is done by first computing 'predicted' values, TTILDA for temperature and NTILDA for density. These are all computed under assumed converter conditions of an emitter temperature of TE, a collector temperature of TC, and a Cesium pressure, in Torr, of PN. The neutral Cesium temperature, TAUN, is assumed to vary linearly between the emitter and collector temperatures.

```
*PROCESS;
      /*   PREDICTOR-CORRECTOR PROGRAM FOR UNSTEADY T.E.C.          */
      /*                                                            */


 PREDCOR:PROC( T1, T2, TAU, NEB, NSTEPS, TE, TC, ENR, CNR,
                TDOT1, NDOT1,
                PN, SMR, LAMDAR, KN, NR, ARECN, TCHAR, EGNDB, RE,
                N,I, AN, AT, BN, BT, CN, CT) REORDER;
        DECLARE
           SUMV ENTRY((*) FLOAT DEC(16),FIXED BIN(31),FIXED BIN(31))
                RETURNS(FLOAT DEC(16)),
           SQRT BUILTIN,

          /*THE FOLLOWING TIME VARIABLES ARE NOND BY TCHAR.          */
           (T1,T2,                    /*START & FINISH TIMES.       */
           DT,                        /*ACTUAL TIME STEP USED.      */
           TIME,

           AN,AT,BN,BT,CN,CT,         /*PRED-COR ALPHA,BETA,GAMMA   */

           IVD EXT,                   /*PLASMA POWER GAIN           */

          /*THE FOLLOWING VARIABLES REFER TO THE MOST RECENT TIME    */
           TAU(*),                    /*E- TEMPERATURE (NOND BY TE). */
           NEB(*),                    /*ELECTRON DENSITY (NOND BY NR)*/
           TDOT1(*), NDOT1(*),        /*PREDICTOR STEP TIME DERIV.S  */
          ((ENE,CNE) INIT(0.8),       /*E & C EMITTED DENSITY, NE.   */   1550
           (ECHI,CCHI) INIT(3),       /*EMITTER & COLLECTOR DROPS    */   1560
           (EALPHA,CALPHA) INIT(0.5)  /*E & C ION SPEED PARAMETERS   */   1570
              ) STATIC EXTERNAL,                                          1580

          /*THE FOLLOWING ARE CONSTANT DURING THIS PROGRAM           */
           MUI(0:N+1),                /*ION MOBILITY                 */
           ONE INIT(1),                                                   0180
           I,                         /*CURRENT (NOND BY REF DIFF C) */   0230
           DZ,                        /*ZETA INCREMENT BETWEEN PTS   */   0240
           TCHAR,                     /*AN ELECTRON TRANSIT TIME     */   0250
           ERR,                       /*ACCURACY PARAM FOR SHEATH    */   0260
           TE,TC,                     /*EMITTER & COLLECTOR TEMPERATU*/   0270
           DTAUNDZ,
           PN,                        /*NEUTRAL PRESSURE (TORR)      */   0280
           ENR,CNR,                   /*E. & C. RICHARSON DENSITIES. */   0290
           NR,                        /*REFERENCE ELECTRON DENSITY   */   0300
           EGNDB,                     /*E(0)/KT(E). NON-D BINDING E  */   0310
           ELOSSB EXT,                /*ENERGY LOSS PER IONIZATION   */
           RE,                        /*Q(E-A) =Q0 * E**-RE          */   0320
           SMR,                       /*SQRT OF ELECTRON/ION MASS RAT*/   0330
           LAMDAR,                    /* MFP RATIO,  =RMUR/SMR       */   0340
           RMUR,                      /*MU RATIO,  =SMR*LAMDAR       */   0350
           KN,                        /*KNUDSEN NUMBER               */   0360
           NNR,                       /*REFERENCE NEUTRAL DENSITY.   */   0370
           ARECN,                     /*COEFFICIENT OF RECOMBINATION */   0380
           PI,                        /*  3.14159...                 */   0390
           CA,CSAHA,                  /*CONSTANTS IN MSOURCE EQN     */   0400
                                                                          0410
          /*THE FOLLOWING ARE VECTORS (0:N+1).                       */   0420
           (NNB,TAUN,                 /*NEUTRAL DENSITY & TEMP.      */   0430
                                      /*   NON-D BY EMITTER VALUES   */   0440
```

```
  IF TAU(1)<0.1 THEN DO; TAU(1)=0.1; EFIX='1'B; END;                    1740
  IF TAU(N)<0.1 THEN DO; TAU(N)=0.1; CFIX='1'B; END;                      P
  IF          RE=0.5 THEN MUEA=TAUN;
     ELSE IF RE=0   THEN MUEA=TAUN/SQRT(TAU);
     ELSE IF RE=-.5 THEN MUEA=TAUN/TAU;
     ELSE                MUEA=TAUN*( TAU**(RE-0.5) );
  K=( (RE+2)/FYEN )*MUEA*NEB*TAU;
  PC=NEB*(TAU+TAUN);
  DETA,DETAP=LOG(K(2)/K(1)) * DZ/(K(2)-K(1));

/*DETERMINE EMITTER SHEATH                                              */
  CALL SHEATH(ECHI,ENE,I*KN/NEB(1),TAU(1),ENR/NEB(1),
                TE, SMR, EALPHA, 0.8, ERR);
  IF ECHI<=1E-5 ! ECHI>=20 THEN EFIX='1'B;                              1860

/*FIND EMITTER (0+) DERIVATIVES FROM B.C.                               */
  ET_ETA=(TAU(1)-1)*ENE*NEB(1)/KN - I*(ECHI-TAU(1)/2);                  1870
  ET_Z=ET_ETA/K(1);
  EPC_Z=(SQRT(PI/8/EALPHA)/LAMDAR/KN)*NEB(1)/MUI(1)
          - I/MUEA(1);
  EN_Z=( EPC_Z-NEB(1)*(ET_Z+DTAUNDZ) )/( TAU(1)+TAUN(1) );

/*SOLVE COLLECTOR SHEATH                                                */
  CALPHA=1/TAU(N);                                                      2020
  CNE=0;                                                                2030
  NCMIN=4*I*KN/SQRT(TAU(N));                                            2040
  IF NEB(N)>=NCMIN                                                      2050
     THEN CCHI=TAU(N)*LOG( NCMIN/NEB(N)+ 2.506628*SMR );                  PR
     ELSE DO; CCHI=0;  NEB(N)=NCMIN; CFIX='1'B; END;                    2070

/*DETERMINE DERIVATIVES AT COLLECTOR (1-) FROM B.C.                     */
  CT_ETA=-I*(CCHI-TAU(N)/2);
  CT_Z=CT_ETA/K(N);
  CPC_Z=(SQRT(PI/8/CALPHA)/LAMDAR/KN)*NEB(N)/MUI(N)
          - I/MUEA(N);
  CN_Z=( CPC_Z-NEB(N)*(CT_Z+DTAUNDZ) ) / ( TAU(N)+TAUN(N) );
  CDETA=LOG(K(N)/K(N-1)) * DZ/(K(N)-K(N-1));

/*SET IMAGE POINTS.                                                     */
  TAU(0)=TAU(2)-2*DETAP*ET_ETA;
  TAU(N+1)=TAU(N-1)+2*CDETA*CT_ETA;
  PC(0)=PC(2)-2*DZ*EPC_Z;
  PC(N+1)=PC(N-1)+2*DZ*CPC_Z;
  NEB(0)=NEB(2)-2*DZ*EN_Z;
  NEB(N+1)=NEB(N-1)+2*DZ*CN_Z;

/*INITIALIZE GAMMAP & QKP FOR LOOP.                                     */
  MNS=MUI(1)*NEB(1)+MUI(2)*NEB(2);
  MURS=MUI(2)/MUEA(2) + MUI(1)/MUEA(1)*( 1 -2*DZ*(
                (0.5-RE)*ET_Z/TAU(1) - 0.5*DTAUNDZ/TAUN(1)) );
  GAMMAP=   0.5*( ( (MUI(1)+MUI( 2 ))*(PC( 1 )-PC(0))
              )/DZ +I*MURS );
  QKP=(TAU(1)-TAU(0))/DETA;

  DO J=1 TO N;

     /*UPDATE FOR NEW J.                                                */
     GAMMAM=GAMMAP;
     QKM=QKP;                                                           1220
     DETA=DETAP;
```

```
            +0.5*( ESOURCE(N)-CV(N)*TDOT1(N) );
        IVD=DZ*IVD+ 2*I*(TAU(1)-TAU(N)) - (NEB(1)*ENE/KN)*(TAU(1)-1);
1
      /*   DOT: RETURNS WITH NEW NEBDOT AND TAUDOT.                    */
      /*****************************************************************/   1410
      /*                                                               */   1420
      /*   COLLECTOR EMISSION IS NEGLECTED.                            */
      /*                                                               */   1440
      /*                                                               */   1470
      /*****************************************************************/   1500
DOT:    PROC(NEBDOT, TAUDOT, NEB, TAU) REORDER;
        DECLARE                                                             0980
          CHKDOT BIT(1) EXT INIT('0'B),/*IF 1 PRINT DIAGNOSTIC INFO */
          SHEATH ENTRY(DEC(16),DEC(16),DEC(16),DEC(16),DEC(16),
            DEC(16),DEC(16),DEC(16),DEC(16),DEC(16)),
         (TAUDOT(*),                                                        0990
          NEBDOT(*),
          NEB(*),                                                           1000
          TAU(*),                                                           1010
          PC(0:N+1),                  /*CHARGED PARTICLE PRESSURE    */
          F(15) EXT INIT(5.74E-3, 1.4E-3, 2.3, .2, .027, .00574,
                   .0424, 3.2, 61.893, 11.607, 15473, 27.04),
                                                                            1040
          /*SHEATH VARIABLES                                            */
          NCMIN,                      /*MINIMUM NEB(N) TO ALLOW I.   */   1670

          /*TRANSPORT VARIABLES                                         */
          FYEN EXT INIT(1),           /*YEN THERMAL CONDUCTIVITY FACT*/
          K(0:N+1),                   /*THERMAL CONDUCTIVITY         */
          MNS,                        /*SUM OF MUI*NEB AT J & J+1    */
          MUIS,MURS,                  /*SUM OF MUI & MUR AT J,J+1    */

          /*CONSERVATION EQUATION VARIABLES                             */
          EN_Z,CN_Z,                  /*SPATIAL NEB DERIVS           */   1640
          ET_ETA,ET_Z,CT_ETA,CT_Z,    /*SPATIAL DERIVS OF TAU        */   1630
          EDETA,CDETA,                /*ETA XPACING BETWEEN GRID-PTS */
          EPC_Z,CPC_Z,                /*PC GRADIENT FROM B.C.        */

          /*TEMPORARY ENERGY EQUATION VARIABLES                         */
          QKM,QKP,                                                          1050
          DETA,DETAP,                 /*GRID PT SPACING IN ETA       */
          KDE,                        /*THERMAL COND X D ETA AVE     */
          CONVECTN,                                                         1070
          POHMIC,                                                           1080
          PB,PBP,                     /*ENERGY STORED IN EXCITED STAT*/
          SIGMA)                                                            1110
             FLOAT DEC(16),                                                 1120

          /*TEMPORARY DENSITY EQUATION VARIABLES                        */
          (GAMMAM,GAMMAP,
          D1B,D21B,D32B,P0,IB,NUE,    /*PARAMETERS FOR MSOURCE       */
          A,
          NES2)
             FLOAT DEC(16),
          J FIXED BIN(31);                                                  1130
        ON FINISH PUT SKIP(5) DATA;

      /*SET THERMAL & ELECTRICAL CONDUCTIVITIES AT 0+ (E) &, 1- (C). */    1710
        TAU(0),TAU(N+1)=1;            /*AVOID NEGATIVE VALUES        */
```

```
      MSOURCE,                  /*E- PRODUCTION RATE (NOND)    */    0450
      ESOURCE,                  /*ENERGY SOURCE TERM (NOND)    */    0460
      CV,
      MUEA,                     /*E- MOBILITY AMONG ATOMS.     */
      NDOT2,TDOT2,
      TTILDA,NTILDA)
         (0:N+1) ) FLOAT DEC(16),
      CFIX BIT(1) EXT,          /*DID C-SHEATH REQUIRE FIX?    */
      EFIX BIT(1) EXT,
     (NSTEPS,
      N,                        /*# OF GRID PTS, E TO C INCL.  */
      J,
      COUNT)                    /*PRESENT # OF TIME STEPS.     */
         FIXED BIN(31);
/*HANDLE EXCEPTIONAL CONDITIONS.                                */
  ON FINISH PUT SKIP(5) DATA;
                                                                0600
  PI=3.1415926 + 5.3589793E-8;
  DZ=ONE/(N-1);
  DT=(T2-T1)/NSTEPS;                                            0740
  CFIX,EFIX='0'B;                                               0610
  ERR=1E-3;                                                     0720

/*SET NEUTRAL TEMPERATURE AND DENSITY.                          */
  IF TE=TC THEN TAUN=1;
     ELSE DO J=0 TO N+1;                                          0
             TAUN(J)=1 + (TC/TE-1)*(J-1)/(N-1);                   0
             END;                                                 0
  NNR=965.5E16*PN/TE;                                           0660
  NNB=1/TAUN;                                                   0670
  DTAUNDZ=TAUN(N)-TAUN(1);

/*SET TRANSPORT PARAMETERS.                                     */
  RMUR=LAMDAR*SMR;                                              0700
  MUI=SQRT(TAUN);

/*SET IONIZATION AND SAHA PARAMETERS.                           */
  CA=0.41283*ARECN*TCHAR*(NR/1E14)**2 * (TE/1500)**-4.5;        0680
  CSAHA=LOG( (1.4027E20*NNR/NR/NR) * (TE/1500)**1.5 );          0690
                                                                0710
  DO COUNT=0 TO NSTEPS-1;
     TIME=T1+COUNT*DT;

     /*PREDICTOR STEP                                           */
     CALL DOT(NDOT1,TDOT1,NEB,TAU);
     NTILDA=NEB + AN*DT*NDOT1;
     TTILDA=TAU + AT*DT*TDOT1;

     /*CORRECTOR STEP                                           */
     CALL DOT(NDOT2,TDOT2,NTILDA,TTILDA);
     NEB=NEB + DT*( BN*NDOT1+CN*NDOT2 );
     TAU=TAU + DT*( BT*TDOT1+CT*TDOT2 );
     END;

/*UPDATE TIME DERIV.S, IMAGE POINTS, AND FIND PLASMA POWER GAIN*/
  CV(0),CV(N+1)=0;
  ESOURCE(0),ESOURCE(N+1)=0;
  CALL DOT(NDOT1,TDOT1,NEB,TAU);
  IVD=   0.5*( ESOURCE(1)-CV(1)*TDOT1(1) )
       + SUMV( ESOURCE-CV*TDOT1, 2, N-1)
```

```
      IF J^=N
         THEN DO;
            DETAP=LOG(K(J+1)/K(J)) * DZ/(K(J+1)-K(J));
            MNS=MUI(J)*NEB(J)+MUI(J+1)*NEB(J+1);
            MUIS=MUI(J)+MUI(J+1);
            MURS=MUI(J)/MUEA(J) + MUI(J+1)/MUEA(J+1);
            END;
         ELSE
            MURS=MURS +2*DZ*(MUI(N)/MUEA(N))*((.5-RE)*CT_Z/TAU(N)
                              - 0.5*DTAUNDZ/TAUN(N));

      /*FIND AMBIPOLAR FLUX AT J+1/2.                                  */
      GAMMAP=0.5*( ( MUIS*(PC(J+1)-PC(J))
                )/DZ +I*MURS );


      /*FIND MASS SOURCE AT J.                                         */
      A=CA/TAU(J)**4.5;
      NES2=NNB(J) * TAU(J)**1.5 * EXP( CSAHA-EGNDB/TAU(J) );
      D21B=F(7)*(1+F(8)/TAU(J));
      D32B=F(2)*EXP(F(3)/TAU(J));
      IB=A*NES2*( 1+F(1)/NEB(J) )/( 1+D21B*(1+D32B/NEB(J))/NEB(J)
                                  );
      P0=1+( F(4)/NEB(J) )*( 1+F(5)/NEB(J) )/( 1+F(6)/NEB(J) );
      NUE=NEB(J)*NEB(J)/NES2;
      MSOURCE(J)=NEB(J)*IB*( 1-P0*NUE );

      NEBDOT(J)=RMUR*(GAMMAP-GAMMAM)/DZ + MSOURCE(J);

      KDE=K(J)*(DETA+DETAP)/2;
      QKP=(TAU(J+1)-TAU(J))/DETAP;
                                                                     1250
      CONVECTN=-1.5*I*(DETA*QKP+DETAP*QKM)/(2*KDE);
      SIGMA=NEB(J)*MUEA(J);                                          1270
      POHMIC=I*( I/SIGMA + TAU(J)*( NEB(J+1)-NEB(J-1) )              1280
                                 / (2*DZ*NEB(J)));                   1290
      PBP=( F(9)*NNR/NR )*EXP( -F(10)/TAU(J) );
      PB=( F(11)*NNR/NR )*EXP( -F(12)/TAU(J) );
      CV(J)=1.5*NEB(J) + NNB(J)*(F(10)*PBP+F(12)*PB*NUE)
                                          / (TAU(J)*TAU(J));
      ESOURCE(J)=-ELOSSB*MSOURCE(J)
                       - NNB(J)*PB*( 2*NUE*NEBDOT(J)/NEB(J) );
                                                                     1320
      TAUDOT(J)=( (QKP-QKM)/KDE + CONVECTN + POHMIC + ESOURCE(J) )
            / CV(J);
                                                                     1340
      IF CHKDOT THEN PUT SKIP(2) DATA(NEB(J),TAU(J),MSOURCE(J),
            J,PB,PBP,A,
                D21B,D32B,P0,IB,NUE,NES2,QKP,GAMMAP,DETAP,MURS);
      END;                                                           1350
                                                                     1370
                                                                     1400
   NEBDOT(0),NEBDOT(N+1)=0;
   TAUDOT(0),TAUDOT(N+1)=0;
   IF CHKDOT THEN PUT SKIP(3) DATA;
   END DOT;
   END PREDCOR;                                                      2170
```

APPENDIX B: Symbols and Notation

Some of the important notations used in this thesis are listed below. The meaning of each symbol is given as well as the page where it is defined. Dimensional variables are listed in column (1). Non-dimensional variables are listed in column (2). As the alphabet is finite, some symbols have more than one meaning; the intended meaning should be clear by context. See also figure 2 for a graphic definition of various voltages used.

(1)	(2)	
α	A	ionization coefficient(II-9,II-19,IV-10)
	α_E, α_c	ion speed parameters(II-12,14)
	$\bar{A}$	temperature sensitive part of density dependent ionization coefficient(II-27)
β		recombination rate coefficient(II-9,IV-10)
d		interelectrode gap length(figure 2)
D_a	$\bar{D}_a$	ambipolar diffusion coefficient(II-20,II-28)
e		elementary charge
Γ	$\bar{\Gamma}$	ambipolar flux(II-8,II-17)
Γ_e, Γ_i	I_e, I_i	electron and ion fluxes, respectively(II-2,II-17)
Γ_E	I_E	emitted flux of electrons by the emitter(II-11,II-17)
k		Boltzmann's constant
k_e	K	electron thermal conductivity(II-8,II-17)
	K_n	parameter related to a Knudsen number(II-17)
J	I	total current(II-3,II-17)

	j	ratio of total current to emitted current(II-24)
J_E	I_E	emitted current(II-11,II-17)
n	$\bar{n}$	plasma number density(II-3,II-17)
n_e, n_i		electron and ion number densities, respectively(II-2)
n_E		emitted number density(II-12,II-29)
n_0, n_1	$\bar{n}_0, \bar{n}_1$	plasma density near the emitter and collector, respectively(II-12,II-14)
t	$\bar{t}$	time(II-2,II-17)
t_c		characteristic diffusion time(II-17)
T_e	τ	electron temperature(II-4,II-16)
T_0, T_1	τ_0, τ_1	electron temperature evaluated near the emitter and collector, respectively(II-14,II-16)
T_n	τ_n	neutral temperature(II-7,II-16)
T_E, T_C		emitter and collector temperature, respectively(II-12,II-14)
V_E	χ_E	emitter sheath height(II-12,II-16)
V_c	χ_c	collector sheath height(II-14,II-16)
ψ	χ	electron motive (potential) (II-3,II-16)